Organic Hole Transport Layers for Efficient, Stable and Scalable Inverted Perovskite Solar Cells

Yiguo Yao, Caidong Cheng, Chenyang Zhang, Hanlin Hu, Kai Wang, Stefaan De Wolf**

Y. Yao, C. Cheng, C. Zhang and Prof. K. Wang

Institute of Flexible Electronics (IFE), Northwestern Polytechnical University (NPU), Xi'an 710072, China

Prof. H. Hu

Hoffman Institute of Advanced Materials, Shenzhen Polytechnic, 7098 Liuxian Boulevard, Shenzhen 518055, China.

Prof. S. De Wolf

King Abdullah University of Science and Technology (KAUST), Division of Physical Science and Engineering, and KAUST Solar Center, Thuwal 23955-6900, Saudi Arabia

Email: kaiwang@nwpu.edu.cn; stefaan.dewolf@kaust.edu.sa;

Keywords: inverted perovskite solar cells, organic hole transporting layers, polymer, small molecules, self-assembled monolayers

Abstract

Hole transporting layers (HTLs) are an essential component in inverted, *p-i-n* perovskite solar cells (PSCs) where they play a decisive role in extraction and transport of holes, surface passivation, perovskite crystallization, device stability and cost. Currently, the exploration of efficient, stable, highly transparent and low-cost HTLs is of vital importance for propelling *p-i-n* PSCs toward commercialization. Compared to their inorganic counterparts, organic HTLs offer multiple advantages such as a tunable bandgap and energy levels, easy synthesis and purification, solution processability and overall low cost. In this review, recent progress of organic HTLs, including conductive polymers, small molecules and self-assembled monolayers (SAMs), as utilized in inverted PSCs is systematically reviewed and summarized. Their molecular structure, hole transport properties, energy levels and relevant device properties and resulting performances are presented and analyzed. A summary of design principles and a future outlook towards highly efficient organic HTLs in inverted PSCs is proposed. This review aims to inspire further innovative development of novel organic HTLs for more efficient, stable, and scalable inverted PSCs.

This article has been accepted for publication and undergone full peer review but has not been through the copyediting, typesetting, pagination and proofreading process, which may lead to differences between this version and the Version of Record. Please cite this article as doi: 10.1002/adma.202203794.

1. Introduction

The increased energy demands related to a rapidly developing economy at the global level needs to be compatible with set climate goals, which explains the significant attention towards sustainable, climate-neutral energy resources. For this, solar energy has been of particular promise as arguably the most abundant renewable energy source.[1-2] Therefore, great efforts have been undertaken to improve the power conversion efficiency (PCE), stability, and scalability of solar cells.[3] At present, among emerging photovoltaic (PV) technologies, perovskite solar cells (PSCs) have seen tremendous breakthroughs within the last decade, resulting in PCE increases from 3.8% in 2009 to 25.7% for single-junction lab-scale devices;[4-20] such values are now comparable with those of market-established solar cell technologies such as crystalline silicon (c-Si) and copper indium gallium diselenide (CIGS).[21-22] Moreover, PSCs can be manufactured using low-cost, scalable, simple solution-processing techniques, further underlining the promise of PSCs as a future mainstream technology.[23] Moreover, PSCs can also be integrated as top cell into tandems when combining either with c-Si, CIGS, organic or another PSC as bottom cell technology, yielding PCEs well above those of the sub cells, opening pathways towards affordable ultra-high efficient PV.[24-35] Yet, despite this rapid progress in performance, important questions remain related to the stability and scalability of PSCs, hindering their market entrance; resolving these is a multifaceted challenge, where the perovskite as well its contact layers play important roles.

Generally, the PSC device structure consists of a metal halide perovskite layer acting as photo-absorber (often labeled as *i*-layer), which is sandwiched between two different charge transport layers (CTLs), namely a hole transport layer (HTL, also referred to as *p*-layer) and an electron transport layer (ETL, *n*-layer).[36-38] These CTLs are sandwiched between the perovskite and an outer electrode, which can be transparent, such as fluorine tin oxide (FTO) or indium tin oxide (ITO), or opaque, typically a metal like silver (Ag), aluminum (Al), gold (Au), and copper (Cu). PSCs can be divided in conventional (*n*-*i*-*p*) or inverted (*p*-*i*-*n*) architectures; the notation refers to the layer deposition sequence; for single-junction PSCs the substrate is usually glass, which will be sunward facing. For instance, the conventional *n*-*i*-*p* structure will feature its ETL and HTL as front and back CTLs, respectively, resulting in electron collection at the (transparent) front contact; such *n*-*i*-*p* PSCs either have a mesoporous or a planar structure, which essentially refers to the employed ETL; the former will be the case when employing sintered TiO_x paste, a legacy from dye sensitized solar cells.[39] The *n*-*i*-*p* structure has systematically outperformed its *p*-*i*-*n* counterpart, up to present.[40-41]

Nevertheless, *p-i-n* PSCs offer several advantages. First, high-temperature sintering (>450 °C, required for the mesoporous TiO_2 formation) is avoided, making this technology of particular appeal for applications with limited temperature resilience, such as most tandem solar cells and flexible devices.[42-43] Second, no extrinsic dopant is needed for the CTLs, which can be instrumental towards improved device stability.[44-47] For instance, it is well known that the dopants in 2,2',7,7'-tetrakis[*N*,*N*-di(4-methoxyphenyl)amino]-9,9'-spirobifluorene (Spiro-OMeTAD) – the most commonly used HTL in *n-i-p* PSCs – can accelerate device degradation because of doping-related Li^+ migration across the perovskite layer; moreover the hygroscopic nature of Spiro-OMeTAD, results in facile and undesired moisture ingress into the perovskite.[48-52] Third, *p-i-n* PSCs usually feature a much less pronounced hysteresis in their current-voltage characteristics, compared to *n-i-p* devices.[53-56] Fourth, the fabrication costs of single-junction *p-i-n* PSCs can arguably be lower because for the back electrode a cheaper metal such as Ag, Al or Cu can be used, compared to Au in the *n-i-p* structure. Nevertheless, the maximum PCE of inverted PSCs (~25%) still lags behind their conventional *n-i-p* counterparts, predominantly due to a relatively lower open-circuit voltage (V_{OC}) and fill factor (FF).[34, 57-60] These losses are dominated by the interfaces between the perovskite and the CTLs, where carrier recombination may occur both at the perovskite/ETL and HTL/perovskite sides, depending much on the choice of CTL. For *p-i-n* PSCs, the ETL is usually a fullerene derivative; contrastingly, for the HTL, several options are available, varying from inorganic to organic materials.[61-63] In *p-i-n* PSCs, the basic function of the HTL includes: i) extraction and transport of holes from the perovskite to the (transparent) anode; ii) blocking the flow of electrons to the anode by an energy barrier, to reducing recombination;[64-65] iii) protecting the perovskite layer from moisture and oxygen, thereby reducing corrosion and improving the device stability.[66-67] Besides, the HTL, terminating the substrate, may act as a template for the subsequent deposition and crystallization of the perovskite layer, and therefore has a direct influence on quality of the subsequent perovskite layer. Finally, situated at the light-incident side, the HTL should be as broadband transparent as possible for the solar spectrum, to avoid current losses at the device level.

Although inorganic HTLs (such as NiO_x) possess a high thermal stability and transparency,[68-70] their PV performance is usually inferior to their organic counterparts due to relatively a low intrinsic conductivity and surface defects.[71-72] For instance, it was reported that NiO_x $Ni^{\geq 3+}$ surface species can react with perovskite organo-iodide precursors, resulting in a defective NiO_x/perovskite interface.[73] Besides, most of the inorganic HTLs require either a high-temperature or high-vacuum processing step and may feature a poor wettability with respect to the perovskite precursor ink, in case of solution processing. Lastly, the available materials suitable as inorganic HTL are limited.[74] On

the contrary, organic HTLs can be solution-processed at low temperature, and their properties can be finely adjusted through molecular design.[75] Moreover, combining novel building blocks through organic synthesis can strongly expand the library of organic HTLs, thus showing great potential for further PSC development in terms of performance, stability and scalability. **Figure 1** presents recent trends in the development of organic HTL.

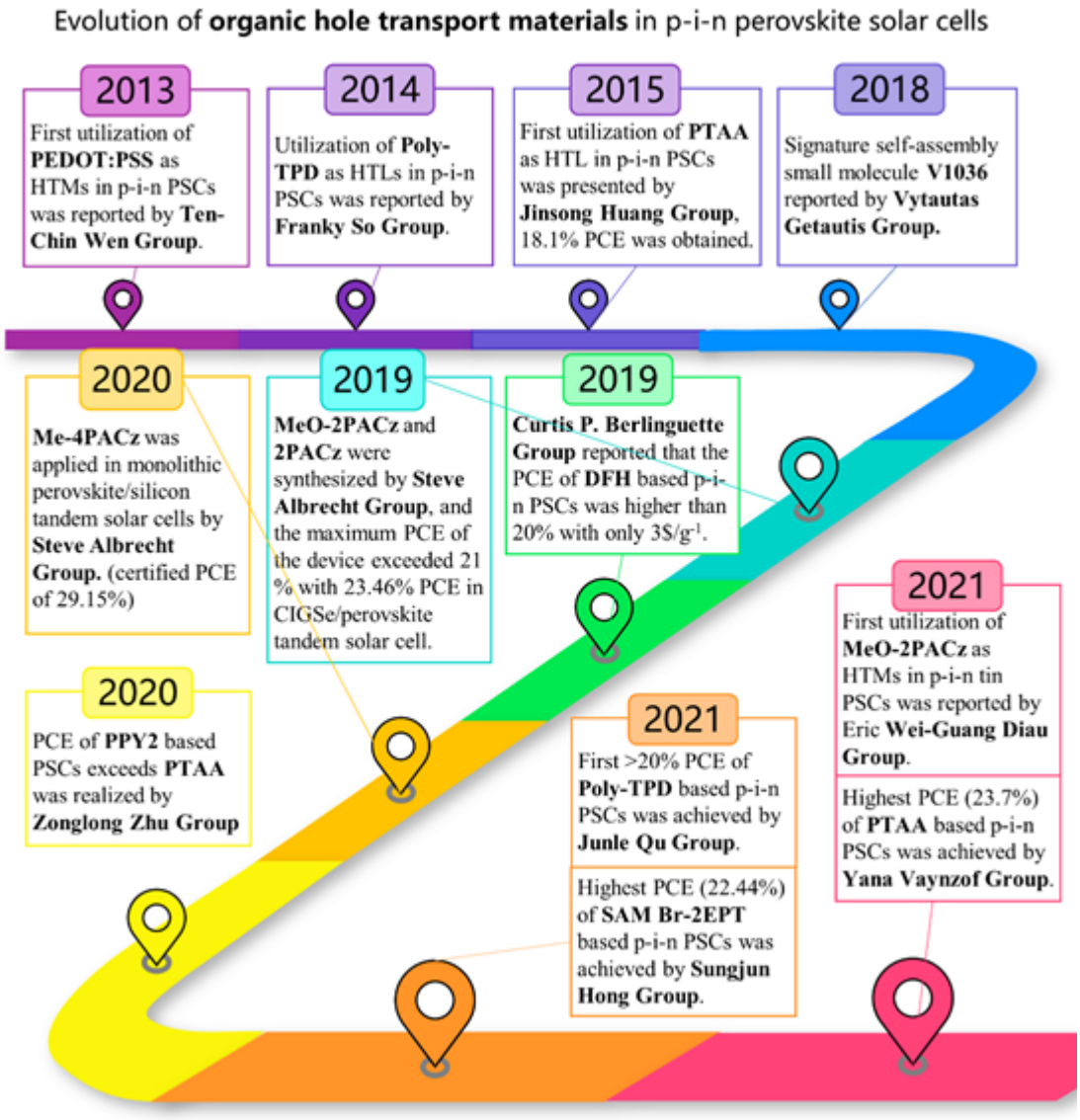

Figure 1. Historical evolution of efficient hole transport layers in the literature.

Although several reviews on dopant-free organic HTLs are available in the literature,[76-78] most of the discussion has been focused on HTLs in *n-i-p* devices, yet the design principles and desired properties for HTLs in *p-i-n* devices differ substantially. For example, a high hydrophobicity is needed in *n-i-p* PSCs to protect the underlying perovskite layer against moisture ingress, whereas a

moderate HTL hydrophobicity is desired in *p-i-n* PSCs to guarantee good wettability of the perovskite-precursor ink. Solvent compatibility between HTL and perovskite may also be different. Moreover, as already stated, the bandgap of HTLs for inverted PSCs should be sufficiently wide to avoid parasitic absorption of solar photons, which may be less of a concern in *n-i-p* devices. In this review, a thorough summary and discussion of the development of organic HTLs aimed for use in *p-i-n* PSCs is presented according to their chemical structure. We categorize organic HTLs into conductive polymers, small molecules (SMs) and emerging self-assembled monolayers (SAMs). In particular, the structure-property relationship and the benefits of organic HTLs towards *p-i-n* PSCs with high performance and stability is presented and analyzed. We then discuss the development and design principles of these materials. Lastly, we provide a brief perspective on future research directions toward realizing highly efficient and stable *p-i-n* PSCs.

2. Conductive polymer HTLs

Conductive polymers have been widely used in organic light-emitting diodes (OLEDs), organic photovoltaics (OPV), and organic field-effect transistors (OFETs). The long conjugated chain facilitates π-electron delocalization throughout the backbone, which is beneficial for intramolecular charge transfer. Meanwhile, the distinct planar and rigid polymer main chains are highly ordered in the solid state, and the aggregates are tightly packed to ensure good intermolecular charge hopping, facilitating charge transport.[79] The alkyl side chain can endow the polymers with good solution processability. [80-81] Also, polymer HTLs are more tolerant to polar solvents because their higher molecular weight compared to small molecules. In this part, we will focus on the latest developments of polymer HTLs, including modifications such as through molecular engineering, bilayer formation, among others. Resulting device performances and stability are discussed and compared.

2.1. PEDOT:PSS

Poly(3,4-ethylenedioxythiophene):poly(styrenesulfonate) (PEDOT:PSS) has historically been the first HTL **(Figure 2a)** used in *p-i-n* PSCs due to its high optical transparency, simple preparation, and well-established use in OPV.[82-83]. The highest occupied molecular orbital (HOMO) and lowest unoccupied molecular orbital (LUMO) energy level of PEDOT:PSS is −5.3 and −2.2 eV, respectively. The hole mobility is 0.045 $cm^2 V^{-1} S^{-1}$ measured from fabricated transistors.[84-85] However, despite these early results, the mismatched energy levels between PEDOT:PSS and perovskite, its insufficient

hole mobility, as well as high acidity continue to hinder PSC performance and stability.[86-87] Wen et al.[88] first reported PEDOT:PSS as HTL in *p-i-n* planar PSCs with as device structure ITO/PEDOT:PSS/$CH_3NH_3PbI_3$/$PC_{61}BM$/BCP/Al in 2013. The optimized device gave a modest PCE of 3.9%. From these beginnings, the performance of PSCs was further optimized by tailoring PEDOT:PSS via strategies such as doping, composite structure, double-layer structure, and solvent post-treatment.

The conductivity of PEDOT:PSS is dependent on the grade of material. For example, the conductivity of PEDOT:PSS (Clevios HTL Solar) is 0.1-1 S cm^{-1}. A higher conductivity of 500 S cm^{-1} is provided by Clevios F HC Solar. Clevios PH 500 and PH 1000 also offer high conductivity of 300 and 850 S cm^{-1}, respectively (reported from Heraeus company). The conductivity of most commonly used PEDOT:PSS in *p-i-n* PSCs (1.6×10^{-3} S cm^{-1}, Clevios PVP Al 4083) is not as high as for the commonly used ETLs (C_{60} or PCBM) in the *p-i-n* device architecture.[89] This results from the insulating nature of PSS, which leads to unbalanced charge transport and loss of photogenerated carriers at the device level.[90] To address this problem, Gong et al.[91] used *N,N*-dimethylformamide (DMF)-treated PEDOT:PSS and poly(methyl-methacrylate) (PMMA)-modified PCBM as HTL and ETL, respectively. This resulted in a balanced charge transport and inhibited charge accumulation and recombination in the device. Moreover, the smoother surface of PEDOT:PSS after DMF treatment resulted in an improved interfacial contact with the overlying perovskite layer, yielding a relatively high V_{OC} (1.02 V) and PCE (18.72%). Resistive losses may be minimized by thinning the PEDOT:PSS. In this context, Sun et al.[92] obtained a PEDOT:PSS monolayer by solvent washing, of which the fabrication process is illustrated in **Figure 2b**. X-ray photoelectron spectroscopy (XPS) spectra, as shown in **Figure 2c** and **2d**, suggested that an In-O-S chemical bond was formed between the PEDOT:PSS monolayer and the underlying ITO, which was argued to facilitate hole transfer and improve device stability. The resultant device gave a PCE of 18.0%, compared to 13.4% for the control device. Qiao et al.[89] obtained PEDOT:PSS with a non-wetting conductive surface by removal of the predominant PSS in PEDOT:PSS via simple solvent-engineering of ethylene glycol and methanol. This resulted in a perovskite with larger crystalline grains on the treated PEDOT:PSS and a significant PCE improvement from 13.23% to 18.18% at the device level, when compared to pristine PEDOT:PSS. Song et al.[93] employed a composite layer of graphene oxide (GO) and PEDOT:PSS as HTL, exhibiting a higher conductivity and better-suited work function for hole extraction from the perovskite layer, compared with simple PEDOT:PSS. The presence of GO in this HTL also increased the crystallinity of perovskite films **(Figure 2e)**, where the device PCE reached 18.09%. Subsequently, Coya et al.[90] reported that the conductivity and device stability can be further improved by evenly dispersing

graphene sheets into PEDOT:PSS; the hydrophobicity of graphene may prevent the adverse reactions caused by the hygroscopicity of PEDOT:PSS and slow down the device degradation. Zhang et al.[94] doped 3-(cyclohexylamino)-2-hydroxy-1-propanesulfonic acid (CAPSO) into PEDOT:PSS. Since the introduction of CAPSO weakened the coulombic force between PEDOT and PSS, the conductivity of the PEDOT:PSS film increased by about three orders of magnitude. Together with a better aligned energy level, an enhanced PCE of 15.7% was achieved for CAPSO-doped PEDOT:PSS based PSCs.

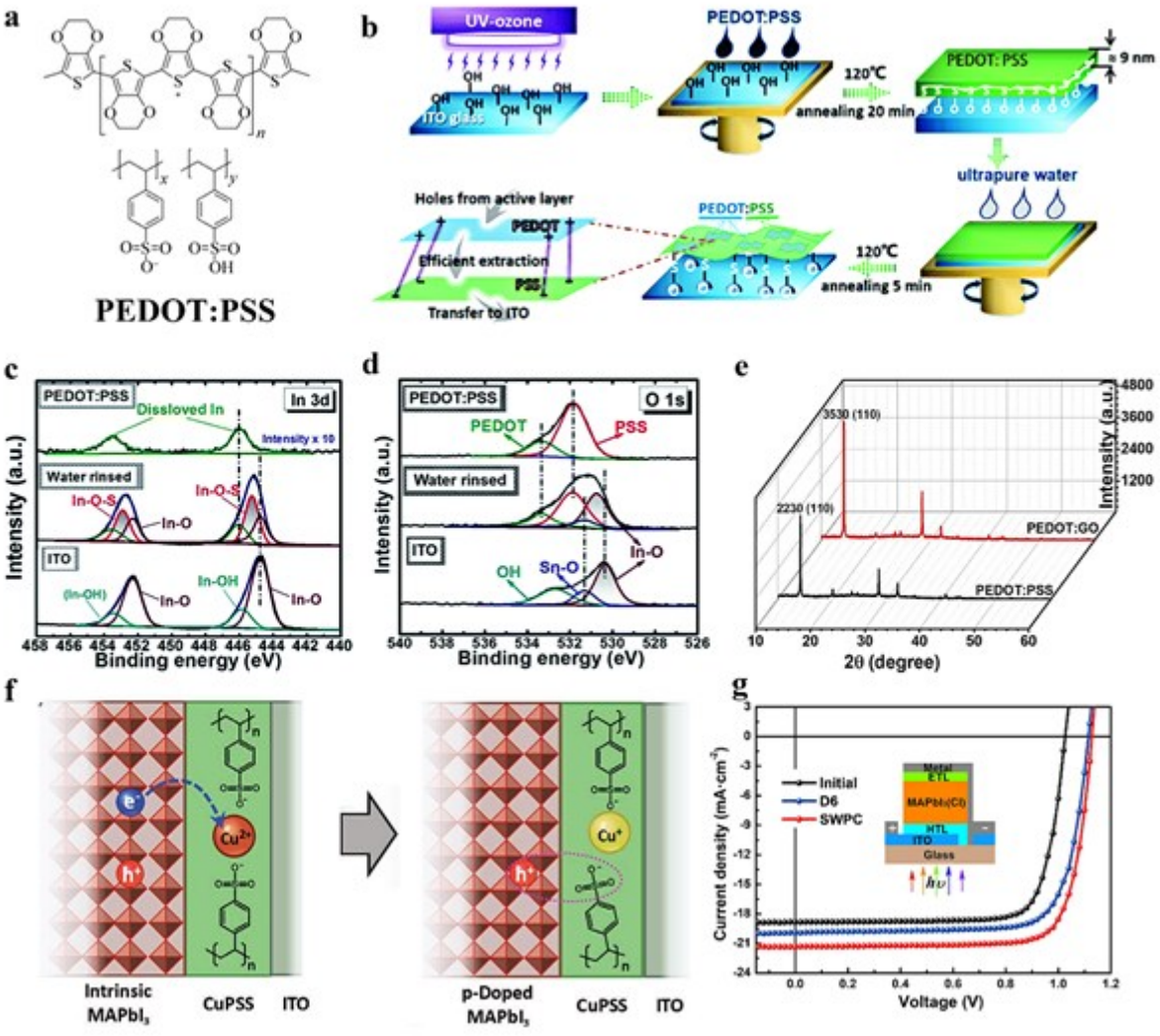

Figure 2. a) Chemical structure of PEDOT:PSS. b) Schematic diagram of the fabrication process of water rinsed PEDOT:PSS films. c, d) XPS spectra of In 3d (c) and O 1s (d) in ITO, PEDOT:PSS and water rinsed PEDOT:PSS. Copyright 2018, Royal Society of Chemistry. e) XRD result of perovskite films on PEDOT:PSS and PEDOT:GO composite films. Copyright 2018, Nature Portfolio. f) Schematic illustration showing p-type doping of Cu:PSS. Copyright 2021, Wiley. g) *J*–*V* curves of the champion devices based on different HTLs (The inset shows the device structure). Copy 2022, Elsevier.

Chemical doping is one of the most powerful methods to improve the electronic conductivity of HTLs. To this end, Song et al.[95] introduced sodium citrate, an alkaline additive, into the PEDOT:PSS solution. This doping increased the work function of PEDOT:PSS, aligning it better with the valence band maximum (VBM) of the perovskite, which is required for efficient hole extraction. It also affected the growth of perovskite, resulting in less carrier recombination. As a consequence, the PCE improved from 15.05% to 18.39% for sodium citrate-doped PEDOT:PSS based devices, compared to the reference device. Chen et al.[96] performed low-temperature annealing after doping PEDOT:PSS with copper (I) thiocyanate (CuSCN), which was found to reduce the HTL/perovskite interfacial energy barrier, thereby improving the charge extraction efficiency, as well as increasing the average size of perovskite crystals; the PEDOT:PSS-CuSCN-based device gave a PCE of 15.3%.

Walker et al.[97] introduced a p-type polyelectrolyte dopant, copper (II) poly (styrene sulfonate) (Cu:PSS). The incorporation of easily reduced Cu^{2+} can increase the work function of HTL and thus match better with VBM of the perovskite (**Figure 2f**), resulting in a higher device V_{OC}. Moreover, optimum mixtures of Cu:PSS with PEDOT:PSS was found to improve the average transmittance due to the highly transparent nature and significantly reduce recombination rates. Together with all these merits, optimized devices incorporating such mixtures delivered an impressive PCE of 19.44%. Huang et al.[98] constructed a gradient heterojunction (GHJ) using a PEDOT:PSS/PEDOT:PSS-VO_X bilayer to suppress nonradiative recombination and improve hole extraction. The PCE of the GHJ PSC was 18.0% and showed good stability with only 20% and 30% relative PCE losses after exposure to full spectrum illumination for 750 h in N_2 atmosphere and for 175 h in air, respectively. Rather than doping PEDOT:PSS, Kim et al.[99] presented a strategy to systematically de-dope PEDOT:PSS with aqueous NaOH, resulting in a raised Fermi level by up to 500 meV. Although the conductivity decreased by de-doping, the charge extraction ability could be maintained by reducing the layer thickness. A significant reduction in carrier recombination at the de-doped PEDOT:PSS/perovskite interface was achieved, leading to increased device performance. Recently, Song et al.[100] proposed a so-called self-woven deposition method to prepare a pinhole-free monolayer PEDOT:PSS mesh. Compared to traditional PEDOT:PSS, this monolayer variant exhibited negligible optical interference, a better energy level alignment and stronger hole extraction ability. Consequently, the resulting inverted PSCs incorporating this monolayer achieved enhanced PCEs of 19.49% and 21.09% for $MAPbI_3$ and $(FASnI_3)_{0.6}(MAPbI_3)_{0.4}$ (see in **Figure 2g**). Besides, relatively high operational and storage stabilities were obtained thanks to the reduction of the unpaired PSS.

2.2. Poly-TPD

Poly(*N*,*N*′-bis(4-butylphenyl)-*N*,*N*'-bis(phenyl)benzidine) (poly-TPD) is also a commonly used polymer HTL in inverted PSCs with a structure as displayed in **Figure 3a**. The HOMO and LUMO energy levels are −5.4 and −2.4 eV, respectively, and its hole mobility, tested by the space charge limited current (SCLC) technique, is around 1×10^{-4} cm^2 V^{-1} S^{-1}.[101-102] So et al.[101] adopted poly-TPD as HTL in inverted PSCs to replace PEDOT:PSS. **Figure 3b** and **3c** show how the average perovskite grain size on poly-TPD is larger than on PEDOT:PSS, which is beneficial to minimize recombination and enhance charge extraction. A maximum PCE of 15.3% was reached on poly-TPD-based devices. Tsang et al.[103] reported a facile surface modification method that can adjust the surface wettability of poly-TPD films by accurately controlling UV-ozone exposure time of the HTL without affecting the bulk properties of the poly-TPD film. As shown in **Figure 3d**, the wetting angle of UV-ozone modified poly-TPD decreases with treatment time, indicating enhanced wettability. Benefiting from a high-quality perovskite and proper energy alignment of poly-TPD, the resulting inverted PSCs showed a PCE >18% together with enhanced stability. Alternatively, Qu et al.[104] developed a solvent-additive engineering method to overcome the non-wetting issue of poly-TPD. It was found that mixing chlorobenzene (CB) and H_2O can improve the direct contact between perovskite and poly-TPD (**Figure 3e** and **3f**), resulting in high-quality perovskite layers with suppressed bulk and interfacial recombination. At the device level, this yielded an excellent PCE of 22.1% with V_{OC} of 1.15 V, J_{SC} of 24.15 mA cm^{-2} and FF of 79.5%, which is one of the highest performances of poly-TPD-based PSCs **(Figure 3g)**. Fang et al.[102] investigated the effect of molecular weight of poly-TPD as HTL on device performance. **Figure 3h** suggests that poly-TPD with a molecular weight of 75 kDa yields reduced carrier recombination and increased conductivity. The resulting PSCs delivered a champion PCE of 19.24% (V_{OC} of 1.13 V) with negligible hysteresis (see **Figure 3i**).

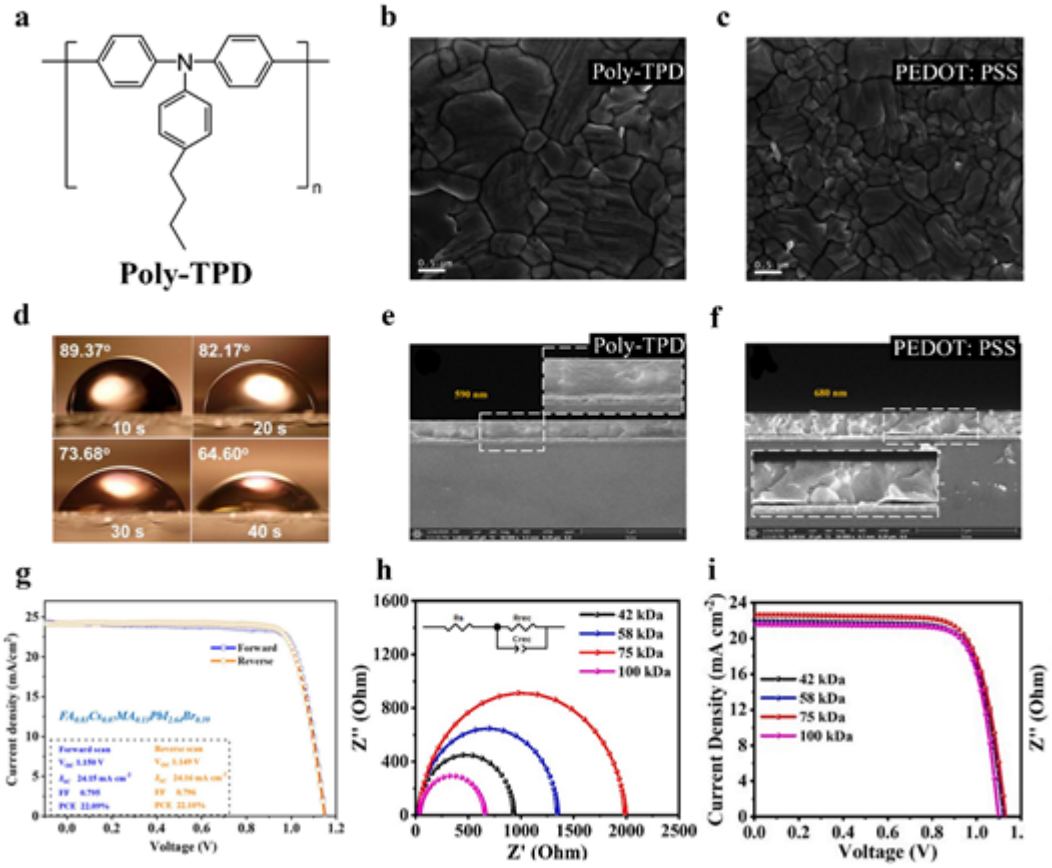

Figure 3. a) Chemical structure of poly-TPD. SEM images of perovskite film based on (b) poly-TPD and (c) PEDOT:PSS. Copyright 2015, Wiley. d) The water contact angles of UVO modified poly-TPD. Copyright 2017, Elsevier. Cross-section SEM of PSCs based on (e) poly-TPD and (f) PEDOT:PSS. g) *J*–*V* curves of $FA_{0.83}Cs_{0.07}MA_{0.13}PbI_{2.64}Br_{0.39}$-based perovskite solar cells. Copyright 2021, Wiley. h) Nyquist plots of PSCs with various PTPD Mws. i) *J*–*V* curves of the champion devices based on different HTLs. Copyright 2021, Elsevier.

2.3. PTAA

Poly(bis(4-phenyl) (2,4,6-trimethylphenyl) amine (PTAA) is the most used polymer HTL for inverted PSCs, owing to its excellent electrical properties and chemical neutrality **(Figure 4a)**. The non-planar molecular structure can provide various carrier transport channels. It shows a hole mobility of (3-6) × 10^{-4} cm^2 V^{-1} S^{-1} tested by the SCLC method with HOMO and LUMO energy levels of −5.2 and−1.8 ~ −1.7 eV, respectively.[84,105-106] The uniformly smooth films and absence of microstructural ordering after annealing reduce recombination at the HTL/perovskite interface.

Meanwhile, the high hydrophobicity is beneficial for the stability of the devices.[107-108] Despite the non-wetting surface, high-quality perovskite thin films can be prepared due to the smooth surface.[109] Miyano et al.[106] reported how PTAA improved the interface quality and carrier transport efficacy, resulting in enhanced performance of PTAA devices (18.1%), compared to PEDOT:PSS references (14.5%). De Wolf et al.[110] used DMF/NMP instead of DMF/DMSO as a co-solvent system to enhance the wettability of perovskite precursor inks on PTAA. **Figure 4b** shows that the higher binding energy of the $MAPbI_3$-NMP adduct (−0.728 eV) with PTAA can inhibit the formation of micro- and nano-scale pinholes compared with $MAPbI_3$-DMSO (−0.174 eV), thus a uniform and dense perovskite layer was obtained. In particular, the device PCE decreased only very slightly with a larger active area from 21.5% (0.1 cm^2) to 19.8% (6.8 cm^2), underlining the attractiveness of this approach for scaled deposition. Moshaii et al.[111] UV treated the PTAA layer for a short time to improve the optical properties of the PTAA layer and achieved full coverage on glass/ITO substrates. The improved perovskite crystallinity significantly promoted charge transfer and reduced recombination, leading to a PCE of 19.17%. Xing et al.[105] introduced M2, a hole conductive small molecule to modify the PTAA surface, specially designed towards good hole extraction and transport properties. With this, the wettability of PTAA film was found to improve greatly too, resulting in a substantially enhanced crystallinity of perovskite. The PCE increased from 18.67% for the PTAA control device to 20.23% for the PTAA/M2 based device.

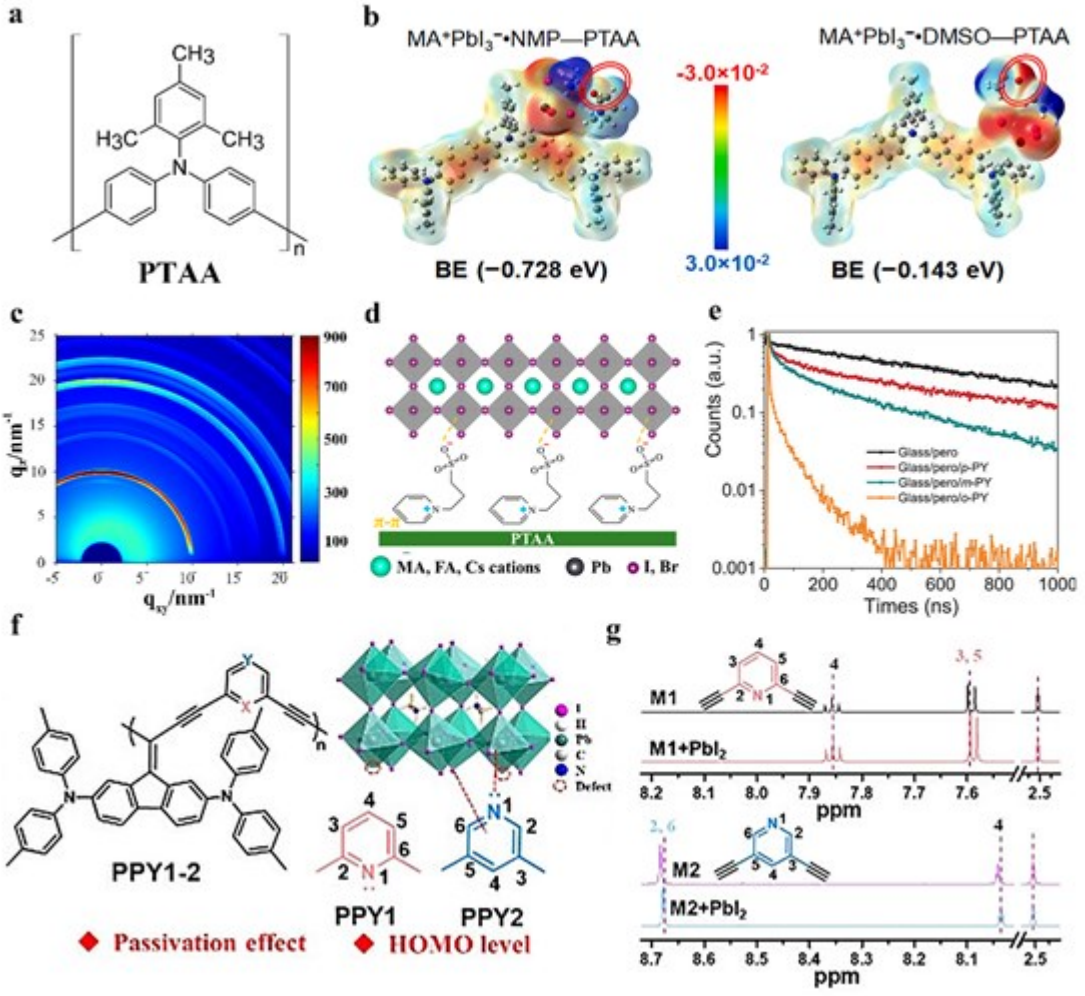

Figure 4. a) Chemical structure of PTAA. b) Electrostatic potential maps and binding energy of $MA^+PbI_3^-$ · DMF-PTAA and $MA^+PbI_3^-$ · DMSO-PTAA. Copyright 2021, Elsevier. c) 2D GIXRD image of $MAPbI_3$ on PTAA HTL with 3wt% MoO_3. Copyright 2022, Elsevier. d) Schematic diagram of the chemical bridge between the perovskites and PTAA. Copyright 2021, American Chemical Society. e) TRPL patterns for the perovskite films covered with different HTLs. Copyright 2021, Wiley. f) The molecular design idea of PPYs. g) The ^{1}H NMR pattern of pyridine-based units M1–2 with or without mixing with PbI_2. Copyright 2021, Wiley.

Despite these improvements, the large energy gap between highest occupied molecular orbital (HOMO) of PTAA and the VBM of perovskite, as well as the insufficient hole mobility within PTAA, may unavoidably increase interfacial carrier recombination, thus lowering the V_{OC} and PCE.[112-113] To address this, doping may increase the conductivity of the HTL and suppress interfacial trap-assisted recombination.[114] Gao et al.[115] introduced MoO_3 as a dopant to modify PTAA. Ultraviolet

photoelectron spectroscopy (UPS) indicated that the HOMO level of PTAA doped by 3wt% MoO_3 downshifted by 0.16 eV, bringing it close to the VBM of perovskite. Simultaneously, the hole mobility and extraction ability were enhanced. The grazing incident X-ray diffraction (GIXRD) 2D pattern in **Figure 4c** confirms formation of high quality polycrystalline $MAPbI_3$ films. Eventually, *p-i-n* PSCs using 3wt% MoO_3-doped PTAA achieved a PCE of 20.06%, compared to 17.71% when using pristine PTAA as HTL. Bao et al.[116] employed PTAA doped with black phosphorus (BP) nanosheets as HTL in *p-i-n* PSCs. Compared with the control device, the BP:PTAA layer significantly improved hole extraction and mobility, thus reducing the interfacial carrier recombination. The champion device gave a PCE of 20.49% with enhanced stability and a remarkably high FF of 83%. Likely this can be attributed in part also to the hydrophobicity induced by BP, resulting in a high-quality perovskite film. Chen et al.[117] synthesized a novel conjugated carbazole-based molecule as a dopant for PTAA, named 9-(diphenyl-phosphanyl)-3-(1,2,2-triphenylvinyl)-9*H*-carbazole (TCzP), which displays a high hole mobility and optimal energy levels for hole extraction from the perovskite. High quality perovskite films were obtained on TCzP-doped PTAA HTLs, which further helped to improve hole extraction at the interface, yielding a PCE of 18.3%. Wang et al.[118] introduced *N,N*'-bis(naphthalen-1-yl)-*N,N*'+-bis(phenyl)benzidine (NPB) as a dopant into PTAA, which again improved the crystal quality of perovskite and optimized the HTL/perovskite interface. In addition, the HOMO level of NPB-doped PTAA was better aligned with the VBM of perovskite resulting in effective hole extraction, and the doped HTLs also showed improved transport properties. As a result, a high PCE of 20.15% was observed. Zhang et al.[119] established a chemical bridge at the PTAA/perovskite interface by using 3-(1-pyridinio)-1-propanesulfonate (PPS) molecules to minimize interfacial recombination of charge carriers, as illustrated in **Figure 4d**. The pyridine unit in PSS was chemically coupled with PTAA phenyl by π-π stacking, and the sulfonate at the other end of the PSS anchored to the perovskite by the strong S-O-Pb coordination bond, thereby improving the HTL/perovskite interfacial properties, resulting in an impressive PCE up to 21.7% with V_{OC} of 1.16 V, J_{SC} of 22.9 mA cm^{-2} and FF of 81.2%.

Song et al.[120] textured PTAA by washing the film prepared from a mixed solution of PTAA and polystyrene (PS) to inhibit internal optical reflection. Compared with the reference device, the J_{SC} increased substantially in magnitude by about 10% without sacrificing another parameter. The PCE was further improved to 21.6% with a remarkable FF of 84% by adding a MgF_2 antireflection coating (ARC) at the outer surface of the glass substrate. The composite use of two kinds of HTLs is also a strategy to enhance targeted properties desired from a HTL.[121] Venkataraman et al.[122] employed a PTAA/CuI bilayer as HTL, which facilitated the growth of larger perovskite grains and increased the built-in potential of the device. The maximum PCE of the PTAA/CuI bilayer device was 20.34%.

Kymakis et al.[123] presented ultra-thin azulene derivatives covered by PTAA as HTL. This thin bilayer resulted in a favorable energy level alignment while reducing parasitic absorption of the HTL and series resistance in the device, yielding a PCE of 18.48% with longer device lifetime. Lately, Zhu et al.[124] reported a molecular engineering strategy on the PTAA structure by removing alkyl groups and attaching multifunctional pyridine units. The introduced pyridine units not only downshifted the HOMO level and enhanced the surface wettability, but also endowed the HTL with a passivation ability and higher hole extraction capacity, which was verified by time-resolved photoluminescence (TRPL) spectra in **Figure 4e**. The device with optimal para-position linking-site HTL delivered a PCE >22% for 0.09 cm^2 and >20% for 1 cm^2 sized PSCs. The relationship between the polymer and PV performance is given in **Table 1**.

2.4. Other Polymer HTLs

In addition to the typical polymer HTLs mentioned above, researchers also synthesized various polymers as HTLs for application in *p-i-n* PSCs. Some of them can achieve impressive PCEs with good stability and low material cost. Zhu et al.[125] reported a novel pyridine-based polymer (PPY2) HTL which is copolymerized 3,5-diethynylpyridine with a diphenylamine-substituted-fluorene unit (Figure 4f). ^{1}H NMR measurements suggest an enhanced lead coordination ability for M2 due to reduced steric hindrance as shown in Figure 4g. Together with suitable energy levels, a high hole mobility and effective passivation of the defects, the resulting *p-i-n* PSCs delivered an encouraging PCE up to 22.41% with superior long-term photostability, outperforming PTAA based control devices (20.98%). Guo et al.[126] employed a commercially available polymer poly[3-(4-carboxybutyl)thiophene-2,5-diyl] (P3CT) as HTL. The carboxyl groups in the side chain of P3CT can not only anchor onto the ITO surface to tune its work function, but also passivate the defects of the overlying perovskite interface. This resulted in uniform perovskite films with better quality; consequently, the champion device reached a PCE of 21.33% with V_{OC} of 1.12 V, J_{SC} of 22.78 mA cm^{-2} and FF of 83.6%. Their group and Wu et al.[127] reported that the PCE for devices based on Na and Rb doped P3CT as HTL was slightly lower than that of P3CT based devices, which was 19.08% and 20.52%, respectively. Xu et al. designed conjugated polyelectrolyte based on a copolymer of benzene and thiophene unit and incorporated K^+ ions into the copolymer to create an HTL. Thanks to the superior defect passivation and hole extraction ability, the inverted PSC device exhibited a PCE of 20.01% and enhanced long-term stability.[128] Recently, Fang et al. developed a surface sulfidation treatment (SST) to construct stable heterojunctions for *p-i-n* PSCs. The formed strong Pb-S bonds upshifted the Femi level and

induced an back-surface field through band bending, aiding in minimizing interface recombination and charge extraction. The resulting *p-i-n* PSCs incorporating P3CT-Na as HTL exhibited a PCE >24%, one of the highest values for *p-i-n* PSCs to date.[129] Saidaminov et al.[130] demonstrated a strategy of doping Cl into polyaniline (PAN) to endow the HTL with surface coordination ability, thereby improving the quality of perovskite thin films. Meanwhile, the nonradiative recombination at the interface was reduced due to passivation of defects, resulting in a PCE of 20.7% for *p-i-n* PSCs. Jen et al.[131] synthesized two novel cross-conjugated isopentanes, PPE1 and PPE2, by connecting 2,7-diphenylamine-terminated fluorene units to ethylene methylene as side chains. Both PPEs possess proper energy levels, moderate hole mobilities and a good surface wettability. PPE2 based devices displayed an impressive PCE of 21.3% owing to the resulting high-quality perovskite thin films with good surface passivation.

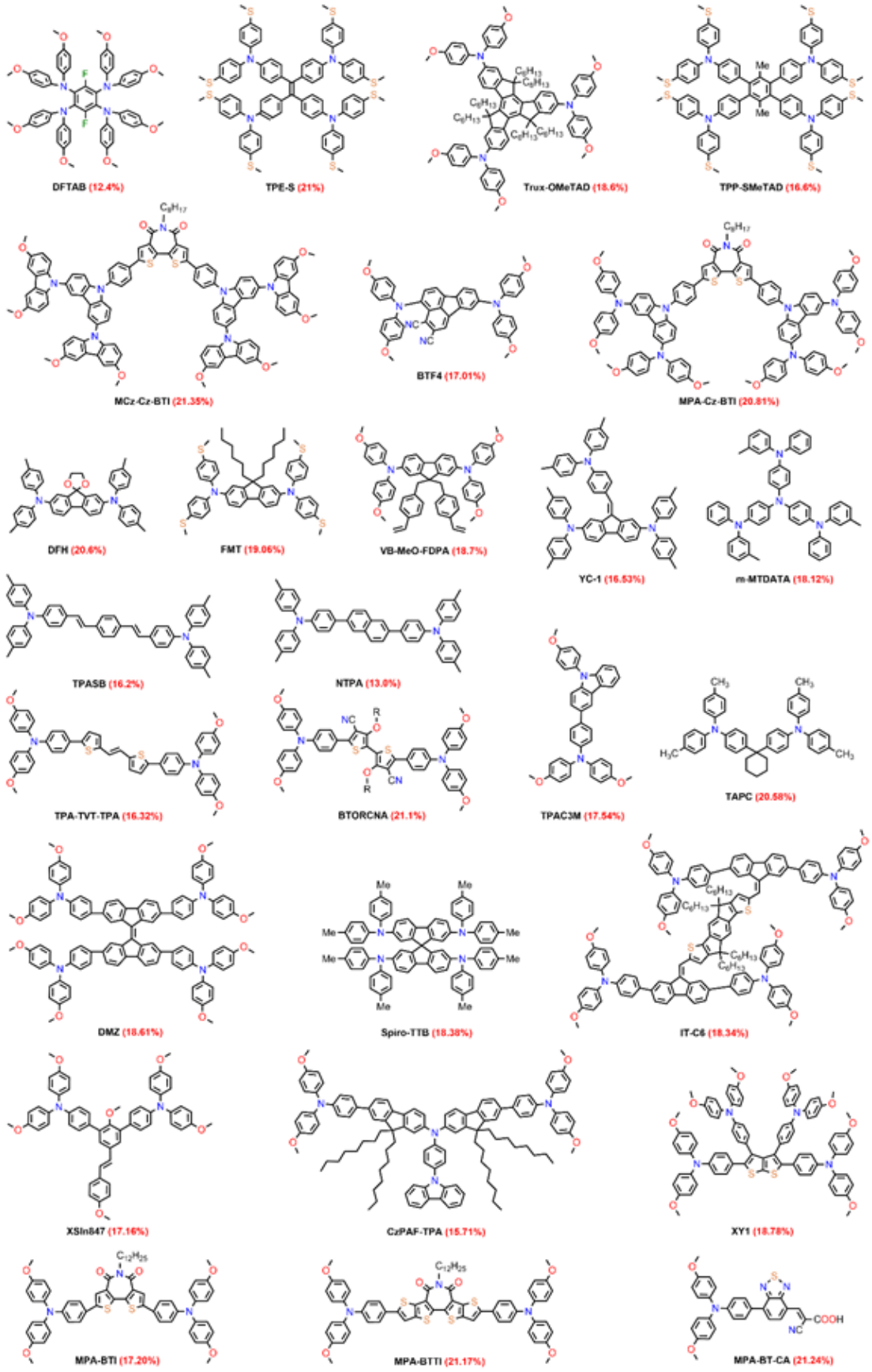

Figure 5. Small molecular structure of diarylamines and triarylamines as discussed in this paper.

Note: a. A:B denotes that B doped into A; b.The parameters in the table are the self tested

ructure of PSCs based on distinct polymer HTLs.

Device structure	V_{OC}/V	J_{SC}/(mA/cm^2)	FF/%	PCE/%	Ref.
ITO/PEDOT:PSS/MAPbI$_3$/PCBM/Al	0.8	10.32	63	5.2	[86]
ITO/PEDOT:PSS/MAPbI$_3$/PCBM/Ag	1.04	22.41	72	16.16	[87]
ITO/PEDOT:PSS/MAPbI$_3$/PCBM/Ag	1.02	22.30	67	15.72	[71]
ITO/PEDOT:PSS/PEDOT:TOS/MAPbI$_{3-x}$(BF$_4$)$_x$/PCBM/Al	1.02	21.33	82.3	18.09	[75]
ITO/PEDOT:PSS/MAPbI$_{3-x}$(BF$_4$)$_x$/PCBM/Ag	0.960	20.43	80.1	13.17	[74]
ITO/SnO$_2$/PEDOT:PSS/MAPbI$_{3-x}$(BF$_4$)$_x$/PCBM/BCP/Ag	1.134	21.016	79.01	18.39	[75]
ITO/PEDOT:PSS/MAPbI$_3$/PCBM/C$_{60}$/LiF/Al	1.02	19.1	78.3	15.3	[76]
ITO/Au:PSS@PEDOT:PSS/MAPbI$_3$/PC$_{61}$BM/Al	1	23.37	81	19.44	[77]
ITO/PEDOT:PSS/PEDOT:PSS-VO$_x$/MAPbI$_3$/PCBM/C$_{60}$/LiF/Al	1.02	22.36	77	16	[78]
ITO/PEDOT:PSS/MAPbI$_3$/C$_{60}$/BCP/Ag	1.13	21.03	76.34	13.49	[100]
ITO/PTB7-TH/MAPbI$_3$/PCBM/C$_{60}$/BCP/Ag	1.1	22	69.7	13.3	[101]
ITO/PTB7-TH/MAPbI$_3$/C$_{60}$/BCP/Ag	1.04	23.2	73.4	18.19	[102]
ITO/PTB7-TH:F4-TCNQ/MAPbI$_3$/PCBM/BCP/Cu	1.13	24.13	73.3	22.09	[104]
ITO/PTB7-TH/MAPbI$_3$/PCBM/BPhen/Al	1.051	23.33	77.1	20.01	
ITO/PTB7-TH:F4-TCNQ/MAPbI$_3$/PCBM/BPhen/Al	1.129	22.1	73.2	17.44	[104]
ITO/PTAA/MAPbI$_3$:KCl/PCBM/ALD/Ag	1.09	21.01	73	16.07	[105]
ITO/PTAA/Cs$_{0.05}$[MA$_{0.17}$FA$_{0.83}$]$_{0.95}$Pb(I$_{0.83}$Br$_{0.17}$)$_3$/PC$_{61}$BM/BCP/Ag	1.06	22.14	76	17.17	[111]
ITO/PTAA/MAPbI$_3$/Cs$_{0.05}$[MA$_{0.17}$FA$_{0.83}$]$_{0.95}$Pb(I$_{0.83}$Br$_{0.17}$)$_3$/PCBM/Cu	1.14	22.37	77.4	20.22	[112]
ITO/PTAA:WO$_3$/MAPbI$_3$/PC$_{61}$BM/BCP/Au	1.14	22.13	77.43	20.05	[113]
ITO/PTAA:BF/MAPbI$_3$/PC$_{61}$BM/BCP/Ag	1.105	22.43	82.0	20.49	[110]
ITO/PTAA:IL4F/MAPbI$_3$/PC$_{61}$BM/C$_{60}$/LiF/Al	1.1	21.12	79	18.3	[114]
ITO/PTAA:NPB/MAPbI$_3$/PC$_{61}$BM/Ag	1.14	22.0	78.4	20.12	[115]
ITO/PTAA/PCBM/MAPbI$_{3-x}$Cl$_x$/PC$_{61}$BM/BCP/Ag	1.10	23	81.2	21.1	[117]
ITO/PTAA/MAPbI$_3$(Cl)/PC$_{61}$BM/BCP/Ag	1.136	22.3	83.3	20.6	[120]
ITO/PTAA/CuI/Cs$_{0.05}$FA$_{0.95}$PbI$_3$/PCBM/C$_{60}$/Al	1.03	24.6	77.4	20.34	[122]
ITO/SnO$_2$/PTAA/Cs$_{0.05}$FA$_{0.85}$PbI$_{0.9}$Br$_{0.1}$/PCBM/BCP/Ag	1.11	21.07	73.88	16.46	[123]
ITO/PTAA/Cs$_{0.05}$[FA$_{0.9}$MA$_{0.1}$]$_{0.95}$Pb(I$_{0.9}$Br$_{0.1}$)$_3$/C$_{60}$/BCP/Ag	1.134	23.33	81.39	22.39	[124]
ITO/PTAA/[FA$_{0.92}$MA$_{0.08}$]$_{0.9}$Cs$_{0.1}$PbI$_{0.92}$Br$_{0.08}$]$_3$/C$_{60}$/BCP/Ag	1.10	23.30	84	22.41	[125]
ITO/PTAA/[FA$_{0.17}$MA$_{0.94}$PbI$_{3.11}$]$_{0.95}$[PbI$_2$]$_{0.05}$/C$_{60}$/ZrAcAc/Ag	1.14	22.10	83.0	21.33	[126]
ITO/PTAA-Me/[FA$_{0.17}$MA$_{0.94}$PbI$_{3.11}$]$_{0.95}$[PbI$_2$]$_{0.05}$/C$_{60}$/ZrAcAc/Ag	1.09	21.05	81.0	19.06	
ITO/PTAA-KD/MAPbI$_3$-xClx/C$_{60}$/BCP/Ag	1.144	21.07	82.78	20.32	[127]
FTO/CL-PAAN/Cs$_{0.05}$FA$_{0.9}$MA$_{0.05}$PbI$_{2.55}$Br$_{0.45}$/PCBM/C$_{60}$/BCP/Ag	1.11	22.3	78.0	20.1	[130]
ITO/PTAA/[FA$_{0.83}$MA$_{0.17}$]$_3$Pb(I$_{0.85}$Br$_{0.15}$)$_3$/PCBM/BCP/Ag	1.19	22.03	80	21.39	[131]
ITO/ITO$_2$/FA$_{0.85}$MA$_{0.15}$Pb(I$_{0.85}$Br$_{0.15}$)$_3$/PCBM/CBD/BCP/Ag	1.1	22.72	80.01	20.01	[128]

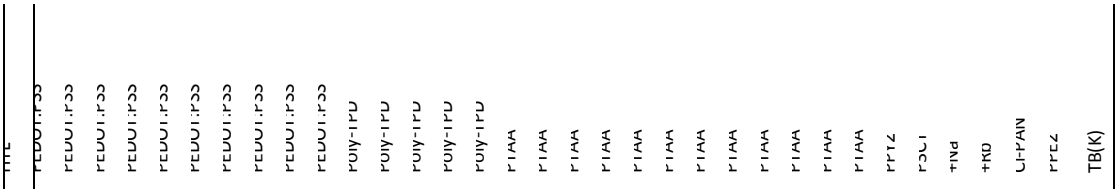

3. Small molecules

Although quite high PCEs have been obtained for inverted PSCs with polymers as HTLs, small molecule HTLs (SM-HTLs) have advantages in terms of well-defined molecular weights and structures,[132-135] adjustable photophysical properties, promising yields, high purity and small inter-batch differences.[136] Some molecular design strategies have been proposed, such as counterion, donor-acceptor (D-A) alternation, extended π-π conjugation, among others. In terms of their structure, SM-HTLs applied in *p-i-n* PSC can be divided into those with diphenylamine (DPA), triphenylamine (TPA) and the ones without DPA and TPA units **(Figure 5).**

3.1. Diarylamine

Bis(4-methoxyphenyl) amine can transfer positive charge effectively and is considered to be a hole transport group to improve charge mobility at the molecular level.[137-138] Eid et al.[139] reported two kinds of SM-HTLs consisting of tetrakis(*N,N*-bis(4-methoxyphenyl)aniline) attached on two different rigid middle cores, namely, DFTAB and TAE. Compared to TAE and PEDOT:PSS, DFTAB showed a better aligned HOMO level with the VBM of the perovskite, obtaining 12.4% of PCE when integrated into *p-i-n* PSCs. Yip et al.[140] synthesized a new small molecule HTL (TPE-S) based on tetraphenylethylene (TPE) core and four MeS-modified arms **(Figure 6a)**. XPS analysis, as shown in **Figure 6b** and **6c** showed that the Pb 4f peak shifted to a lower binding energy, and the N 1s and S 2p peaks of TPE-S moved to a higher binding energy compared with the reference sample, which implies that the lone electron pairs on N atoms can interact with Pb^{2+} to form strong Pb-S and S-I interactions. The coordination bond of S-Pb^{2+} can effectively passivate defects in perovskites, restraining unwanted carrier recombination. XRD and SEM results demonstrated that TPE-S can adjust the crystallinity of the perovskite, resulting in the formation of dense and high-quality perovskite film, significantly suppressing light-induced phase segregation in the perovskite and enhancing the photostability of the device. $CsPbI_2Br$ and $FA_{0.9}Cs_{0.1}PbI_3$ based devices incorporating

TPE-S as HTL displayed remarkable PCEs of 15.4% and 21.0% with improved stability, compared to PEDOT:PSS based PSCs.

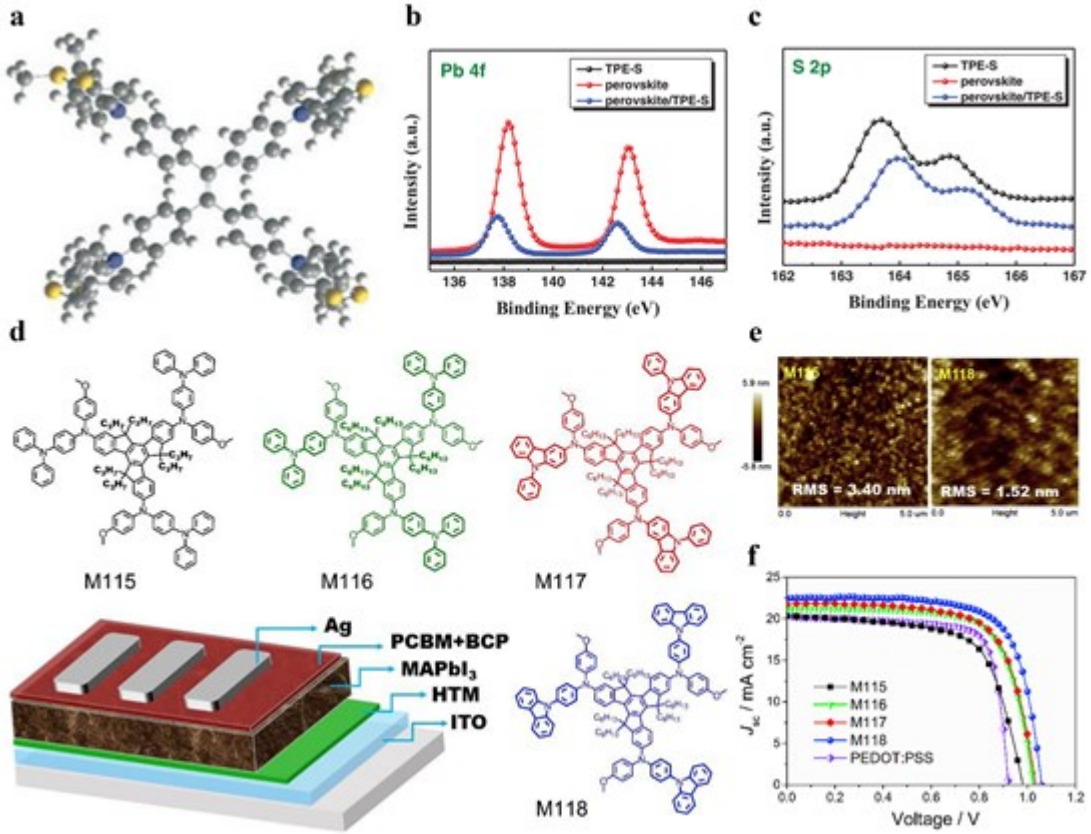

Figure 6. a) Molecular structure of TPE-S. b, c) XPS spectra of Pb 4f (c) and S 2p (d), in TPE-S, perovskite and bilayered perovskite/TPE-S films, respectively. Copyright 2020, Wiley. d) Chemical structure of M115-118 and structure diagram of inverted PSC. e) AFM topography images of perovskite based on M115 and M118. f) *J*–*V* curves of the PSCs for M115-M118 as HTLs. Copyright 2019, Elsevier.

Truxene core, 10,15-dihydro-5*H*-diindeno[1,2-*a*;1',2'-*c*]fluorine, exists in a planar heptacyclic structure. This highly planar, rigid, and completely conjugated moiety displays a C_{3h} symmetry structure, which enables a high hole mobility. It was initially adopted to construct HTLs for *n-i-p* PSCs, giving promising device performance.[141-142] Later on, it was modified to develop HTLs for inverted PSCs. Chen et al.[143] designed and synthesized a new HTL that promoted good contact

between perovskite and the anode below, Trux-OMeTAD, which consists of a truxene core with arylamine terminals and hexyl side chains. Photoluminescence (PL) spectra and TRPL showed that HTLs annealed at 150 °C can enhance the fluorescence quenching of perovskites compared with HTLs without annealing, which is consistent with the improved hole extraction and transport properties observed in such annealed HTLs. Together with a high mobility of 3.60×10^{-3} $cm^2 V^{-1}s^{-1}$, *p-i-n* PSCs resulted in a PCE of 18.6%. Subsequently, the same group replaced truxene with tetraphenyl (1,4-dimethyl-2,3,5,6-tetraphenylbenzene) as the core and prepared two HTLs with different terminal substituents, one with methoxy (TPP-OMeTAD) and the other with a methyl-sulfanyl group (TPP-SMeTAD).[144] Time-of-flight secondary-ion mass spectrometry (TOF-SIMS) showed the presence of the molecules in the perovskite and the formation of a HTL/perovskite heterojunction. This heterojunction can help to minimize recombination and provide efficient hole extraction and transport, thus improving device performance. PL and TRPL measurements exhibited a slightly higher quenching efficiency for TPP-SMeTAD derived from stronger interaction between S atom and Pb^{2+} ion and a better aligned energy level with the perovskite, thereby yielding devices with a PCE of 16.6%. Liang et al.[145] also designed and synthesized four new types of HTLs (M115-118) with truxene as a core and surrounded by cyclic aromatic amines (MDPDA, MPCA and CPMA) **(Figure 6d)**. They systematically studied the effects of the length of alkyl and peripheral aromatic amines on their optoelectronic properties. The introduction of hexyl chains on the conjugated skeleton is beneficial for hole transport, evidenced by a high hole mobility of 1.75×10^{-3} $cm^2 V^{-1} s^{-1}$ as obtained for M118. Meanwhile, atomic force microscopy (AFM) measurements, as shown in **Figure 6e**, indicate that the surface roughness of M118 is lower than that of M115-117, suggesting that the hexyl chain on the conjugated skeleton can provide better solubility and film-forming properties. With a high quality perovskite film and high mobility, the *J-V* curves in **Figure 6f** show that the best PCE of the M118 based device reached 17.1%. In terms of molecular engineering, constructing a D-A alternating structure is thought to be desirable for HTLs in inverted PSCs, as in such case the energy level and mobility can be tuned by appropriate selection of donor and acceptor units. Besides, the intramolecular charge transfer (ICT) and high dipole moment can induce a built-in potential to further boost charge extraction. Li et al.[146] synthesized 2,3-dicyano-fluoranthene as the electron-withdrawing unit and diarylamine as electron donor unit to construct D-A type HTLs. The stacking mode of BTF3-4 based on single crystal X-ray analysis is shown in **Figure 7a**. The molecules showed appropriate energy levels with the perovskite and strong molecular accumulation, especially for the quasi-three-dimensional herringbone assembly formed by BTF4, which promotes hole extraction and transport. Conventional and inverted PSCs using BTF4 as HTL achieved PCEs of 18.03% and 17.01%,

respectively. He et al.[147] developed a series of D-A type dendritic HTL using BTI as the core, and diphenylamine (PA) and carbazole (Cz) units as peripheral unit. **Figure 7b** illustrates how their HOMO levels gradually downshifted with increasing number of carbazole units in the branch, and the hole mobility decreased slightly. Photothermal deflection spectroscopy (PDS) experiment showed that the perovskite films on MPA-Cz-BTI and MCz-Cz-BTI possessed a high electronic order, which may reduce nonradiative recombination. Together with a significantly suppressed density of interface trap states, inverted devices based on MPA-Cz-BTI and MCz-Cz-BTI obtained good PCEs of 20.8% and 21.35% with ultrahigh FFs of 85.2% and 83.5%, as shown in **Figure 7c-e**, respectively.

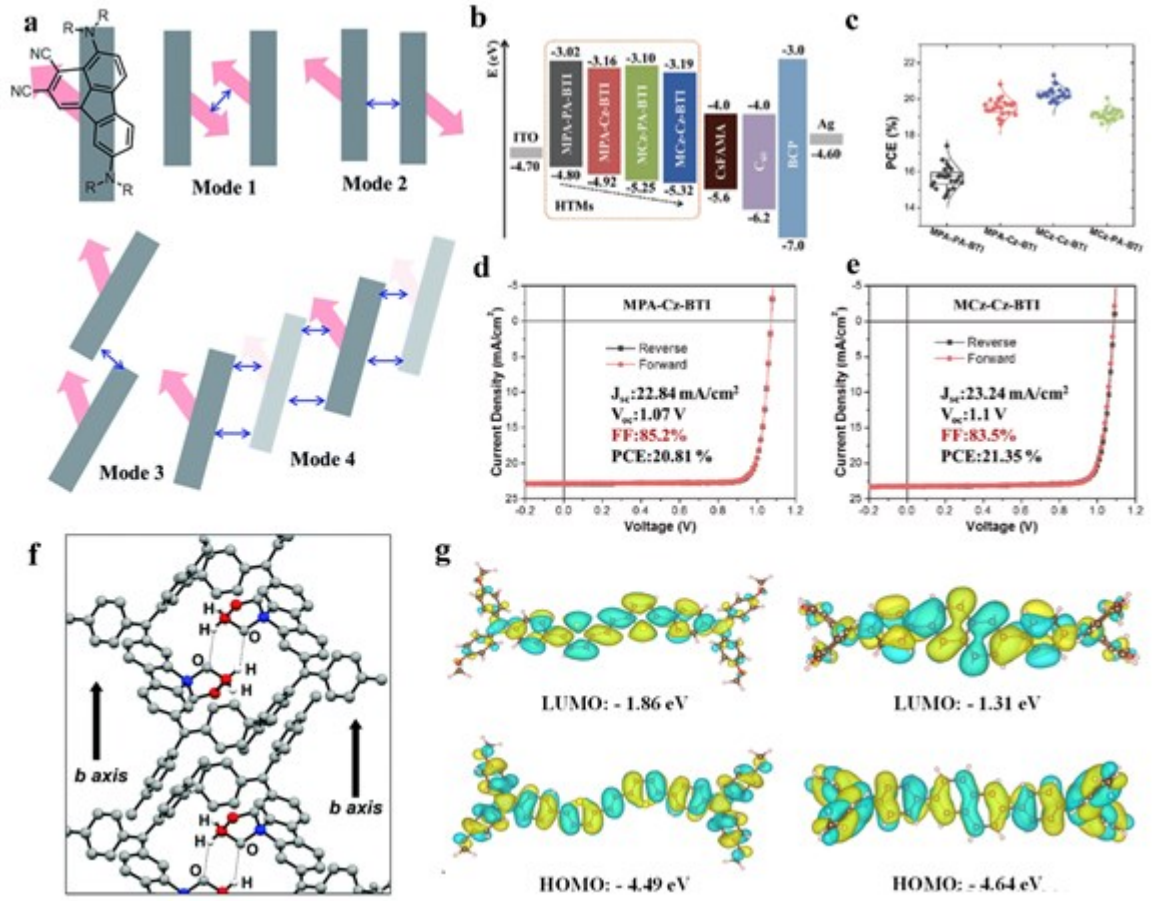

Figure 7. a) Schematic diagram of π-stacking mode of BTF3-4 based on single crystal X-ray analysis. Copyright 2018, Royal Society of Chemistry. b) Energy level alignments of different components in PSCs. c) Statistics of the PCE values for the PSCs with different HTLs. *J–V* curves for the optimal PSCs with (d) MPA-Cz-BTI and (e) MPA-Cz-BTI HTLs. Copyright 2021, Springer Link. f) The ball-and-stick model presents the tendency of CH-O interaction between DFH molecules. Copyright 2019, Royal Society of Chemistry. g) The electron density of HOMO and LUMO of TPA-TVT-TPA and TPA-NAP-TPA, respectively. Copyright 2017, Wiley.

Fluorene is also a popular core unit to construct HTLs in PSCs. Berlinguette et al.[148] designed a new HTL N^2,N^2,N^7,N^7-tetra-ptolylspiro[fluorene-9,2'-[1,3]dioxolane]-2,7-diamine (DFH) via simple reaction of inexpensive reagents and a facile purification process. **Figure 7f** shows the C-H-O and C-H-π interaction between adjacent DFH molecules parallel to the b-axis. The strong intermolecular interaction enabled a high intrinsic hole mobility (1.00×10^{-3} $cm^2 V^{-1} s^{-1}$). The annealed film also accommodated growth of large perovskite crystalline domains. The resultant *p-i-n* PSCs yielded a PCE > 20%. Li et al.[149] designed and synthesized a linear HTL comprising 9,9-dihexyl-9*H*-fluorene core and *N, N*-di-p-methylthiophenylamine terminal (denoted as FMT). The molecule was synthesized straightforwardly from commercial monomers in two steps. The FMT film was nearly transparent to the visible light and possessed desired thermal stability. The methylthio group on the para-position of diphenylamine was beneficial to lowering HOMO level to match the VBM of perovskite. Under the best conditions, the FMT-based device attained a PCE as high as 19.06%, superior to 13.9% of the PEDOT:PSS based control device. Shao et al.[150] synthesized a series of diphenylamine derivatives with different substituents that can be thermally crosslinked. Specifically, VB-MeO-FDPA with aromatic side chain and methoxy substitution presented better energy alignment with the perovskite layer and higher conductivity, which facilitated the charge extraction and transfer from perovskite to the anode. A remarkable PCE of 18.7% was obtained with negligible hysteresis.

3.2. Triarylamine

Triarylamine has been widely used as a HTL in OLEDs because of its excellent hole transport properties, morphological and thermal stability[151]. The pseudo-3D conjugated architecture of triphenylamine endows the resultant molecule with isotropic charge transport. Fu et al.[152] explored a small molecule, 4,4',4''-tris(*N*-3-methylphenyl-*N*-phenylamino) triphenylamine (*m*-MTDATA). The conductivity and hole mobility increased to 1.8×10^{-2} $mS\,cm^{-1}$ and 4.4×10^{-1} $cm^2 V^{-1} s^{-1}$ upon thermal annealing at 150 °C. Together with favorable energy level, the PCE of *p-i-n* PSCs based on *m*-MTDATA significantly boosted to 18.12% with minimal initial performance loss over 1000 hours, compared to 13.44% for PEDOT:PSS based control devices. Chen et al.[153] studied the effects of various amounts of methoxy groups on the photoelectric properties of triphenylamine dibenzofulvene derivatives connected by SP^2-hybridized carbon atoms. The device based on YC-1 without methoxy group as HTL displayed a highest PCE of 16.53%. Subsequently, they used YC-1 as interface modification layer between NiO_X and perovskite to passivate the surface defects of NiO_X. The existence of YC-1 can

enlarge the grain size of perovskites and reduce the number of grain boundary defects, both of which improve charge extraction. Compared with traditional NiO_X HTLs (17.16%), the PCE of the optimized champion device boosted to 19.37%. McCulloch et al.[154] presented two small molecules, which respectively taken biphenyl (BTPA) and naphthalene (NTPA) as the core and two *N*,*N*-bis(4-methoxyphenyl)aniline groups as the flank. The hole mobility of NITP and BTPA after thermal annealing was 1.10×10^{-3} $cm^2 V^{-1} s^{-1}$ and 4.70×10^{-4} $cm^2 V^{-1} s^{-1}$, respectively. The perovskite layer based on NTPA and BTPA showed a higher peak strength compared with PEDOT:PSS as verified by XRD, indicating a larger crystal domain. The PCE of inverted PSCs based on these two HTLs was 13% and 12.1%, respectively. Sonar et al.[155] designed and synthesized molecules TPA-TVT-TPA and TPA-NAP-TPA with triphenylamine methoxy as end-capping groups, and thienylvinylenethienyl (TVT) and naphthalene (NAP) as cores, respectively. **Figure 7g** shows the electron distribution and the estimated energy level. TPA-TVT-TPA shows a wider absorption band and smoother surface of the device, which may be related to the larger conjugated backbone of TPA-TVT-TPA. The PCE of these HTLs based devices was 16.32% for TPA-TVT-TPA and 14.63% for TPA-NAP-TPA, respectively. Xu et al.[156] employed two novel small molecule HTLs with linear π-conjugated structure, 4,4'-bis(4-(di-*p*-toyl)aminostyryl)biphenyl (TPASBP) and 1,4'-bis(4-(di-*p*-toyl)aminostyryl)benzene (TPASB) as HTLs in *p-i-n* PSCs. The perovskite ($MAPbI_3$) films formed on both films showed larger grains and less grain boundaries than standard PEDOT:PSS HTL. TPASB presented a slightly higher hole mobility of 1.65×10^{-3} $cm^2 V^{-1} s^{-1}$ and the PCE based on TPASB reached 17.6%. Guo et al.[157] reported two novel SM-HTLs, BTORA and BTORCNA, which featured an intramolecular S-O interaction-embedded simple structure consisting of a bithiophene-bridged two triphenylamine segments. Compared with the control HTL without intramolecular noncovalent interactions, both BTORA and BTORCNA showed a better suited energy level, enhanced thermal stability and defect-passivation effect. **Figure 8a** presents the stacking direction of BTORCNA molecules in pure films. Single crystal analysis revealed that the short S-O distance (2.92 Å) confirmed the intramolecular interactions, leading to highly planar backbone and compact intermolecular stacking. Further attachment of electron-withdrawing CN groups in BTORCN provided more favorable surface properties and energy level arrangement, so that PCE of BTORCNA based devices significantly increased to 21.1% with a V_{OC} of 1.10 V, J_{SC} of 22.84 mA cm^{-2} and FF of 84% (**Figure 8c**). Moreover, it showed excellent long-term stability with negligible efficiency loss of BTORCNA-based devices after one month of storage.

Park et al.[158] synthesized three triarylamine derivatives as HTLs (TPAC0M, TPAC2M and TPAC3M), which shared the same conjugation skeleton of triarylamine derivatives backbone and contained different numbers and positions of methoxy groups. The number of methoxy units did not cause

noticeable changes in the optical properties and electrical conductance, but the charge extraction and recombination behavior were improved with increasing attached methoxy units. XPS and TRPL characterization revealed that the methoxy units could passivate defect sites at the HTL/perovskite interface, thus reducing recombination losses and improving hole extraction. Consequently, an increase in PCE up to 17.54% was attained. Wang et al.[159] introduced small molecule 4,4'-cyclohexylidenebis[*N,N*-bis(4-methylphenyl)benzenamine] (TAPC) as HTL for inverted PSCs. Because of the conjugated structure and partial crystallization of TAPC, a high conductivity of 1.19×10^{-2} mS cm^{-1} and mobility of 1.11×10^{-2} $cm^2 V^{-1} s^{-1}$ can be achieved by optimized thermal annealing at 120 °C. Moreover, the smooth, uniform and hydrophobic TAPC film was beneficial to obtain a larger perovskite grain size with less unreacted PbI_2, resulting in reducing recombination losses in the device. By using TAPC as the HTL, the best device achieved a PCE of 18.80%. In *p-i-n* PSCs, thick HTLs may cause large charge transport resistance and transit time as well as parasitic absorption.[92] Cheng et al.[160] reported a monomolecular layers (ML) strategy for three widely investigated HTLs (TAPC, PEDOT:PSS, PTAA) by solvent washing of pristine HTLs (p-HTLs) layer. **Figure 8d** and **8e** displays that contact angle of perovskite on ML-HTLs was much smaller than that on p-HTLs, favoring a high coverage and uniform perovskite layer. Moreover, it was found the ML-HTL generally raised the effective work function of ITO towards a better energy level alignment by the formation of interface dipoles. Ultimately, a substantially improved FF of 81.86% and a champion PCE of 20.58% were achieved with ML-TAPC based device.

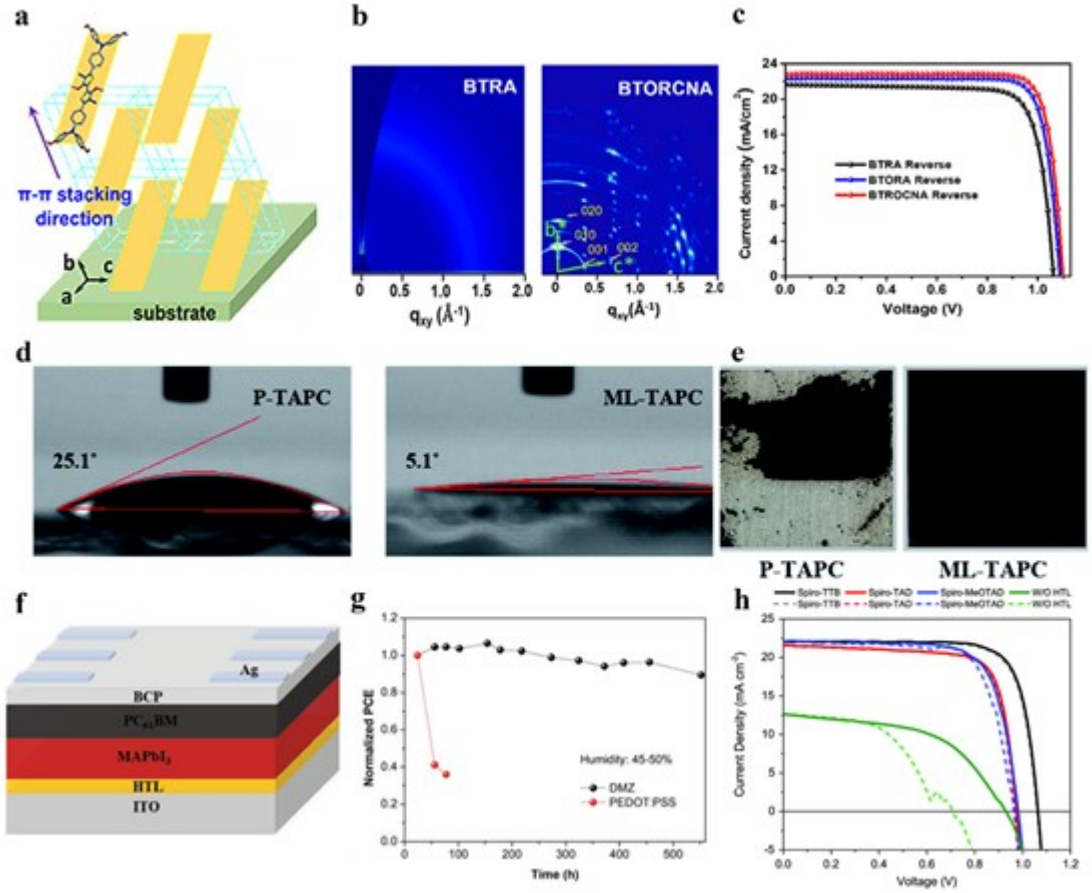

Figure 8. a) The stacking orientation of BTORCNA molecules in the film. b) 2D GIWAXS pattern of BTRA and BTORCNA film. c) The best *J*–*V* characteristics curves of the devices with different HTLs. Copyright 2022, Wiley. d) Contact angle of perovskite precursor on p-TAPC and ML-TAPC. e) The appearance of perovskite films on HTLs. Copyright 2020, Royal Society of Chemistry. f) The inverted PSC structure. g) The stability measurement of unpackaged devices based on different HTLs. Copyright 2019, Wiley. h) The *J*–*V* curves for the optimal PSCs with different HTLs. Copyright 2019, Wiley.

Huang et al.[161] reported a small molecule HTL (named DMZ) composed of four triphenylamine units as side arms and a bifluorenylidene as the core and applied it to the PSC device illustrated in **Figure 8f**. HTLs with flexible core can adjust their configuration according to the interaction between side arm and perovskite or the interaction between side arm itself, which may lead to a good balance between high mobility and low charge recombination. After optimizing the thickness of the HTL, 18.61% of PCE was obtained by using thin (13 nm) DMZ HTL layer. As shown in **Figure 8g**, 90% of the maximum PCE can be maintained for more than 556 hours without encapsulation in air (RH=

45%-50%). Che et al.[162] synthesized two rationally designed HTLs with butterfly-shaped triarylamine groups based on a dibenzofulvene-bridged indacenodithiophene (IDT) core (attaching hexyl and octyl chains), namely, IT-C6 and IT-C8, respectively. IT-C6 with a shorter hexyl chain revealed a higher hole mobility (9.94×10^{-4} $cm^2 V^{-1} s^{-1}$), more suitable band arrangement, a better interface contact and passivation effect. The champion device with IT-C6 achieved 18.34% of PCE with a high FF of 82.32%. Spiro-based hole transport molecules have been overwhelmingly used in normal architecture devices. Guo et al,[163] have proved that spiro-based hole transport molecules can be used as efficient HTLs in *p-i-n* PSC too. Three types of triphenylamine derivatives were studied: 2,2',7,7'-tetra(*N,N*-di-tolyl)amino-9,9-spirobifluorene (Spiro-TTB), 2,2',7,7'-tetra-kis-(diphenylamino)-9,9'spirobifluorene (Spiro-TAD), and Spiro-MeOTAD. The $MAPbI_3$ perovskite layer was deposited by an orthogonal solvent composed of GBL and DMSO to avoid dissolution of the HTL layer. The well-aligned energy levels and high hole mobility (1.97×10^{-3} $cm^2 V^{-1} s^{-1}$) of Spiro-TTB enabled a V_{OC} up to 1.09 V and PCE of 18.38% (as seen in **Figure 8h**). Xue et al.[164] synthesized X-shaped and Y-shaped nonlinear molecules via a facile synthesis route. The Y-shaped structure of XSln847 can achieve tight molecular stacking with higher hole mobility and stronger photoluminescence quenching, yielding a PCE of 17.16%.

Guo et al.[165] adopted 4-methoxy-*N*-(4-methoxyphenyl)-*N*-phenylaniline as the donor fragment and imide-functionalized thiophene derivatives as the acceptor moiety, which are 2,2'-bithiophene (MPA-BTI) to 2,2'-bithieno[3,2-*b*] thiophene (MPA-BTTI), to construct D-A-type HTLs. The imide functionalized cores can simultaneously ensure good intermolecular π-π stacking due to the planar structure and provide passivation through carbonyl groups.[166] Accompanied with a well-matched energy level and excellent film properties, the inverted device based on MPA-BTTI achieved a high PCE of 21.17% with negligible hysteresis. Moreover, it showed good long-term stability and maintained 90% of the initial PCE under 500 h constant light exposure. It was previously reported that the interaction between S in sulfides and Pb^{2+} is strong, which can passivate the trap states in the perovskite. The thiophene ring possesses a high hole mobility, but the coordination ability of S on the thiophene ring is much weaker than that of sulfides and mercaptan. Therefore, Wong et al.[53] prepared a XY1 HTL attaching four methoxy substituted triphenylamine group on thieno[2,3-*b*] thiophene core. Compared with PEDOT:PSS, XY1 exhibited a higher hole transport ability and a well aligned energy level with the VBM of the perovskite, yielding a PCE of 18.78%. Jin et al.[167] reported a SM-HTL, *N*-(4-(9*H*-carbazol-9-yl)phenyl)-7-(4-(bis(4-methoxyphenyl)amino)phenyl)-*N*-(7-(4-(bis(4-methoxyphenyl)amino)phenyl)-9,9-dioctyl-9*H*-fluoren-2-yl)-9,9-dioctyl-9*H*-fluoren-2-amine (CzPAF-TPA). The appropriate HOMO level of −5.07 eV, a high hole mobility due to the extended

conjugation, and a pin-hole free uniform film, enabled a PCE of 15.71% and 12.46% for devices on rigid and flexible substrates, respectively. Guo et al.[168] proposed an anchoring group-assisted D-A molecular modification molecule (MPA-BT-CA) like **Figure 9a**. The TRPL spectrum in **Figure 9b** indicates that the charge recombination between MPA-BT-CA and perovskite interface is weakened, and the hole extraction efficiency at the interface is improved. It is well known that the uncoordinated Pb^{2+} ions located at grain boundaries and surfaces are the main defect sources, forming harmful trap states with adverse effects on charge separation and transport.[169-170] **Figure 9c** shows that there is an obvious shift in the BT part in the ^{1}H NMR spectrum, which is mainly due to the strong combination between 2-cyanoacrylic acid (CA) and Pb^{2+}. As anchoring group, CA shows a tunable energy level, and capability to passivate perovskite defects, leading to a champion PCE of 21.24% with V_{OC} of 1.13 V, J_{SC} of 22.25 mA cm^{-2}, FF of 84.8% (**Figure 9d**).

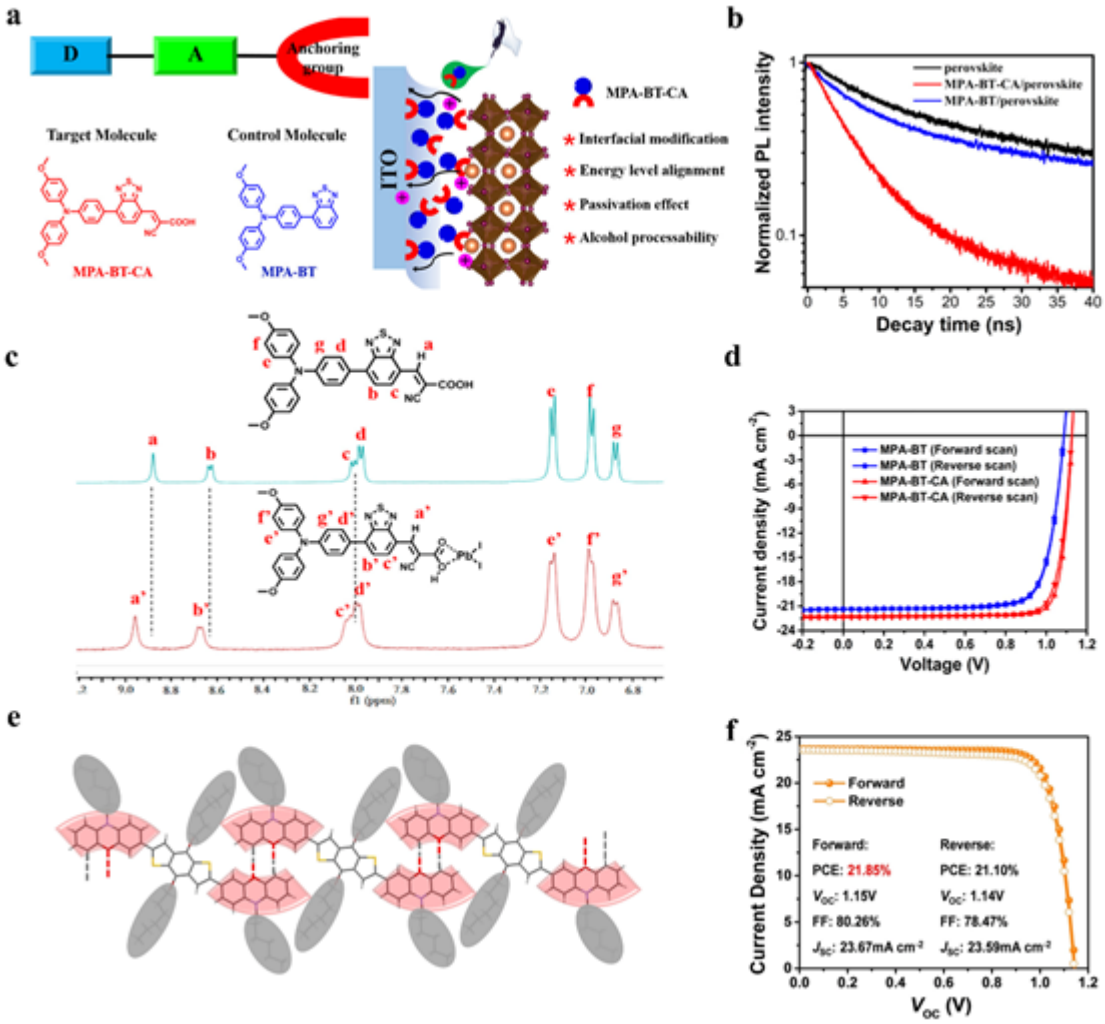

Figure 9. a) Chemical structure of MPA-BT-CA and its multifunctional schematic diagram. b) TRPL measurement spectrogram of the perovskite films on different HTLs. c) ^{1}H NMR spectra of MPA-BT-CA with or without PbI_2. d) The champion *J*–*V* curves of the PSCs with MPA-BT-CA and MPA-BT as HTLs. Copyright 2020, American Chemical Society. e) Assembly illustration of phenoxazine-based D-π-D molecules. f) *J*–*V* curves of the champion device based on N01. Copyright 2021, Wiley.

3.3. Other structures

In 2018, Nakamura et al.[171] constructed a new class of organic/inorganic hybrid molecules, an alkanediylsulfonate disodium salt bearing a benzo[1,2-*b*:4,5-*b'*]dipyrrol core. In particular, the 3-F-br-4C molecule could form a thin and compact film when coated on ITO with a matched energy level with $MAPbI_3$. The corresponding *p-i-n* device resulted in a PCE of 17.2% with minimal hysteresis. Chen et al.[172] designed a series of D-A-D type SM-HTLs, where 2,2' and 3,3' substituted thienoisoindigo (TII) was the electron acceptor core, and 1,3-di(9*H*-carbazol-9-yl) benzene, *N*-phenylcarbazole, triphenylamine, and benzene is the peripheral electron donor (named H3-7). The SEM and AFM images show that H7 films are smoother and perovskite films on H7 are more uniform with larger grain sizes compared to films on PEDOT:PSS. However, the weaker hole extraction ability of H7 than PEDOT:PSS resulted in a relatively low PCE of 12.0%, similar to that of the PEDOT:PSS based device. Tsang et al.[173] reported two HTLs consisting of a benzo[1,2-*b*:4,5-*b'*]dithiophene (BDT) core and two phenothiazine (PTZ) or phenoxazine (POZ) terminal units. Bromohexyl can promote dipole-dipole interactions between HTL molecules, resulting in a more ordered molecular arrangement. Meanwhile, the lone pair electrons around the bromine atom act as a Lewis-base, which can passivate the defects at the HTL/perovskite interface through coordination with Pb ions. Single-crystal XRD analysis suggested that the molecular packing patterns and intermolecular distance of the redox centers affect the inherent hole extraction and transport capabilities. The N-N distance between adjacent molecule is much closer for BDT-POZ, thus benefiting hole-hopping across the HTLs. As a result, the BDT-POZ film exhibited a higher hole extraction and mobility than BDT-PTZ. Consequently, BDT-POZ devices yielded a higher PCE of 19.16% than the BDT-PTZ ones of 18.26%. Later on, Jen et al.[174] synthesized two D-π-D type HTLs consisting of BDT as the core and bromohexyl substituted POZ (N01) or hexyl substituted POZ (N02) as the terminal donor unit; the structure of N01 is illustrated in **Figure 9e**. Single-crystal XRD showed that N01 could self-assemble into an ordered lamellar structure by multiple weak intramolecular interaction including C-H···O, C-H···Br and π-π interactions. Therefore, N01 exhibited a higher hole mobility of 1.1×10^{-4} $cm^2 V^{-1} s^{-1}$

and better hole extraction ability. Besides, bromohexyl-induced self-assembly exhibited stronger interactions with Pb ions, favoring defect passivation and interfacial charge transport. Consequently, *p-i-n* devices based on N01 yielded an impressive PCE of 21.85% with J_{SC} of 23.67 mA cm^{-2} and V_{OC} of 1.15 V (**Figure 9f**).

Janssen et al.[175] reported a fused azapolyheteroaromatic small molecule, namely anthradi-7-azaindole (ADAI). ADAI molecules can integrate hydrogen-bonded donor and acceptor sites in the conjugated skeleton by condensation of 7-azacyclohexane building blocks. These molecules could self-assemble to form an interface layer, which improved the morphology of the perovskite and reduced non-radiation recombination. The *p-i-n* device based on ADAI as HTL reached a PCE >16%. Hereafter, they extended π-conjugated nuclei from anthracene used in ADAI to pyrene to synthesize pyrenodiindole (PDI) and pyrenodi-(7-azaindole) (PDAI) as HTLs in narrow-bandgap PSCs.[176] Both PDI and PDAI exhibited similar hole transport characteristics compared to PEDOT:PSS. The use of thin PDAI as HTL in PSCs changed the optical interference and reduced parasitic absorption in the near-infrared region, thus improving the J_{SC}. Consequently, a higher PCE of 16.1% was achieved for PDAI and PDI, outperforming 15.1% for PEDOT:PSS. The relationship between the small molecule and PV performance is given in **Table 2**.

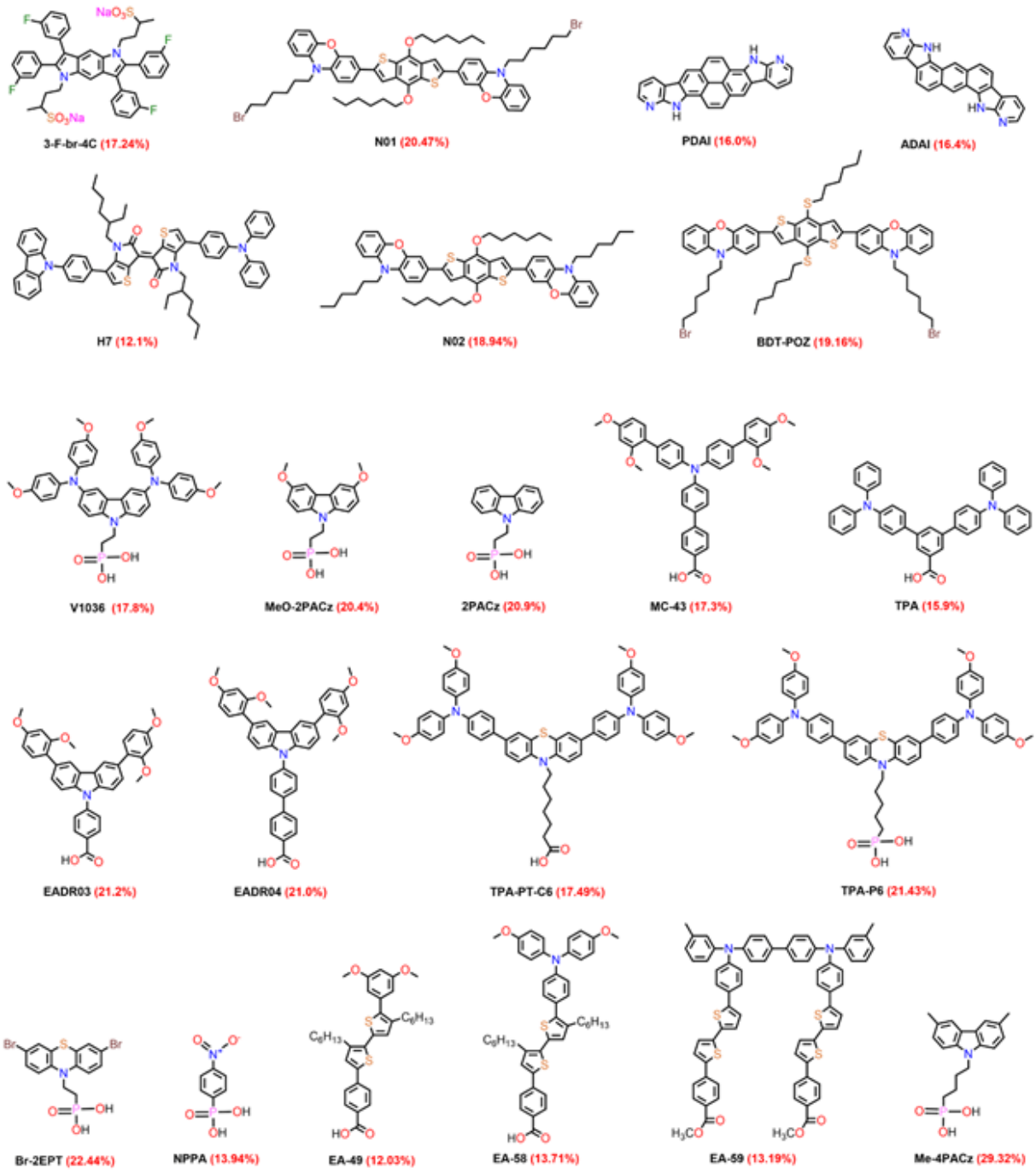

Figure 10. Other categories of small molecules and SAM structures mentioned in this article.

Table 2. The photoelectric properties and device structure of PSCs based on distinct HTLs. The device parameters were self tested at the laboratory.

HTL	HOMO/ LUMO (eV)	Hole mobility ($cm^2 V^{-1} s^{-1}$)	Conductivity ($S\ cm^{-1}$)	Thick/ (nm)	Device structure	V_{OC}/ (V)	J_{SC}/($mA\cdot cm^{-2}$)	FF/ (%)	PCE/ (%)	Refs.
XY1	−5.44/−2.42	3.76×10^{-4}			ITO/HTL/$(CsPbI_3)_{0.05}[(FAPbI_3)_{0.83}(MAPbBr_3)_{0.17}]_{0.95}$/$C_{60}$/BCP/Au	1.11	22.21	76.18	18.78	[53]
TAE	−4.90/−2.20	2.40×10^{-5}		20	ITO/HTL/$MAPbI_3$/PCBM/Ag	1.00	16.70	66.0	11.60	[139]
DFTAB	−5.20/−2.10	1.60×10^{-5}		20	ITO/HTL/$MAPbI_3$/PCBM/Ag	1.07	17.50	69.0	12.40	
TPE-S	−5.29/−2.54	1.20×10^{-5}		10	ITO/HTL/$CsPbI_2Br$/PCBM/ZnO/Ag	1.26	15.60	78.5	15.40	[140]
Trux-OMeTAD	−5.28/−2.30	3.60×10^{-3}		15	ITO/HTL/$MAPbI_3$/PCBM/ZnO/NPs/Al	1.02	23.20	79.0	18.60	[143]
TPP-SMeTAD	−5.18/−1.94	0.74×10^{-4}			ITO/HTL/$MAPbI_3$+HTL/PCBM/ZnO/NPs/Al	1.07	20.15	77.0	16.60	[144]
M118	−5.27/−2.17	1.75×10^{-3}		30	ITO/HTL/$MAPbI_3$/PCBM/BCP/Ag	1.06	22.4	72.0	17.10	[145]
BTF4	−5.02/−3.38	1.17×10^{-4}			ITO/HTL/$(FAPbI_3)_{0.85}(MAPbBr_3)_{0.15}$/PCBM/LiF/Ag	1.03	21.50	76.8	17.01	[146]
MCz-Cz-BTI	−5.32/−3.19	1.16×10^{-4}			ITO/HTL/CsFAMA/C_{60}/BCP/Ag	1.10	23.24	83.5	21.35	[147]
DFH	−5.27/−2.29	1.00×10^{-3}	7.4×10^{-6}	40	ITO/HTL$MA_{0.9}FA_{0.1}PbI_{3-x}Cl_x$/$C_{60}$/BCP/Ag	1.09	22.70	83.0	20.6	[148]
FMT	−4.89/−1.94	2.28×10^{-6}		10	ITO/HTL/$MAPbI_3$/PCBM/Al	1.07	22.52	79.27	19.06	[149]
VB-MeO-FDPA	−5.20/−2.60	3.00×10^{-4}		10	ITO/HTLs/$MAPbI_{3-X}Cl_X$/PCBM/PEI/Ag	1.15	20.89	77.8	18.70	[150]
m-MTDATA	−5.10/−2.00	4.40×10^{-5}	1.8×10^{-5}		ITO/HTL/$Cs_{0.05}(FA_{0.85}MA_{0.15})_{0.95}Pb(I_{0.85}Br_{0.15})_3$/$C_{60}$/BCP/Cu	1.035	22.50	77.8	18.12	[152]
YC-1	−5.28/−2.71				ITO/NiO_x/HTL/$MAPbI_3$/PCBM/BCP/Ag	1.079	22.49	81.1	19.37	[153]
NTPA	−5.27/−2.34	1.10×10^{-3}		30	ITO/HTL/$MAPbI_3$/PCBM/Ag	0.98	17.40	70.8	12.10	[154]
BTPA	−5.20/−2.20	4.70×10^{-4}		30	ITO/HTL/$MAPbI_3$/PCBM/Ag	1.02	17.40	73.3	13.00	
TPA-TVT-	−5.37/−3.07	2.10×10^{-5}			ITO/HTL/$MAPbI_3$/PCBM/BCP/Ag	1.07	21.49	71.0	16.32	[155]

TPA										
TPASB	−5.49/−2.85	1.65×10^{-3}			ITO/HTL/$MAPbI_3$/PCBM/Al	1.05	20.80	80.0	17.6	[156]
BTORCNA	−5.20/−2.90	1.81×10^{-4}			ITO/HTL/$(FA_{0.17}MA_{0.94}PbI_{3.11})_{0.95}$	1.10	22.84	84.0	21.10	[157]
BTORA	−4.84/−2.96	9.52×10^{-5}			$(PbCl_2)_{0.05}/C_{60}$/BCP/Ag	1.09	22.33	83.4	20.27	
TPAC3M	−4.96/−1.71	1.10×10^{-5}		40-50	ITO/HTL/$MAPbI_3$/PCBM/ZnO/Al	1.00	22.79	78.0	17.54	[158]
TAPC	−5.50/−2.00	4.99×10^{-4}	1.19×10^{-5}	30	ITO/HTL/$MAPbI_3$/PCBM/Ag	1.04	22.32	81.15	18.80	[159]
ML-TAPC	−5.39/-	3.70×10^{-2}		22	ITO/HTL/$MAPbI_{3-X}Cl_X/MoO_3$/Ag	1.10	22.77	81.9	21.6	[160]
DMZ	−5.15/−2.88	3.71×10^{-5}		13	ITO/HTL/$MAPbI_3$/PCBM/BCP/Ag	1.02	22.62	81.05	18.61	[161]
IT-C6	−4.74/−2.46	9.94×10^{-4}		25	ITO/HTL/$(FAPbI_3)_{0.85}(MAPbBr_3)_{0.15}$/PCBM/Zrcac/Ag	1.055	21.17	82.32	18.34	[162]
Sprio-TTB	−5.30/−2.23	1.97×10^{-3}		10	ITO/HTL/$MAPbI_3$/PCBM/BCP/Ag	1.07	22.02	78.0	18.38	[163]
XSln847	−5.26/−2.10	9.66×10^{-5}			ITO/HTL/$MAPbI_3$/PCBM/BCP/Ag	1.08	22.34	71.15	17.16	[164]
MPA-BTTI	−5.24/−3.32	2.02×10^{-4}	1.35×10^{-5}		ITO/HTL/$MAPbI_3/C_{60}$/BCP/Ag	1.12	23.23	81.4	21.17	[165]
CzPAF-TPA	−5.07/−2.20	3.13×10^{-4}			ITO/HTL/$MAPbI_3$/PCBM/ZnO/Al	1.05	20.00	74.58	15.71	[167]
MPA-BT-CA	−5.29/−3.90	8.70×10^{-6}		23	ITO/HTL/$(FA_{0.17}MA_{0.94}PbI_{3.11})_{0.95}$ $(PbCl_2)_{0.05}/C_{60}$/BCP/Ag	1.13	22.25	84.8	21.24	[168]
BDPSO 3F-br-4C	−5.37/−2.98	4.00×10^{-5}		8	ITO/HTL/$MAPbI_3/C_{60}$/BCP/Ag	1.06	20.20	80.0	17.2	[171]
H7	−5.31/−3.43			10	ITO/HTL/$MAPbI_3$/PCBM/BCP/Ag	0.93	20.86	75.0	12.10	[172]
BDT-POZ	−5.35/−2.78	2.10×10^{-4}			ITO/HTL/$MAPbI_3/C_{60}$/BCP/Ag	1.04	22.56	81.7	19.16	[173]
BDT-PTZ	−5.42/−2.81	9.80×10^{-5}				1.02	22.43	79.8	18.26	
N01	−5.09/−2.43	1.10×10^{-4}		60	ITO/HTL/$MAPbI_3/C_{60}$/BCP/Ag	1.08	23.65	80.15	20.47	[174]
ADAI		1.10×10^{-4}		10	ITO/HTL/$MAPbI_3$/PCBM/LiF/Al	1.03	19.90	77.0	15.90	[175]
PDAI	−4.89/−2.57	2.90×10^{-3}			ITO/HTL/$(FASnI_3)_{0.6}(MAPbI_3)_{0.4}/C_{60}$/BCP/Ag	0.77	29.00	72.0	16.00	[176]

4. Self-Assembled Monolayers (SAMs) based HTL (SAM-HTL)

SAMs are ordered organic molecules with a thickness of one or few molecules assemblies that spontaneously form on substrates by adsorption of the anchoring group (**Figure 10**). Unlike PTAA or other conjugated organic molecules that are expensive or tedious to synthesize, SAMs offer an opportunity for cheap, scalable and stable HTLs in *p-i-n* PSCs due to the low materials consumption, simple fabrication and relatively easy modification. Moreover, the chemical bath deposition method of SAMs can be implemented for large-area PSCs and modules, as well as bottom solar cells with complex surfaces, such as textured silicon wafers, giving them great potential for perovskite based tandem solar cells.[177-178]

4.1. General features of SAM-HTLs

Normally, the SAM molecules consist of three parts, namely i) an anchoring group that binds to the surface of substrate, ii) the linker that connects the anchoring group and terminal group, iii) a terminal group (sometimes called functional group in the literature) that contacts directly to the perovskite upper layers. The anchoring group type will determine the binding energy with the substrate surface, and it greatly affects the interfacial dipole, contact resistance, coverage ratio and work function of substrate. The detailed anchoring group types and anchoring mechanisms are discussed below. The linkage unit is responsible for the interaction between the molecules during the self-assembly process, affecting the packing properties and tilt angle relative to the surface. Structurally, the linkage can be an inactive aliphatic chain and a conjugated aromatic unit. The varied linkage types can induce different supermolecular structures with Van der Waals interactions and charge transport abilities at the interface, thereby influencing the charge extraction/transport at the interface. The terminal group can form a new surface, acting as a growth template for the subsequent perovskite layer. If the terminal group consists of active unit such as amines, thiols and other functional groups which can interact with the perovskite, it could influence the dynamic growth, crystalline quality and even the work function of the subsequent perovskite layer.

4.2. Deposition methods of SAM-HTL

For the preparation of SAM-based HTLs, mainly two types are widely used, dip and spin coating. The dip-coating method is applied by immersion of the substrate into the SAMs solution, which

allows self-assembly of the molecules on the surface of substrate. The adsorption can be modulated by the choice of solvent, the concentration, and dipping time. This method does not require any specialized equipment and is easy scalable at the laboratory level.[77] The slow growth rate and use of toxic organic solvent are the main drawbacks. In contrast, in the spin-coating method the SAMs are dispensed onto the substrate at certain speed. This method is simpler and only takes few minutes, consequently, it is more widely used in laboratory but has limited scalability. Both methods are often followed by thermal annealing

4.3. Adhesion Mechanism of SAM-HTLs

The adhesion mechanism is dependent on the anchoring group and the chemical properties of the substrate surface. Since most SAM-HTLs feature carboxyl acid or phosphonic acid as anchoring groups, here, we focus on the mechanism of these two cases. The carboxyl acid group possesses two oxygen atoms, allowing two binding sites with the ITO surface. The monodentate binding forms by condensation of the anchoring OH group with the hydroxyl group on the ITO surface. The bidentate coordination forms by a further condensation by the hydrogen atom transferred to the surface hydroxyl group.[179] Different from carboxyl acid, the phosphonic anchoring group has two hydroxyls and one phosphonic group, endowing the mono-, bi-, and tridentate binding mode depending on the substrate surface and reaction conditions. The mono- and bidentate bonding are formed via protonation of the surface hydroxyl group and releasing one water molecule, leading to a strong P-O-M bond.[179] In terms of the tridentate bonding, the hydrogen atom is transferred to the surface hydroxyl group following by hetero-condensation, generating the vacancy for oxygen atom in SAMs and forming the third bond.[180] These oxygen atoms can bind to the same or different metal atoms simultaneously, depending on the surface conditions. It is not surprising that phosphonic acid has the strongest binding energy, according to the binding energy calculation between TiO_2 and 15 different anchoring group.[181]

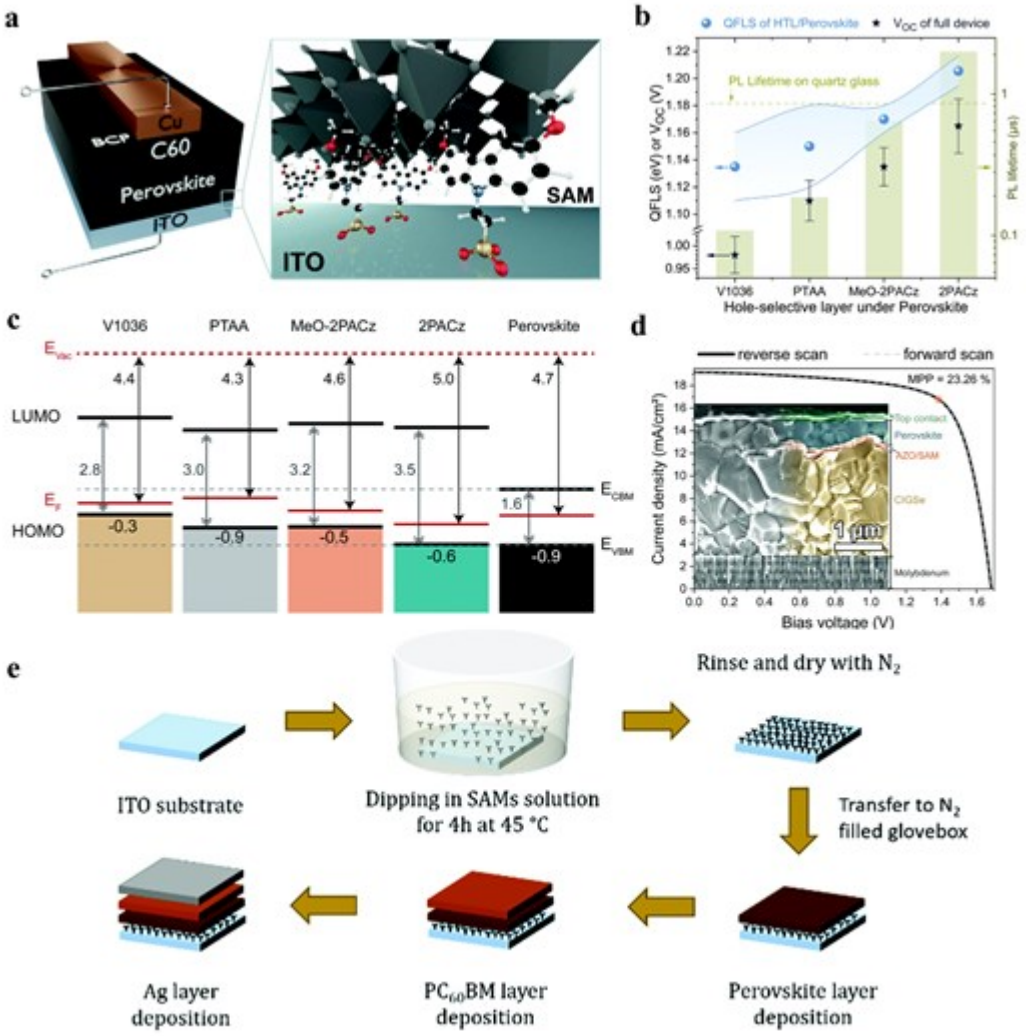

Figure 11. a) Configuration of inverted device and the magnification shows the arrangement of SAM molecules between perovskite and ITO. b) Summary of PL and TRPL measurements. c) Energy level diagram about devices based on values from UPS measurements. d) The *J*–*V* curve of a monolithic CIGSe/perovskite tandem solar cell, inset: cross-section SEM image of tandem cell. Copyright 2019, Royal Society of Chemistry. e) The fabrication process diagram of the PSC. Copyright 2019, Royal Society of Chemistry.

4.4. SAM-HTL types

Although SAMs have been widely used in organic electronics and as interlayers in PSCs, the first SAM-based HTL in *p-i-n* PSCs was only reported in 2018. Getautis and coworkers designed and synthesized a new molecule, called V1036 and composed of phosphonic acid as anchoring group,

ethyl as linker and dimethoxydiphenylamine substituted carbazole as terminal group. It was found that mixing certain amounts of the electrically inactive filler molecule C4 can optimize the ionization potential and wettability, and fill pinholes. Benefitting from this, *p-i-n* PSCs based on the mixed V1036 and C4 reached a PCE of 17.8% with average FF close to 80%, comparable to PTAA based reference devices. Moreover, these PSCs exhibited a 0.3 mA cm^{-2} higher J_{SC} than the PTAA-based devices due to reduced parasitic absorption. This study showed for the first time the great application potential of SAMs as HTLs.[182] Following this work, the same group further designed and synthesized two new SAM-HTLs, MeO-2PACz and 2PACz **(Figure 11a)**. In comparison to V1036, these molecules possess a simpler structure with and without a substituted carbazole unit by methoxy (MeO-2PACz and 2PACz, respectively). Correspondingly, the synthesis route is short and cheap starting materials are used. **Figure 11b** indicates the formation of a better passivated surface for 2PACz based PSCs. **Figure 11c** presents an energy level diagram of different HTLs, from which along with a weakened electron-donating substitution at the 3,6-positions of carbazole, a deeper HOMO level trend is observed. 2PACz showed the closest alignment to the VBM of perovskite. Thanks to the reduced nonradiative recombination and well-suited energetic alignment, a maximum PCE of 20.9% and a V_{OC} up to 1.19 V were demonstrated based on a triple-cation perovskite, outperforming the PTAA-based devices. Furthermore, by integrating the SAM into monolithic perovskite/CIGSe tandem solar cells **(Figure 11d)**, a stabilized, certified PCE of 23.26% on an active area of 1.03 cm^2 was achieved.[183]

Palomares and coworkers synthesized two SAM HTLs, TPA and MC-43, with triphenlyamine as terminal group, phenyl unit as linker, and carboxylic acid as anchoring group.[184] **Figure 11e** displays the preparation process of the SAMs. By replacing PEDOT:PSS in *p-i-n* PSC, the PSCs based on MC-43 attained a champion PCE of 17.3% with a FF of 80%, V_{OC} of 1.07 V and J_{SC} of 20.3 mA cm^{-2}, which are among the highest values for $MAPbI_3$ PSCs in the literature. Recently, the same group rationalized the design of two new molecules EADR03 (4'-(3,6-bis(2,4-dimethoxyphenyl)-9*H*-carbazol-9-yl) benzoic acid) and EADR04 (4'-(3,6-bis(2,4-dimethoxyphenyl)-9*H*-carbazol-9-yl)-[1,1'-biphenyl]-4-carboxylic acid). Although PTAA has a small energy offset with the VBM of perovskite, the SAM-HTL based devices showed higher V_{OC}, indicating the enhanced charge transport ability and passivation effect of SAMs compared to PTAA. With the insertion of LiF and an ARC, these two SAM-HTLs based devices yielded a high PCE of 21% **(Figure 12a** and **12b)**. More importantly, a superior device stability was attained based on these two materials compared to PTAA based reference devices. These results highlight how SAMs based on a carboxylic acid anchoring group are also promising to achieve highly stable and efficient devices.[185]

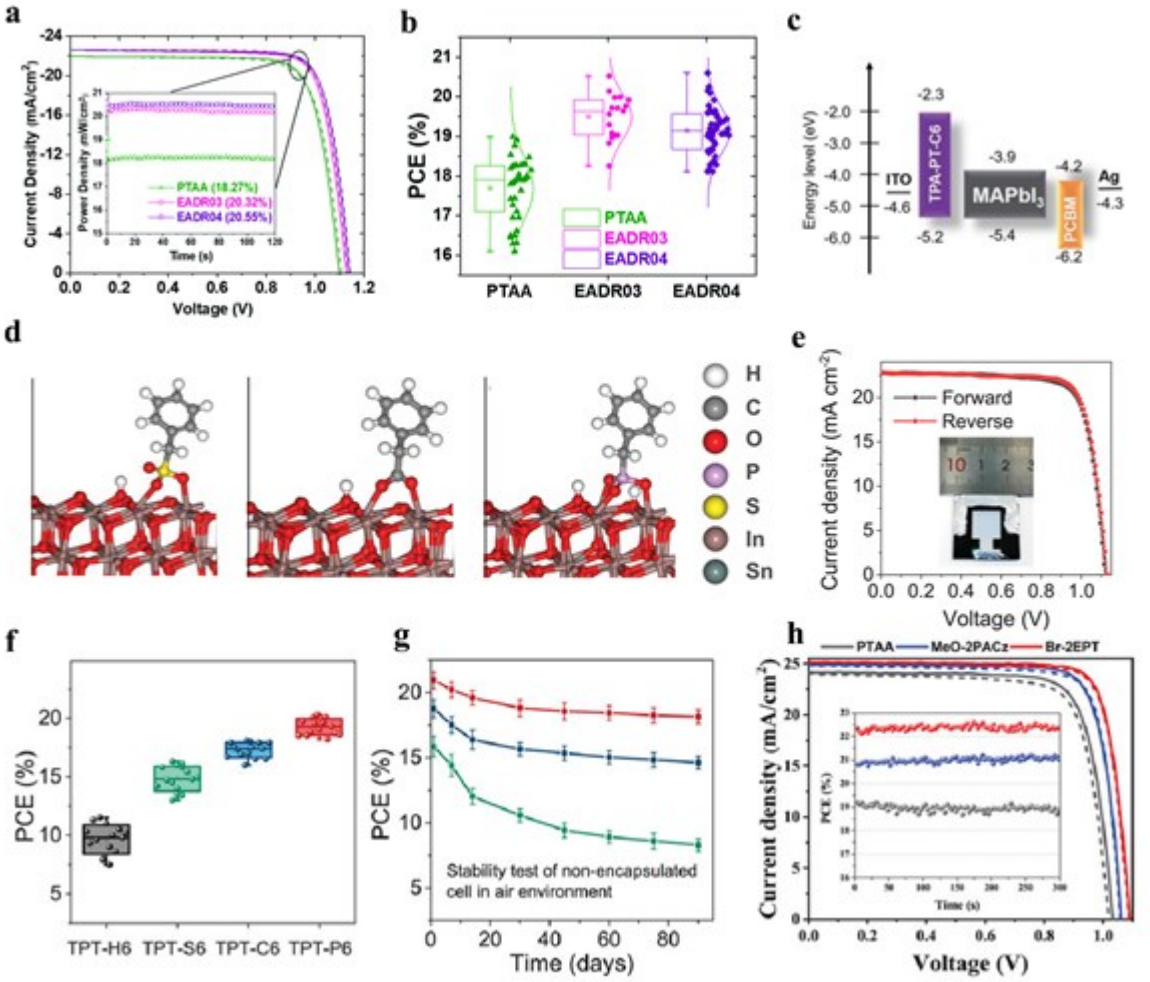

Figure 12. a) Champion *J*–*V* curves of the PSCs with PTAA, EADR03 and EADR04 as HTLs. b) Statistics of the PCE values for the PSCs with different HTLs. Copyright 2021, Royal Society of Chemistry. c) Energy level alignment of different components in PSCs. Copyright 2019, Wiley. d) Adsorption model of different SAM molecule on the ITO (111) surface. e) The *J*–*V* curves of large area PSCs based on TPT-P6. f) Statistics of the PCE values for the PSCs with different HTLs. g) Long-time stability test of non-encapsulated cell in environment with a relative humidity of 30%. Copyright 2021, Wiley. h) The champion *J*–*V* curves of the PSCs and reverse scan (V_{OC} to $J_{SC,}$ solid) with respective MPP tracks in the inset. Copyright 2021, Wiley.

Besides the commonly scrutinized carbazole and triphenylamine units, some researchers reported SAM-HTLs based on phenothiazine. In comparison to carbazole and triphenylamine building blocks, phenothiazine is relatively cheaper, and the sulphur atom may passivate interfacial trap states. Zhu

et al. designed and synthesized a SAM-HTL called TPA-PT-C6, consisting of carboxyl acid as anchoring group, hexyl as linker, and dimethoxydiphenylamine substituted phenothiazine as terminal group.[186] **Figure 12c** shows the matched energy level alignment with $MAPbI_3$ for TPA-PT-C6. They proposed an anchoring-based co-assembly strategy by mixing TPA-PT-C6 with a hydrophilic ammonium salt CA-Br. The introduction of a proper amount of CA-Br can mitigate the nonwetting problem for perovskite deposition and improves the electronic contact at the SAMs/perovskite interface. A high PCE of 17.49% and 12.67% was achieved for inverted PSCs with area of 1.02 cm^2 and aperture area of 36 cm^2, respectively, which is promising for large-area PSCs. Further, to investigate the effect of the anchoring group on device performance, the same group designed and synthesized a series of SAMs based on phenothiazine, featuring different anchoring groups such as -SO_3H, -COOH, and -PO_3H_2 for TPT-S6, TPT-C6, and TPT-P6, respectively. Calculations and experiments confirmed how the phosphonic acid group formed the strongest chemical binding between the phosphate and ITO surface (as illustrated in **Figure 12d**). TPT-P6 generated an ordered and dense monolayer on ITO surface and showed a good hole transport ability. **Figure 12e** presents an example of large area PSC modules. The resultant inverted PSCs delivered a remarkable PCE of 21.43% (0.09 cm^2) and 20.09% (1.0 cm^2) with superior stability (**Figure 12f**).[187] Hong et al. reported a SAM-HTL, Br-2EPT, comprising of a brominated phenothiazine moiety as terminal unit, ethyl as linker, and phosphonic acid as anchoring group.[188] The Br-terminal unit can pull down the HOMO level due to its electron-withdrawing ability and change the perovskite crystallinity through chemical interaction. When integrated into inverted PSCs as HTL, it yielded a minimized nonradiative loss and a well-matched energy level with perovskite, resulting in a PCE >22% with an average FF close to 81% (**Figure 12g** and **12h)**. The device also demonstrated outstanding stability after 100 h of continuous MPP tracking, highlighting the stable and high-performance PSC could be achieved based on phenothiazine-based SAMs.

To gain a deeper understanding of the effect of the terminal group, Tao and coworkers systematically studied phenylphosphonic acid carrying electron-donating or electron-withdrawing *p*-substituents. Five SAM-HTLs, 4-methoxyphenyl-phosphonic acid (MxPPA), 4-methylphenylphosphonic acid (MyPPA), phenylphosphonic acid (PPA), 4-cyanophenylphosphonic acid (CPPA), and 4-nitrophenylphosphonic acid (NPPA) were studied in $MAPbI_3$-based inverted PSCs. It was found that variation of the terminal group with different electron push/pull ability could adjust the work function and the wettability, thus influence the perovskite quality and the device performance.[189] Demic et al. presented five novel SAM-HTLs to compare the effect of an electron donating and withdrawing terminal group on the performance of inverted PSCs.[190] Contiguous

thiophene rings were utilized as the linker to provide better conjugation. Similarly, the terminal group have an impact on the work function and wetting ability. EA-49 gave the best PCE owing to the well-suited energy level and the methoxy terminal group can passivate the trap state of perovskite layer. The same group designed and synthesized three SAMs bearing carboxyl acid as anchoring group, bithophene as linker, and varied terminal group (triphenylamine for EA-54, dimethoxydiphenylamine for EA-58, carbazole for EA-63).[191] Although the HOMO level of EA-63 matched better with the VBM of $MAPbI_3$ and EA-63 based *p-i-n* PSC exhibited higher V_{OC}, EA-58 based PSC afforded better PCE due to higher FF, which was attributed to the surface passivation of methoxy group through a coordination bond. Apart from the terminal group modification, they designed and synthesized two SAM-HTLs to study the effect of linker group. One molecule was bridged by a bithiophene linker and the other one was enriched with two hexyl chains.[192] It was found that the branched and long hexyl chain partially hinder the formation of conformal and dense monolayer due to steric hindrance, which may cause current leakage, inducing additional recombination losses, thus resulting in slightly lower PCE of 11.11% than the analogue without hexyl chains (PCE of 13.19%).

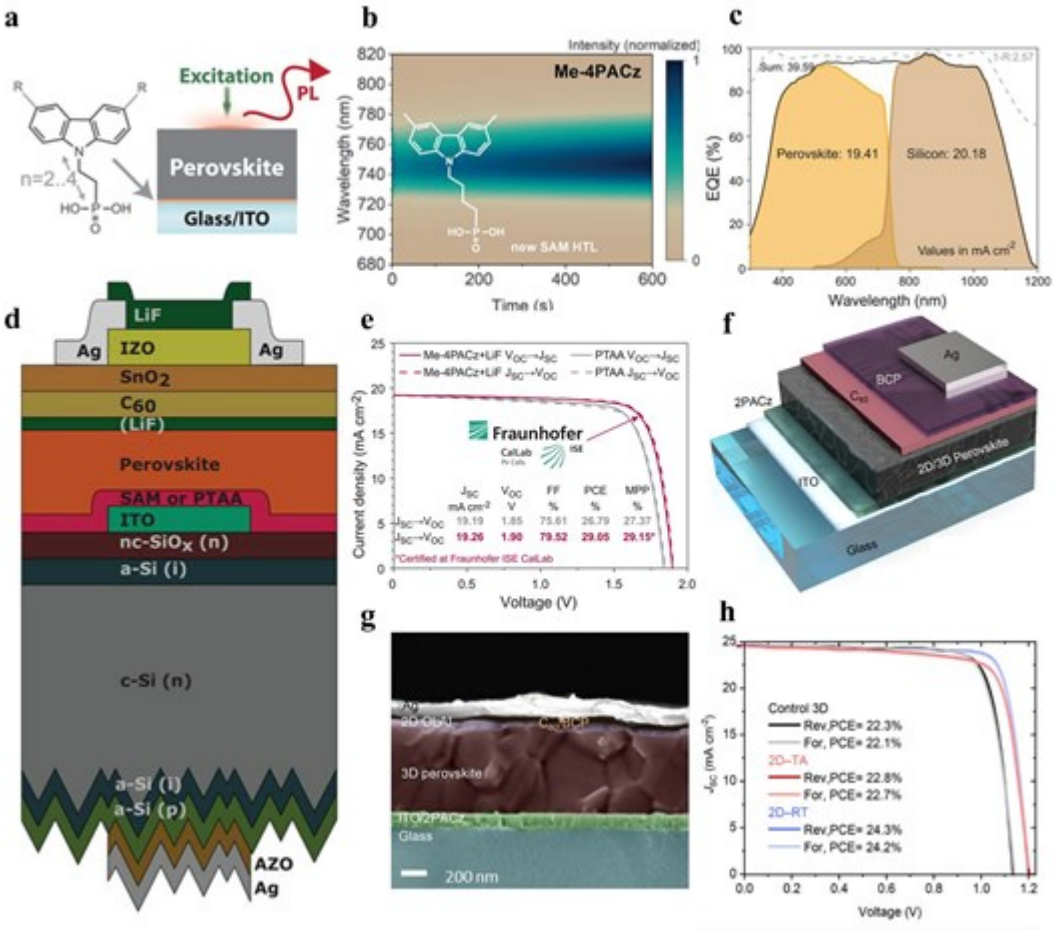

Figure 13. a) Schematic illustration of photoluminescence (PL) experiments and chemical structures of carbazole-based SAMs. b) The phase stability of perovskite-type absorption materials on Me-4PACz was analyzed. c) The EQE spectra and reflection (1-R) of certified tandem cell internal measurement. d) The structure of monolithic perovskite/silicon tandem solar cells. e) Certified *J-V* curves of perovskite/silicon tandems. Copyright 2020, American Association for the Advancement of Science. f) Device structure of inverted PSC g) Cross-section SEM image of inverted PSC. h) The champion *J-V* curves of PSC. Copyright 2022, American Association for the Advancement of Science.

Table 3. The Photoelectric properties and device structure of PSCs based on distinct SAM HTLs.

HTL	HOMO/ LUMO(eV)	Device structure	V_{OC}/ V	J_{SC}/ (mA·cm^{-2})	FF/ %	PCE/ %	Refs.
V1036	−5.09/−2.34	ITO/V1036/C4/$Cs_{0.05}(MA_{0.17}FA_{0.83})_{0.95}Pb(I_{0.83}Br_{0.17})_3$/$C_{60}$/BCP/Cu	1.09	21.9	81.0	17.8	[182]
MeO-2PACz	−5.1/−1.9	ITO/MeO-2PACz/$Cs_{0.05}(MA_{0.17}FA_{0.83})_{0.95}Pb(I_{0.83}Br_{0.17})_3$/$C_{60}$/BCP/Cu	1.144	22.2	80.5	20.4	[183]
2PACz	−5.6/−2.1	ITO/2PACz/$Cs_{0.05}(MA_{0.17}FA_{0.83})_{0.95}Pb(I_{0.83}Br_{0.17})_3$/$C_{60}$/BCP/Cu	1.188	21.9	80.2	20.9	
2PACz	−5.1/−1.9	CIGSe/AZO/2PACz/$Cs_{0.05}(MA_{0.17}FA_{0.83})_{0.95}Pb(I_{0.83}Br_{0.17})_3$/$C_{60}$/$SnO_2$/IZO/Ag/LiF	1.68	19.17	71.9	23.26[a]	
MC-43	−5.1/-	ITO/MC-43/$Cs_{0.05}(MA_{0.17}FA_{0.83})_{0.95}Pb(I_{0.83}Br_{0.17})_3$/$PC_{60}$BM/Ag	1.07	20.3	80.0	17.3	[184]
TPA	−5.3/-	ITO/TPA/$Cs_{0.05}(MA_{0.17}FA_{0.83})_{0.95}Pb(I_{0.83}Br_{0.17})_3$/$PC_{60}$BM/Ag	1.06	19.4	76.9	15.9	
EADR03	−5.05/−1.77	ITO/EADR03/$Cs_{0.05}FA_{0.79}MA_{0.16}Pb(I_{0.84}Br_{0.16})_3$/LiF/$C_{60}$/BCP/NaF/Cu	1.156	22.9	80.0	21.2	[185]
EADR04	−5.06/−1.74	ITO/EADR04/$Cs_{0.05}FA_{0.79}MA_{0.16}Pb(I_{0.84}Br_{0.16})_3$/LiF/$C_{60}$/BCP/NaF/Cu	1.164	22.6	80.0	21.0	
TPA-PTC6	−5.20/−2.34	ITO/TPA-PTC6/CABr/$MAPbI_3$/PCBM/BCP/Ag	1.039	21.8	77.35	17.49	[186]
TPT-P6	−5.20/−2.32	ITO/TPT-P6/$Cs_{0.05}MA_{0.12}FA_{0.83}Pb(I_{0.85}Br_{0.15})_3$/$C_{60}$/BCP/Ag	1.125	23.50	81.08	21.43	[187]
Br-2EPT	−5.47/−2.12	ITO/Br-2EPT/$Cs_{0.05}(FA_{0.92}MA_{0.08})_{0.95}Pb(I_{0.92}Br_{0.08})_3$/$C_{60}$	1.09	25.11	82.0	22.44	[188]

		/BCP/Cu					
NPPA	−5.30/-	ITO/NPPA/$Cs_{0.05}(FA_{0.92}MA_{0.08})_{0.95}Pb(I_{0.92}Br_{0.08})_3$/PCBM/Ag	1.07	18.44	70.0	13.94	[189]
EA-49	−5.07/-	ITO/EA-49/$MAPbI_3$/$PC_{60}BM$/Ca/Ag	1.024	17.95	68.15	12.03	[190]
EA-58	−4.80/-	ITO/EA-58/$MAPbI_3$/$PC_{60}BM$/Ca/Ag	0.967	19.08	76.37	13.71	[191]
EA-59	−4.92/-	ITO/EA-59/$MAPbI_3$/$PC_{61}BM$/Ca/Ag	1.09	17.98	71.56	13.19	[192]
Me-4PACz	−5.8/−2.5	Ag/AZO/a-Si(p)/a-Si(i)/c-Si(n)/a-Si(i)/nc-SiO_x(n)/ITO/Me-4PACz/$Cs_{0.05}(FA_{0.77}MA_{0.23})_{0.95}Pb(I_{0.77}Br_{0.23})_3$/$C_{60}$/$SnO_2$/IZO/Ag/LiF	1.87	19.37	81.06	29.32[a]	[193]
MeO-2PACz	−5.1/-	ITO/MeO-2PACz/$FASnI_3$/C_{60}/BCP/Ag	0.475	20.3	67.3	6.49	[196]

[a] Certified PCE. All the other PCEs are in-house measurements.

Researchers have successfully integrated SAM-HTLs into perovskite/silicon tandem solar cells. Albrecht et al. designed a SAM with methyl group substitution, called Me-4PACz ([4-(3,6-dimethyl-9*H*-carbazol-9-yl)butyl]phosphonicacid) (**Figure 13a** and **13b**).[193] The influence of the aliphatic chain length n (n=2, 4, 6) in carbazole-based nPACz and methyl substitution (Me-nPACz) on device performance was investigated and an optimum performance was found at n=2 for nPACz and n=4 for Me-nPACz. Thanks to the fast hole extraction and efficient passivation of the SAM interface, the PSC could reach a V_{OC} value of >1.23 V and FF up to 84% using a perovskite bandgap of 1.68 eV. When transferred into a monolithic perovskite/silicon tandem solar cell with device structure shown in **Figure 13c** and **13d**, a certified PCE of 29.15% was obtained **(Figure 13e)**, surpassing other monolithic and four-terminal perovskite-based tandem solar cells. Moreover, the tandem solar cells retained 95% of their initial PCE after 300 h when monitored at 25°Cand in ambient air with 30% to 40% relative humidity, outperforming the PTAA-based control device. Recently, De Wolf et al. passivated the defects at the perovskite top surface employing oleylammonium-iodide molecules for single-junctions PSCs. The resulting Ruddlesden-Popper phase 2D-perovskite layer at the top was tailored in its dimensionality by tuning the annealing conditions, followed by systematic characterized. A maximum PCE of 24.3% was fabricated for a single-junction PSC with structure ITO/2PACz/3D-perovskite/2D-perovskite/C_{60}/BCP/Ag (**Figure 13f-h)**. Moreover, the encapsulated device retained >95% of the initial value after >1000 hours at damp-heat test conditions, whereas the control devices retained PCE <90% for only 100 hours.[194] A pronounced advantage of SAMs is that they can realize a conformal coverage on rough surface, such as FTO, textured silicon wafers

and so on. For perovskite/silicon tandem solar cells, De Wolf and coworkers incorporated 2PACz onto a textured silicon heterojunction solar cell, acting as SAM-HTL for the top perovskite sub cell. Benefiting from the reduced nonradiative recombination loss and suppressed phase segregation by addition of carbazole in the perovskite precursor solution, they reported a certified PCE of 28.2% for double-sided, textured monolithic perovskite/silicon solar cell over ~1cm^2 and the device when encapsulated attained over 93% of its initial performance for more than 40 days when tested in a hot and humid outdoor environment.[195]

The outstanding property of the SAM-HTLs also attracts the interest in the Sn-based PSC community. Recently, the first trial of a Sn-based PSC utilizing 2PACz, Me-4PACz and MeO-2PACz as HTL was reported by Diau and coworkers.[196] Combining preheating of the glass/ITO substrate and a two-step perovskite deposition approach, the device performance was promoted to PCE of 6.5% with excellent long-term stability without encapsulation, indicating the promising application of SAM-HTL in lead-free perovskite solar cells. The relationship between the SAM-HTL and PV performance is given in **Table 3**.

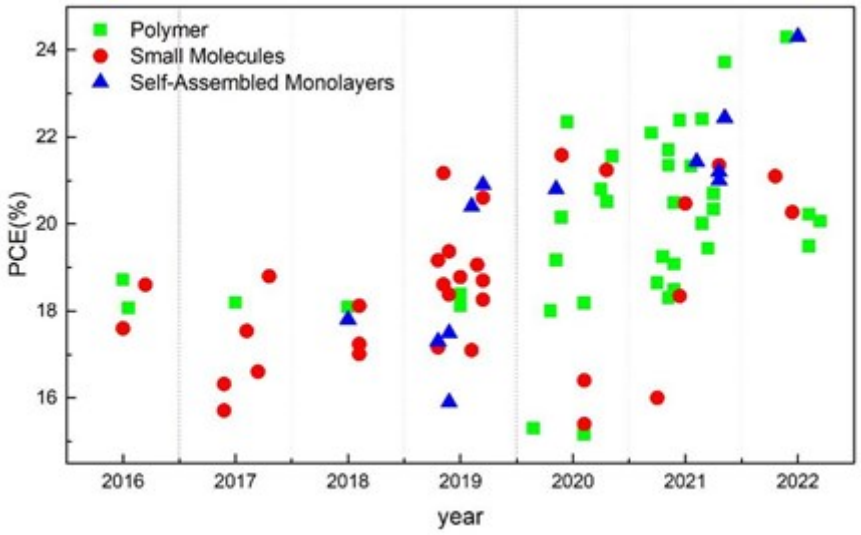

Figure 14. Summary of PCE (%) development of organic HTL (polymers, small molecules, self-assembled monolayers) for inverted (*p-i-n*) PSCs in the literature.

Table 4. Summary of stability results and test conditions (left), and number of synthetic steps, overall yield of the products and estimated cost value (right) of select HTLs. The PCEs were in-house measured at the respective laboratories.

No	Molecule	Light	T /°C	Humidity /%	atmosphere	Initial PCE/%	encapsulate	Time	Num. of steps	Overall yield/%	Value/ USD/g	Ref
1	XY1	AM1.5G	RT	30-40	N_2	18.78	NO	T_{95}-200h	1	51		[53]
2	MCz-Cz-BTI	AM1.5G	RT	30-40	N_2	21.35	Yes	T_{80}-900h	4	18		[147]
		dark	RT	55-60	N_2	21.35	NO	T_{95}-1400h				
3	DFH								2	73	3	[148]
4	FMT	Dark	60	30-40	N_2	18.2	NO	T_{59}-132h	2	64	41.8	[149]
5	BTORCNA	dark	RT	30-40	N_2	21.1	NO	T_{100}-30d	6	48	58	[157]
6	MPA-BTTI	dark	RT	20	N_2	21.17	NO	T_{90}-60d	3	31		[165]
	MPA-BTTI	AM1.5G	RT	30-40	Air	21.17	Yes	T_{90}-500h				
	PEDOT:PSS	dark	RT	20	N_2	17.11	NO	T_{50}-15d				
	PTAA	dark	RT	20	N_2	19.85	NO	T_{80}-40d	4	23.7	423.3	[197]
7	MPA-BT-CA	dark	RT	30-40	Air	21.24	NO	T_{70}-100h	2	68	46	[168]
8	N01	LED	65	30-40	N_2	20.47	NO	T_{80}-300h	3	37		[174]
9	TPT-P6	Dark	RT	30-40	N_2	21.43	NO	T_{90}-90d	2	42		[187]
10	Br-EPT	AM1.5G	RT	15-25	Air	22.44	NO	T_{100}-100h	3	35	31.48	[188]
	MeO-2PACz	AM1.5G	RT	15-25	Air	22.44	NO	T_{97}-100h	3	35		
11	Me-4PACz	LED	25	30-40	Air	29.13	NO	$T_{95.5}$-300h	4	45		[193]

5. Stability and Scalability

Since long-term stability is still one of the major factors limiting the commercialization of PSCs, stability results are essential to assess the properties of HTLs. Such results of several representative HTLs-based PSCs under various test conditions are summarized and referenced in **Table 4**. The acidity and hygroscopic character of PEDOT:PSS severely affects the stability of the resultant PSCs. PTAA, poly-TPD and most other polymer HTLs show extended device stability after elimination of the drawbacks of PEDOT:PSS. SM-HTLs exhibit good device stability, where the MCz-Cz-BTI based device retained 95% of its initial PCE after 1400 h under dark with RH of 55-60% RH. Some of the SMs

showed higher device stability than PTAA based reference devices. An unencapsulated device based on MPA-BTTI maintained 90% of initial PCE after 60 days, outperforming the PTAA based device under the same aging condition. It also showed good thermal and light stability. Thermal stability test showed that MPA-BTTI retained 94% of its initial PCE after thermal stress at 80 °C for 800 h in a glove box. MPA-BTTI based devices maintained 90% of their initial PCE after 500 h continuous illumination. Encouragingly, impressive stability was achieved for SAM based devices. Hong et al. reported that the PTAA based reference lost more than 15% of its initial PCE after 100 h under 1 sun AM 1.5G illumination in ambient air condition with RH of 15-25%. The MeO-2PACz based reference device retained 97% of its initial efficiency. Interestingly, the Br-2EPT based device showed a slightly increased efficiency after aging at the same conditions, demonstrating its superior light-soaking response. Considering that the stability of these SAM based devices in air is comparable or better than most SMs tested in glove box, a greater potential of SAMs for long-term stability is expected. This is related to their compact, good film morphology and simple molecular structure, which is chemically robust against to oxygen, moisture, thermal and diffusion of ions.

Besides efficiency and stability, cost and processability are critical for up-scaling. The synthetic steps, overall yield of the products and estimated cost value for most relevant HTLs are shown too in **Table 4**. It can be seen that the high costs of polymer HTLs (for instance 423.3 $ per g for PTAA as of writing) limits their potential for large-scale applications. SMs and SAMs are viewed to be easier to scale since they do not suffer from batch to batch variability as for polymer HTLs. It is worth noting that a low cost of 3 $ per g of DFH indicates the great potential of SMs and SAMs to further save the cost. To reduce the material cost, simple synthetic route, inexpensive reagents and easy purification procedures are needed.

In terms of processability, most of the larger-area devices so far are fabricated by spin-coating. However, this method is generally perceived to be unsuitable for large throughput processing; moreover, more than 90% of the precursor ink is wasted during the process. To resolve this, several large-area technologies have been developed such as blade coating, slot die coating, dip coating and so on. However, most of the literature so fare merely focus on printing the single perovskite layer, reports of HTL deposited by these scalable techniques are relatively rare. Information about blade coating, slot die coating and similar techniques to deposit the HTL is collected in **Table 5**. Huang et al. fabricated a device (ITO/PTAA/$MAPbI_3$/C_{60}/BCP/Cu) where both PTAA and perovskite layer were prepared via blade coating. They achieved a PCE of 15.3% and 14.6% measured at aperture area of 33.0 cm^2 and 57.2 cm^2, respectively, demonstrating the feasibility of fabricating large-area PSCs via

blade coating technology. Uniform and high-quality deposition of HTL is crucial for large-area production and high-performance PSCs, more effort and study is desired in the future.

Table 5. Some of HTLs deposited by other technology rather than spin-coating and the device performance.

Type	HTL	Coating method	Device structure	area/cm^2	PCE/%	Ref.
Single junction	TPT-P6	Diping	ITO/TPT-P6/$Cs_{0.05}MA_{0.12}FA_{0.83}Pb(I_{0.85}Br_{0.15})_3/C_{60}$/BCP/Ag	1	20.09	[187]
	PEDOT:PSS	Slot-die	ITO/PEDOT:PSS/$MAPbI_{3-x}Cl_x$/PCBM/Ca/Al	0.1	11.16	[198]
	PEDOT:PSS	Slot-die	ITO/PEDOT:PSS/$(BA)_2(MA)_3Pb_4I_{13}$/PC61BM/PEIE/Ag	0.1	8	[199]
	PEDOT:PSS	Slot-die	ITO/PEDOT:PSS/$(MA_{0.6}FA_2)_{0.38}Cs_{0.2}PbI_{2.975}Br_{0.025}$/PCBM/PEIE/Ag	0.1	8.62	[200]
	PEDOT:PSS	Slot-die	ITO/PEDOT:PSS/ $Cs_{0.07}FA_{0.79}MA_{0.14}Pb(I_{0.83}Br_{0.17})_3$/PCBM/PEIE/Au	0.2	11.93	[201]
	PEDOT:PSS	Slot-die	ITO/PEDOT:PSS/$MAPbI_xC_{i3-x}$/PCBM/ZnO/Ag	0.2	4.9	[202]
	PEDOT:PSS	Blade	ITO/PEDOT:PSS/$MAPbI_xC_{i3-x}$/PC61BM/Bis-C60/Ag	2.25	10.44	[203]
	PTAA	Blade	ITO/PTAA/BAA-modified $MAPbI_3$/C60/BCP/Cu	1.1	20	[204]
	PTAA	Blade	ITO/PTAA/SiO_2 NPs/$FA_{0.83}Cs_{0.17}Pb(I_{0.87}Br_{0.13})_3$ /PCBM/BCP/Ag	49.6	9.3	[205]
	PTAA	Blade	ITO/PTAA/$MAPbI_3/C_{60}$/BCP/Cu	63.7	16.4	[206]
	PTAA	Blade	ITO/PTAA/$MAPbI_3/C_{60}$/BCP/Cu	21.5	17.8	[207]
	PTAA	Blade	ITO/PTAA/$MAPbI_3/C_{60}$/BCP/Cu	33	15.3	[208]
	PTAA	Blade	ITO/PTAA/SiO_2 NPs/$FA_{0.83}Cs_{0.17}Pb(I_{0.87}Br_{0.13})_3$ /PCBM/BCP/Ag	0.24	16.9	[209]
tandem	MeO-2PACz	Diping	CIGSe/AZO/2PACz/ $Cs_{0.05}(MA_{0.17}FA_{0.83})_{0.95}Pb(I_{0.83}Br_{0.17})_3/C_{60}/SnO_2$/IZO/Ag/LiF	1.06	22.4	[183]
	PTAA	Blade	Bottom cell/ITO/PTAA /$Cs_{0.05}(FA_{0.77}MA_{0.23})_{0.95}Pb(I_{0.77}Br_{0.23})_3/SnO_2/C_{60}$/ITO/Ag/PDMS	2.56	26.2	[210]
	PEDOT:PSS	Blade	Bottom cell/Au/PEDOT:PSS/ $MA_{0.3}FA_{0.7}Pb_{0.5}Sn_{0.5}I_3/C_{60}$/ALD-$SnO_2$/Ag	20	21.7[a]	[211]

[a] Certified PCE. All the other PCEs were measured in-house at the respective laboratories.

6. Conclusions and Outlook

Since recognizing the advantages of *p-i-n* PSCs, such as promise for commercialization and use in high-performance perovskite/silicon tandem solar cells, significant progress in their PCEs has been achieved, catching up with their *n-i-p* counterparts (as shown in **Figure 14**). In this, HTLs play a critical role in achieving a high PCE and long-term stability. In this review, we comprehensively

summarized organic HTL developments for *p-i-n* PSCs including materials such as conductive polymers, small molecules (SMs), and self-assembled monolayers (SAMs). For polymeric HTLs, attempts to improve device performance including chemical doping, inserting interfacial layers and structural modification are presented. SM-HTLs and SAM-HTLs are viewed to be excellent alternatives to polymers due to their well-defined structure, easy purification and well-adjusted structure. To improve the performance of the SM-HTLs, donor-acceptor (D-A) alternation and expansion of π conjugation have been proven to be efficient strategies due to the intrinsic polarity and high dipole moment, which can induce self-doping and built-in potential to enhance the charge extraction. However, an extended conjugation or D-A strategy will red shift the absorption of the HTL and induce parasitic absorption, mandating careful material optimization. SAM-HTLs offer multiple advantages such as a low material cost, compatibility with substrates with complex and large-area surfaces, tunable bandgap, higher transmittance and green-solvent processability. **Figure 14** summarizes the PCE vs. year of publications for polymers, SMs and SAMs HTLs. Emerging SAM-HTLs have shown a particularly rapid development, providing now among the highest performance for *p-i-n* PSCs.

On the basis of the discussion in this review, we propose the following design principles for HTLs for *p-i-n* PSCs: 1) well-aligned HOMO/LUMO levels to efficiently extract and block photogenerated holes and electrons, respectively; 2) sufficiently high hole mobility for efficient hole transport; 3) high transparency, enabled through a sufficiently wide band-gap to avoid competition of light absorption with perovskite; 4) a suitable solubility for solution processing, and sufficient chemical resilience against solvent washing such as DMF and DMSO, which are commonly used as solvents for perovskite precursors. Ideally, it should also be possible to be deposited on complex and large-area surfaces and dissolved in an eco-friendly solvent; 5) moderate hydrophobicity to ensure dense and smooth film morphology; 6) high stability to light, thermal and water during the device operation time; 7) low material cost.

Most of the reported HTLs were explored with one specific perovskite composition; some HTLs showed universality when employing various perovskite compositions ($MAPbI_3$, double cation, triple cation perovskite). At present, it is difficult to precisely classify which HTL is more suitable for a particular perovskite. Nevertheless, some correlations between HTLs and the perovskite type can be identified. First, the perovskite bandgap and energy levels can be tailored by cation and halide engineering. Therefore, for a particular perovskite, a well-aligned HOMO-LUMO energy level with the given perovskite is one of the selection criteria for a suitable HTL. Second, the HTL plays a critical

role in the crystallization process of the perovskite film. The S atom, carbonyl, pyridine and other Lewis base groups in the molecular structure of the HTLs can passivate the under-coordinated Pb ion through coordination. Here, an enhanced quality of perovskite polycrystalline film was observed for some HTL material system due to its suitable surface wettability and defect-passivation effect. Moreover, these coordination interactions can suppress light-induced phase segregation and defect formation, and thus improve the photostability of the device, especially for mixed-cation mixed-halide and all-inorganic perovskite. Besides, it was found the bottom side of mixed-cation mixed-halide perovskite has more inhomogeneities and sub-microscale imperfections.[212] These undesired complex phases, accumulating at the buried interfaces, limit device performance. HTLs with a functional passivation unit can mitigate these undesirable imperfections by varying the morphology and crystallographic structure through molecule-assisted microstructural reconstruction. Therefore, for mixed-cation mixed-halide (organic-inorganic hybrid and all-inorganic perovskite), the HTLs with functional passivation unit are more suitable.

Besides passivation, SAM-based PSCs showed a higher stability compared to PTAA-based cells under light-soaking stress.[183] A large number of excess charge carriers under illumination could lead to a lowered energetic threshold of ionic movement.[213] Negami et al. argued that light-induced iodide diffusion to the perovskite/HTL interface and the electrochemical reaction to form I_2 degrade the performance of PSCs.[214] In this regarding, polymers with long backbone and some SMs with complex molecular structure may suffer from partially structural damage due to the diffusion of I_2. Contrastingly, SAM and SMs with a simple molecular structure are more chemically robust, do not easily undergo structural destruction, nor lead to accumulation of ions. Considering realistic operation conditions at evaluated temperature and under sunlight, HTLs with compact and superior morphology, excellent passivation and relatively simple chemical structure can mitigate degradation processes such as through water penetration, ion migration and other undesirable changes.

Despite the stimulating studies summarized in this review, some challenges and issues need to be addressed that could accelerate the progress in future studies. Based on this review, the following research directions are worth attention. 1) as defect passivation is an efficient method to enhance the efficiency and stability of PSCs, the incorporation of passivation functional groups should be increasingly considered when designing molecules. These functional groups will interact with perovskite deposition and crystallization and influence the quality of perovskite layer. However, it is still unclear what precise HTL characteristics are necessary to form high-quality perovskite film. Some groups claim the functional groups may facilitate perovskite growth, while other groups

reported a nonwetting surface improves film quality. Therefore, the relationship between the functional group and film quality of perovskite requires detailed investigations. 2) The role of dipole moment of SAM-HTLs is still not fully clear. Besides charge extraction, the V_{OC} is also related to the built-in potential, induced by the intrinsic polarity and high dipole moment. The dipole moment effect is believed to be amplified when a monolayer is applied, therefore controlling the dipole moment of SAMs is an important topic to develop new SAMs. The modification of various anchoring and terminal groups is an efficient way to regulate the dipole strength and direction, thus systematic research on this is desired. 3) The selection of HTLs is still relatively limited and there is still much room in exploring new HTLs. The design of new HTLs is mainly from experience of previous literatures and the knowledge learned from similar research fields such as molecular electronics. However, precise prediction of the properties of new HTLs is still elusive. While theoretical calculations mainly provide information of energy levels and molecular configuration,[215] it hardly predicts the overall device performance, where results are typically only obtained after laborious material synthesis and device testing. To save resources and time, a machine learning method should be developed as a powerful computational tool by establishing databases containing reported materials.[216] A fast prescreening and better prediction of the designed materials could be achievable by this data-driven method.[217-218] Therefore, with a HTL database collected from literatures and summarized structure-performance relationship, the accelerated process of new and highly efficient HTLs is expected.

Finally, recent progress of organic HTLs in *p-i-n* PSCs is comprehensively summarized and we hope it can facilitate the innovations of ideal HTLs and the commercialization of PSCs. Meanwhile, the knowledge gained from studies on inverted PSCs can be implemented for developing efficient lead-free PSCs and perovskite light-emitting diodes (PeLEDs), expanding the application of these organic HTLs.

Conflict of Interest

The authors declare no conflict of interest.

Acknowledgements

We thank the financial support from NSF of China (62104197), the Funds for Basic Scientific Research in Central Universities (G2020KY0537).

Received: ()

Revised: ()

Published online: ()

References

[1] L. Hammarström, S. Hammes-Schiffer, *Accounts Chem. Res.* **2009**, *42*, 1859.

[2] M. A. Green, A. Ho-Baillie, H. J. Snaith, *Nat. Photonics* **2014**, *8*, 506.

[3] A. K. Jena, A. Kulkarni, T. Miyasaka, *Chem. Rev.* **2019**, *119*, 3036.

[4] A. Kojima, K. Teshima, Y. Shirai, T. Miyasaka, *J. Am. Chem. Soc.* **2009**, *131*, 6050.

[5] NREL, Best Research-Cell Efficiency Chart, https://www.nrel.gov/pv/cell-efficiency.html accessed: March 2022.

[6] J. H. Im, C. R. Lee, J. W. Lee, S. W. Park, N. G. Park, *Nanoscale* **2011**, *3*, 4088.

[7] H.-S. Kim, C.-R. Lee, J.-H. Im, K.-B. Lee, T. Moehl, A. Marchioro, S.-J. Moon, R. Humphry-Baker, J.-H. Yum, J. E. Moser, M. Grätzel, N.-G. Park, *Sci. Rep.* **2012**, *2*, 591.

[8] M. M. Lee, J. Teuscher, T. Miyasaka, T. N. Murakami, H. J. Snaith, *Science* **2012**, *338*, 643.

[9] J. Burschka, N. Pellet, S.-J. Moon, R. Humphry-Baker, P. Gao, M. K. Nazeeruddin, M. Grätzel, *Nature* **2013**, *499*, 316.

[10] M. Liu, M. B. Johnston, H. J. Snaith, *Nature* **2013**, *501*, 395.

[11] S. D. Stranks, G. E. Eperon, G. Grancini, C. Menelaou, M. J. Alcocer, T. Leijtens, L. M. Herz, A. Petrozza, H. J. Snaith, *Science* **2013**, *342*, 341.

[12] N. J. Jeon, J. H. Noh, Y. C. Kim, W. S. Yang, S. Ryu, S. I. Seok, *Nat. Mater.* **2014**, *13*, 897.

[13] H. Zhou, Q. Chen, G. Li, S. Luo, T. B. Song, H. S. Duan, Z. Hong, J. You, Y. Liu, Y. Yang, *Science* **2014**, *345*, 542.

[14] N. J. Jeon, J. H. Noh, W. S. Yang, Y. C. Kim, S. Ryu, J. Seo, S. I. Seok, *Nature* **2015**, *517*, 476.

[15] E. Bi, H. Chen, F. Xie, Y. Wu, W. Chen, Y. Su, A. Islam, M. Grätzel, X. Yang, L. Han, *Nat. Commun.* **2017**, *8*, 15330.

[16] M. Cai, Y. Wu, H. Chen, X. Yang, Y. Qiang, L. Han, *Adv. Sci.* **2017**, *4*, 1600269.

[17] K. T. Cho, S. Paek, G. Grancini, C. Roldán-Carmona, P. Gao, Y. Lee, M. K. Nazeeruddin, *Energy Environ. Sci.* **2017**, *10*, 621.

[18] J. K. Nam, S. U. Chai, W. Cha, Y. J. Choi, W. Kim, M. S. Jung, J. Kwon, D. Kim, J. H. Park, *Nano Lett.* **2017**, *17*, 2028.

[19] Y. B. Wang, Y. F. Yue, X. D. Yang, L. Y. Han, *Adv. Energy Mater.* **2018**, *8*, 1800249.

[20] Y. B. Wang, T. Wu, J. Barbaud, W. Kong, D. Cui, H. Chen, X. D. Yang, L. Y. Han, *Science* **2019**, *365*, 687.

[21] J. Ramanujam, U. P. Singh, *Energy Environ. Sci.* **2017**, *10*, 1306.

[22] Y. M. Yang, A. Yu, B. Hsu, W. C. Hsu, A. Yang, C. W. Lan, *Prog. Photovoltaics* **2015**, *23*, 340.

[23] L. Chao, T. Niu, W. Gao, C. Ran, L. Song, Y. Chen, W. Huang, *Adv. Mater.* **2021**, *33*, 2005410.

[24] F. Fu, J. Li, T. C. Yang, H. Liang, A. Faes, Q. Jeangros, C. Ballif, Y. Hou, *Adv. Mater.* **2022**, 2106540.

[25] S. Qin, C. Lu, Z. Jia, Y. Wang, S. Li, W. Lai, P. Shi, R. Wang, C. Zhu, J. Du, J. Zhang, L. Meng, Y. Li, *Adv. Mater.* **2022**, *34*, 2108829.

[26] D. Wang, H. Guo, X. Wu, X. Deng, F. Li, Z. Li, F. Lin, Z. Zhu, Y. Zhang, B. Xu, A. K. Y. Jen, *Adv. Funct. Mater.* **2021**, *32*, 2107359.

[27] J. Y. Kim, J. W. Lee, H. S. Jung, H. Shin, N. G. Park, *Chem. Rev.* **2020**, *120*, 7867.

[28] F. H. Isikgor, F. Furlan, J. Liu, E. Ugur, M. K. Eswaran, A. S. Subbiah, E. Yengel, M. De Bastiani, G. T. Harrison, S. Zhumagali, C. T. Howells, E. Aydin, M. Wang, N. Gasparini, T. G. Allen, A. u. Rehman, E. Van Kerschaver, D. Baran, I. McCulloch, T. D. Anthopoulos, U. Schwingenschlögl, F. Laquai, S. De Wolf, *Joule* **2021**, *5*, 1566.

[29] Z. Li, Y. Zhao, X. Wang, Y. Sun, Z. Zhao, Y. Li, H. Zhou, Q. Chen, *Joule* **2018**, *2*, 1559.

[30] J. Liu, E. Aydin, J. Yin, M. De Bastiani, F. H. Isikgor, A. U. Rehman, E. Yengel, E. Ugur, G. T. Harrison, M. Wang, Y. Gao, J. I. Khan, M. Babics, T. G. Allen, A. S. Subbiah, K. Zhu, X. Zheng, W. Yan, F. Xu, M. F. Salvador, O. M. Bakr, T. D. Anthopoulos, M. Lanza, O. F. Mohammed, F. Laquai, S. De Wolf, *Joule* **2021**, *5*, 3169.

[31] P. Wang, W. Li, O. J. Sandberg, C. Guo, R. Sun, H. Wang, D. Li, H. Zhang, S. Cheng, D. Liu, J. Min, A. Armin, T. Wang, *Nano Lett.* **2021**, *21*, 7845.

[32] W. Chen, Y. Zhu, J. Xiu, G. Chen, H. Liang, S. Liu, H. Xue, E. Birgersson, J. W. Ho, X. Qin, J. Lin, R. Ma, T. Liu, Y. He, A. M.-C. Ng, X. Guo, Z. He, H. Yan, A. B. Djurišić, Y. Hou, *Nat. Energy* **2022**, *7*, 229.

[33] M. De Bastiani, A. J. Mirabelli, Y. Hou, F. Gota, E. Aydin, T. G. Allen, J. Troughton, A. S. Subbiah, F. H. Isikgor, J. Liu, L. Xu, B. Chen, E. Van Kerschaver, D. Baran, B. Fraboni, M. F. Salvador, U. W. Paetzold, E. H. Sargent, S. De Wolf, *Nat. Energy* **2021**, *6*, 167.

[34] Y. Hou, E. Aydin, M. De Bastiani, C. Xiao, F. H. Isikgor, D. J. Xue, B. Chen, H. Chen, B. Bahrami, A. H. Chowdhury, A. Johnston, S. W. Baek, Z. Huang, M. Wei, Y. Dong, J. Troughton, R. Jalmood, A. J. Mirabelli, T. G. Allen, E. Van Kerschaver, M. I. Saidaminov, D. Baran, Q. Qiao, K. Zhu, S. De Wolf, E. H. Sargent, *Science* **2020**, *367*, 1135.

[35] M. De Bastiani, M. Babics, E. Aydin, A. S. Subbiah, L. Xu, S. De Wolf, *Sol. RRL* **2021**, *6*, 2100493.

[36] L. Calio, S. Kazim, M. Grätzel, S. Ahmad, *Angew. Chem. Int. Ed.* **2016**, *55*, 14522.

[37] X. Yin, L. Guan, J. Yu, D. Zhao, C. Wang, N. Shrestha, Y. Han, Q. An, J. Zhou, B. Zhou, Y. Yu, C. R. Grice, R. A. Awni, F. Zhang, J. Wang, R. J. Ellingson, Y. Yan, W. Tang, *Nano Energy* **2017**, *40*, 163.

[38] X. Yin, C. Wang, D. Zhao, N. Shrestha, C. R. Grice, L. Guan, Z. Song, C. Chen, C. Li, G. Chi, B. Zhou, J. Yu, Z. Zhang, R. J. Ellingson, J. Zhou, Y. Yan, W. Tang, *Nano Energy* **2018**, *51*, 680.

[39] C. Zuo, H. J. Bolink, H. Han, J. Huang, D. Cahen, L. Ding, *Adv. Sci.* **2016**, *3*, 1500324.

[40] H. Min, M. Kim, S.-U. Lee, H. Kim, G. Kim, K. Choi, J. H. Lee, S. I. Seok, *Science* **2019**, *366*, 749.

[41] M. Kim, G.-H. Kim, T. K. Lee, I. W. Choi, H. W. Choi, Y. Jo, Y. J. Yoon, J. W. Kim, J. Lee, D. Huh, H. Lee, S. K. Kwak, J. Y. Kim, D. S. Kim, *Joule* **2019**, *3*, 2179.

[42] P. Docampo, J. M. Ball, M. Darwich, G. E. Eperon, H. J. Snaith, *Nat. Commun.* **2013**, *4*, 2761.

[43] Y. Li, L. Meng, Y. M. Yang, G. Xu, Z. Hong, Q. Chen, J. You, G. Li, Y. Yang, Y. Li, *Nat. Commun.* **2016**, *7*, 10214.

[44] K. Rakstys, C. Igci, M. K. Nazeeruddin, *Chem. Sci.* **2019**, *10*, 6748.

[45] H. D. Pham, T. C. J. Yang, S. M. Jain, G. J. Wilson, P. Sonar, *Adv. Energy Mater.* **2020**, *10*, 1903326.

[46] W. Zhou, Z. Wen, P. Gao, *Adv. Energy Mater.* **2018**, *8*, 1702512.

[47] G. W. Kim, H. Choi, M. Kim, J. Lee, S. Y. Son, T. Park, *Adv. Energy Mater.* **2020**, *10*, 1903403.

[48] K. Gao, Z. Zhu, B. Xu, S. B. Jo, Y. Kan, X. Peng, A. K. Y. Jen, *Adv. Mater.* **2017**, *29*, 1703980.

[49] T. H. Schloemer, J. A. Christians, J. M. Luther, A. Sellinger, *Chem. Sci.* **2019**, *10*, 1904.

[50] Z. Song, A. Abate, S. C. Watthage, G. K. Liyanage, A. B. Phillips, U. Steiner, M. Graetzel, M. J. Heben, *Adv. Energy Mater.* **2016**, *6*, 1600846.

[51] S. Wang, Z. Huang, X. Wang, Y. Li, M. Gunther, S. Valenzuela, P. Parikh, A. Cabreros, W. Xiong, Y. S. Meng, *J. Am. Chem. Soc.* **2018**, *140*, 16720.

[52] A. Dualeh, T. Moehl, M. K. Nazeeruddin, M. Grätzel, *ACS Nano* **2013**, *7*, 2292.

[53] X. Yang, J. Xi, Y. Sun, Y. Zhang, G. Zhou, W.-Y. Wong, *Nano Energy* **2019**, *64*, 103946.

[54] H. S. Kim, I. H. Jang, N. Ahn, M. Choi, A. Guerrero, J. Bisquert, N. G. Park, *J. Phys. Chem. Lett.* **2015**, *6*, 4633.

[55] W. S. Yang, B. W. Park, E. H. Jung, N. J. Jeon, Y. C. Kim, D. U. Lee, S. S. Shin, J. Seo, E. K. Kim, J. H. Noh, S. I. Seok, *Science* **2017**, *356*, 1376.

[56] J. H. Heo, H. J. Han, D. Kim, T. K. Ahn, S. H. Im, *Energy Environ. Sci.* **2015**, *8*, 1602.

[57] F. Li, X. Deng, F. Qi, Z. Li, D. Liu, D. Shen, M. Qin, S. Wu, F. Lin, S. H. Jang, J. Zhang, X. Lu, D. Lei, C. S. Lee, Z. Zhu, A. K. Jen, *J. Am. Chem. Soc.* **2020**, *142*, 20134.

[58] Z. Yu, Z. Yang, Z. Ni, Y. Shao, B. Chen, Y. Lin, H. Wei, Z. J. Yu, Z. Holman, J. Huang, *Nat. Energy* **2020**, *5*, 657.

[59] R. Azmi, E. Ugur, A. Seitkhan, F. Aljamaan, A. S. Subbiah, J. Liu, G. T. Harrison, M. I. Nugraha, M. K. Eswaran, M. Babics, Y. Chen, F. Xu, T. G. Allen, A. U. Rehman, C. L. Wang, T. D. Anthopoulos, U. Schwingenschlogl, M. De Bastiani, E. Aydin, S. De Wolf, *Science* **2022**, *376*, 73.

[60] Z. Li, B. Li, X. Wu, S. A. Sheppard, S. Zhang, D. Gao, N. J. Long, Z. Zhu, *Science* **2022**, *376*, 416.

[61] M. Stolterfoht, C. M. Wolff, J. A. Márquez, S. Zhang, C. J. Hages, D. Rothhardt, S. Albrecht, P. L. Burn, P. Meredith, T. Unold, D. Neher, *Nat. Energy* **2018**, *3*, 847.

[62] W. Yan, Y. Li, Y. Li, S. Ye, Z. Liu, S. Wang, Z. Bian, C. Huang, *Nano Energy* **2015**, *16*, 428.

[63] J.-S. Yeo, R. Kang, S. Lee, Y.-J. Jeon, N. Myoung, C.-L. Lee, D.-Y. Kim, J.-M. Yun, Y.-H. Seo, S.-S. Kim, S.-I. Na, *Nano Energy* **2015**, *12*, 96.

[64] W. Yan, Y. Li, W. Sun, H. Peng, S. Ye, Z. Liu, Z. Bian, C. Huang, *RSC Adv.* **2014**, *4*, 33039.

[65] Y. Zhang, W. Liu, F. Tan, Y. Gu, *J. Power Sources* **2015**, *274*, 1224.

[66] W. Yan, Y. Li, Y. Li, S. Ye, Z. Liu, S. Wang, Z. Bian, C. Huang, *Nano Res.* **2015**, *8*, 2474.

[67] Z. Zhou, S. Pang, Z. Liu, H. Xu, G. Cui, *J. Mater. Chem. A* **2015**, *3*, 19205.

[68] J. Y. Jeng, K. C. Chen, T. Y. Chiang, P. Y. Lin, T. D. Tsai, Y. C. Chang, T. F. Guo, P. Chen, T. C. Wen, Y. J. Hsu, *Adv. Mater.* **2014**, *26*, 4107.

[69] S. Sajid, A. M. Elseman, H. Huang, J. Ji, S. Dou, H. Jiang, X. Liu, D. Wei, P. Cui, M. Li, *Nano Energy* **2018**, *51*, 408.

[70] Z. Zhu, Y. Bai, T. Zhang, Z. Liu, X. Long, Z. Wei, Z. Wang, L. Zhang, J. Wang, F. Yan, S. Yang, *Angew. Chem. Int. Ed.* **2014**, *53*, 12571.

[71] H. Park, R. Chaurasiya, B. H. Jeong, P. Sakthivel, H. J. Park, *Adv. Photonics Res.* **2021**, *2*, 2000178.

[72] C. C. Boyd, R. C. Shallcross, T. Moot, R. Kerner, L. Bertoluzzi, A. Onno, S. Kavadiya, C. Chosy, E. J. Wolf, J. Werner, J. A. Raiford, C. de Paula, A. F. Palmstrom, Z. J. Yu, J. J. Berry, S. F. Bent, Z. C. Holman, J. M. Luther, E. L. Ratcliff, N. R. Armstrong, M. D. McGehee, *Joule* **2020**, *4*, 1759.

[73] L. Bertoluzzi, C. C. Boyd, N. Rolston, J. Xu, R. Prasanna, B. C. O'Regan, M. D. McGehee, *Joule* **2020**, *4*, 109.

[74] W. Han, G. Ren, Z. Li, M. Dong, C. Liu, W. Guo, *J. Energy Chem.* **2020**, *46*, 202.

[75] R. Rhee, S. Im, H. Lee, J. H. Lee, Y. Kim, D. H. Chun, C. Park, S. Lee, J. H. Kim, J. H. Park, *ACS Sustain. Chem. Eng.* **2020**, *8*, 8004.

[76] F. Ali, C. Roldán-Carmona, M. Sohail, M. K. Nazeeruddin, *Adv. Energy Mater.* **2020**, *10*, 2002989.

[77] S. Y. Kim, S. J. Cho, S. E. Byeon, X. He, H. J. Yoon, *Adv. Energy Mater.* **2020**, *10*, 2002606.

[78] K. Choi, H. Choi, J. Min, T. Kim, D. Kim, S. Y. Son, G.-W. Kim, J. Choi, T. Park, *Sol. RRL* **2019**, *4*, 1900251.

[79] D. Venkateshvaran, M. Nikolka, A. Sadhanala, V. Lemaur, M. Zelazny, M. Kepa, M. Hurhangee, A. J. Kronemeijer, V. Pecunia, I. Nasrallah, I. Romanov, K. Broch, I. McCulloch, D. Emin, Y. Olivier, J. Cornil, D. Beljonne, H. Sirringhaus, *Nature* **2014**, *515*, 384.

[80] Y. Liu, L. A. Renna, Z. A. Page, H. B. Thompson, P. Y. Kim, M. D. Barnes, T. Emrick, D. Venkataraman, T. P. Russell, *Adv. Energy Mater.* **2016**, *6*, 1600664.

[81] X. Li, X. Liu, X. Wang, L. Zhao, T. Jiu, J. Fang, *J. Mater. Chem. A* **2015**, *3*, 15024.

[82] Y. Yang, C. Zhu, F. Lin, T. Chen, D. Pan, X. Guo, *Acta Chim. Sin.* **2019**, *77*, 964.

[83] L. V. Kayser, D. J. Lipomi, *Adv. Mater.* **2019**, *31*, 1806133.

[84] D. B. Khadka, Y. Shirai, M. Yanagida, J. W. Ryan, K. Miyano, *J. Mater. Chem. C* **2017**, *5*, 8819.

[85] Q. Wei, M. Mukaida, Y. Naitoh, T. Ishida, *Adv. Mater.* **2013**, *25*, 2831.

[86] K.-G. Lim, S. Ahn, Y.-H. Kim, Y. Qi, T.-W. Lee, *Energy Environ. Sci.* **2016**, *9*, 932.

[87] K. M. Reza, S. Mabrouk, Q. Qiao, *Proc. Nat. Res. Soc* **2018**, *2*, 02004.

[88] J. Y. Jeng, Y. F. Chiang, M. H. Lee, S. R. Peng, T. F. Guo, P. Chen, T. C. Wen, *Adv. Mater.* **2013**, *25*, 3727.

[89] K. M. Reza, A. Gurung, B. Bahrami, S. Mabrouk, H. Elbohy, R. Pathak, K. Chen, A. H. Chowdhury, M. T. Rahman, S. Letourneau, H.-C. Yang, G. Saianand, J. W. Elam, S. B. Darling, Q. Qiao, *J. Energy Chem.* **2020**, *44*, 41.

[90] C. Redondo-Obispo, T. S. Ripolles, S. Cortijo-Campos, A. L. Álvarez, E. Climent-Pascual, A. de Andrés, C. Coya, *Mater. Des.* **2020**, *191*, 108587.

[91] K. Chen, Q. Hu, T. Liu, L. Zhao, D. Luo, J. Wu, Y. Zhang, W. Zhang, F. Liu, T. P. Russell, R. Zhu, Q. Gong, *Adv. Mater.* **2016**, *28*, 10718.

[92] L. Hu, M. Li, K. Yang, Z. Xiong, B. Yang, M. Wang, X. Tang, Z. Zang, X. Liu, B. Li, Z. Xiao, S. Lu, H. Gong, J. Ouyang, K. Sun, *J. Mater. Chem. A* **2018**, *6*, 16583.

[93] J. C. Yu, J. A. Hong, E. D. Jung, D. B. Kim, S. M. Baek, S. Lee, S. Cho, S. S. Park, K. J. Choi, M. H. Song, *Sci. Rep.* **2018**, *8*, 1070.

[94] Z. Zhao, L. Yuan, J. Huang, J. Shi, Y. Cao, W. Zi, W. Zhang, *Org. Electron.* **2020**, *78*, 105557.

[95] W. Hu, C. Y. Xu, L. B. Niu, A. M. Elseman, G. Wang, B. Liu, Y. Q. Yao, L. P. Liao, G. D. Zhou, Q. L. Song, *ACS Appl. Mater. Interfaces* **2019**, *11*, 22021.

[96] L. Xu, Y. Li, C. Zhang, Y. Liu, C. Zheng, W. Lv, M. Li, Y. Chen, W. Huang, R. Chen, *Sol. Energy Mater. Sol. Cells* **2020**, *206*, 110316.

[97] A. Ali, Y. Ahn, K. A. Khawaja, J. H. Kang, Y. J. Park, J. H. Seo, B. Walker, *Adv. Funct. Mater.* **2021**, *31*, 2009246.

[98] L. Xu, M. Qian, C. Zhang, W. Lv, J. Jin, J. Zhang, C. Zheng, M. Li, R. Chen, W. Huang, *Nano Energy* **2020**, *67*, 104244.

[99] Y.-C. Chin, M. Daboczi, C. Henderson, J. Luke, J.-S. Kim, *ACS Energy Lett.* **2022**, *7*, 560.

[100] C. Xu, Y. Yao, G. Wang, J. Dong, G. Xu, Y. Zhong, D. Lu, X. Zhao, D. Liu, G. Zhou, X. Yang, P. Li, L. Chen, Q. Song, *Chem. Eng. J.* **2022**, *428*, 132074.

[101]D. Zhao, M. Sexton, H.-Y. Park, G. Baure, J. C. Nino, F. So, *Adv. Energy Mater*. **2015**, *5*, 1401855.

[102] X. Hu, C. Tao, J. Liang, C. Chen, X. Zheng, J. Li, J. Li, Y. Liu, G. Fang, *Sol. Energy* **2021**, *218*, 368.

[103] X. Xu, C. Ma, Y. Cheng, Y.-M. Xie, X. Yi, B. Gautam, S. Chen, H.-W. Li, C.-S. Lee, F. So, S.-W. Tsang, *J. Power Sources* **2017**, *360*, 157.

[104] F. Zhang, Y. Hou, S. Wang, H. Zhang, F. Zhou, Y. Hao, S. Ye, H. Cai, J. Song, J. Qu, *Sol. RRL* **2021**, *5*, 2100190.

[105] Y. Li, B. Wang, T. Liu, Q. Zeng, D. Cao, H. Pan, G. Xing, *ACS Appl. Mater. Interfaces* **2022**, *14*, 3284

[106] J. Xu, J. Dai, H. Dong, P. Li, J. Chen, X. Zhu, Z. Wang, B. Jiao, X. Hou, J. Li, Z. Wu, *Org. Electron.* **2022**, *100*, 106378.

[107] W. Zhang, J. Smith, R. Hamilton, M. Heeney, J. Kirkpatrick, K. Song, S. E. Watkins, T. Anthopoulos, I. McCulloch, *J. Am. Chem. Soc.* **2009**, *131*, 10814.

[108] J. Huang, Y. Yuan, Y. Shao, Y. Yan, *Nat. Rev. Mater.* **2017**, *2*, 17042.

[109] C. Bi, Q. Wang, Y. Shao, Y. Yuan, Z. Xiao, J. Huang, *Nat. Commun.* **2015**, *6*, 7747.

[110] F. H. Isikgor, A. S. Subbiah, M. K. Eswaran, C. T. Howells, A. Babayigit, M. De Bastiani, E. Yengel, J. Liu, F. Furlan, G. T. Harrison, S. Zhumagali, J. I. Khan, F. Laquai, T. D. Anthopoulos, I. McCulloch, U. Schwingenschlögl, S. De Wolf, *Nano Energy* **2021**, *81*, 105633.

[111] Z. Bagheri, F. Matteocci, E. Lamanna, D. Di Girolamo, A. G. Marrani, R. Zanoni, A. Di Carlo, A. Moshaii, *Sol. Energy Mater. Sol. Cells* **2020**, *215*, 110606.

[112] J. Luo, J. Xia, H. Yang, L. Chen, Z. Wan, F. Han, H. A. Malik, X. Zhu, C. Jia, *Energy Environ. Sci.* **2018**, *11*, 2035.

[113] Y. Kim, E. H. Jung, G. Kim, D. Kim, B. J. Kim, J. Seo, *Adv. Energy Mater.* **2018**, *8*, 1801668.

[114] Q. Wang, C. Bi, J. Huang, *Nano Energy* **2015**, *15*, 275.

[115] C. Wang, Z. Su, L. Chen, H. Zhang, W. Hui, D. Liang, G. Zheng, L. Zhang, Z. Tang, W. Wen, J. Tang, Q. Huang, F. Song, Q. Chen, X. Gao, *Appl. Surf. Sci.* **2022**, *571*, 151301.

[116] W. Dong, S. Xiong, J. Yang, W. Qiao, Q. Zeng, X. Wang, Y. Yao, Q. Bao, *Org. Electron.* **2021**, *89*, 106052.

[117] L. Xu, Y. Liu, W. Qiu, Y. Li, H. Wang, M. Li, L. Xian, C. Zheng, Y. Chen, R. Chen, *J. Power Sources* **2021**, *506*, 230120.

[118] H. Liu, H.-R. Liu, F. Yang, J.-E. Yang, J. Song, M. Li, Z. Li, W. C. Tsoi, M. Chinweokwu Eze, Z.-Y. Liu, H. Ma, M. Gao, Z.-K. Wang, *J. Power Sources* **2020**, *448*, 227420.

[119] Q. Zhou, J. Qiu, Y. Wang, M. Yu, J. Liu, X. Zhang, *ACS Energy Lett.* **2021**, *6*, 1596.

[120] C. Y. Xu, W. Hu, G. Wang, L. Niu, A. M. Elseman, L. Liao, Y. Yao, G. Xu, L. Luo, D. Liu, G. Zhou, P. Li, Q. Song, *ACS Nano* **2020**, *14*, 196.

[121] X. Liu, Y. Cheng, C. Liu, T. Zhang, N. Zhang, S. Zhang, J. Chen, Q. Xu, J. Ouyang, H. Gong, *Energy Environ. Sci.* **2019**, *12*, 1622.

[122] H. Javaid, V. V. Duzhko, D. Venkataraman, *ACS Appl. Energy Mater.* **2021**, *4*, 72.

[123] N. Tzoganakis, B. Feng, M. Loizos, M. Krassas, D. Tsikritzis, X. Zhuang, E. Kymakis, *J. Mater. Chem. C* **2021**, *9*, 14709.

[124] X. Xu, X. Ji, R. Chen, F. Ye, S. Liu, S. Zhang, W. Chen, Y. Wu, W. H. Zhu, *Adv. Funct. Mater.* **2021**, *32*, 2109968.

[125] X. Sun, Z. Li, X. Yu, X. Wu, C. Zhong, D. Liu, D. Lei, A. K. Jen, Z. Li, Z. Zhu, *Angew. Chem. Int. Ed.* **2021**, *60*, 7227.

[126] Q. Liao, Y. Wang, X. Yao, M. Su, B. Li, H. Sun, J. Huang, X. Guo, *ACS Appl. Mater. Interfaces* **2021**, *13*, 16744.

[127] S. Li, B. He, J. Xu, H. Lu, J. Jiang, J. Zhu, Z. Kan, L. Zhu, F. Wu, *Nanoscale* **2020**, *12*, 3686.

[128] L. Zhang, X. Zhou, J. Xie, S. Chen, S. Bae, J. Kim, B. Xu, *J. Mater. Chem. A* **2020**, *8*, 8238.

[129] X. Li, W. Zhang, X. Guo, C. Lu, J. Wei, J. Fang, *Science* **2022**, *375*, 434.

[130] Y. Mei, Z. Shen, S. Kundu, E. Dennis, S. Pang, F. Tan, G. Yue, Y. Gao, C. Dong, R. Liu, W. Zhang, M. I. Saidaminov, *Chem. Mater.* **2021**, *33*, 4679.

[131] X. Sun, X. Deng, Z. Li, B. Xiong, C. Zhong, Z. Zhu, Z. Li, A. K. Jen, *Adv. Sci.* **2020**, *7*, 1903331.

[132] W. Li, C. Liu, Y. Li, W. Kong, X. Wang, H. Chen, B. Xu, C. Cheng, *Sol. RRL* **2018**, *2*, 1800173.

[133] L. Zhang, X. Zhou, X. Zhong, C. Cheng, Y. Tian, B. Xu, *Nano Energy* **2019**, *57*, 248.

[134] W. Nie, H. Tsai, R. Asadpour, J. C. Blancon, A. J. Neukirch, G. Gupta, J. J. Crochet, M. Chhowalla, S. Tretiak, M. A. Alam, H. L. Wang, A. D. Mohite, *Science* **2015**, *347*, 522.

[135] X. Zheng, B. Chen, J. Dai, Y. Fang, Y. Bai, Y. Lin, H. Wei, Xiao C. Zeng, J. Huang, *Nat. Energy* **2017**, *2*, 17102.

[136] H. Kang, G. Kim, J. Kim, S. Kwon, H. Kim, K. Lee, *Adv. Mater.* **2016**, *28*, 7821.

[137] M. Jørgensen, K. Norrman, F. C. Krebs, *Sol. Energy Mater. Sol. Cells* **2008**, *92*, 686.

[138] K. Norrman, M. V. Madsen, S. A. Gevorgyan, F. C. Krebs, *J. Am. Chem. Soc.* **2010**, *132*, 16883.

[139] A. E. Labban, H. Chen, M. Kirkus, J. Barbe, S. Del Gobbo, M. Neophytou, I. McCulloch, J. Eid, *Adv. Energy Mater.* **2016**, *6*, 1502101.

[140] K. Jiang, J. Wang, F. Wu, Q. Xue, Q. Yao, J. Zhang, Y. Chen, G. Zhang, Z. Zhu, H. Yan, L. Zhu, H. L. Yip, *Adv. Mater.* **2020**, *32*, 1908011.

[141] J. Wang, Y. Chen, M. Liang, G. Ge, R. Zhou, Z. Sun, S. Xue, *Dyes Pigment.* **2016**, *125*, 399.

[142] K. Rakstys, A. Abate, M. I. Dar, P. Gao, V. Jankauskas, G. Jacopin, E. Kamarauskas, S. Kazim, S. Ahmad, M. Grätzel, M. K. Nazeeruddin, *J. Am. Chem. Soc.* **2015**, *137*, 16172.

[143] C. Huang, W. Fu, C. Z. Li, Z. Zhang, W. Qiu, M. Shi, P. Heremans, A. K. Jen, H. Chen, *J. Am. Chem. Soc.* **2016**, *138*, 2528.

[144] H. Chen, W. Fu, C. Huang, Z. Zhang, S. Li, F. Ding, M. Shi, C.-Z. Li, A. K. Y. Jen, H. Chen, *Adv. Energy Mater.* **2017**, *7*, 1700012.

[145] B. Wang, Q. Zeng, Z. Sun, S. Xue, M. Liang, *Dyes Pigment.* **2019**, *165*, 81.

[146] X. Sun, Q. Xue, Z. Zhu, Q. Xiao, K. Jiang, H. L. Yip, H. Yan, Z. Li, *Chem. Sci.* **2018**, *9*, 2698.

[147] W. Chen, Y. Wang, B. Liu, Y. Gao, Z. Wu, Y. Shi, Y. Tang, K. Yang, Y. Zhang, W. Sun, X. Feng, F. Laquai, H. Y. Woo, A. B. Djurišić, X. Guo, Z. He, *Sci. China Chem.* **2021**, *64*, 41.

[148] Y. Cao, Y. Li, T. Morrissey, B. Lam, B. O. Patrick, D. J. Dvorak, Z. Xia, T. L. Kelly, C. P. Berlinguette, *Energy Environ. Sci.* **2019**, *12*, 3502.

[149] J. Zhang, Q. Sun, Q. Chen, Y. Wang, Y. Zhou, B. Song, N. Yuan, J. Ding, Y. Li, *Adv. Funct. Mater.* **2019**, *29*, 1900484.

[150] Y. Zhang, C. Kou, J. Zhang, Y. Liu, W. Li, Z. Bo, M. Shao, *J. Mater. Chem. A* **2019**, *7*, 5522.

[151] Q. Q. Ge, J. Y. Shao, J. Ding, L. Y. Deng, W. K. Zhou, Y. X. Chen, J. Y. Ma, L. J. Wan, J. Yao, J. S. Hu, Y. W. Zhong, *Angew. Chem. Int. Ed.* **2018**, *57*, 10959.

[152] R. Chen, T. Bu, J. Li, W. Li, P. Zhou, X. Liu, Z. Ku, J. Zhong, Y. Peng, F. Huang, Y. B. Cheng, Z. Fu, *ChemSusChem* **2018**, *11*, 1467.

[153] Y. C. Chen, Y. H. Li, C. L. Chung, H. L. Hsu, C. P. Chen, *Prog. Photovoltaics* **2019**, *28*, 49.

[154] M. Neophytou, J. Griffiths, J. Fraser, M. Kirkus, H. Chen, C. B. Nielsen, I. McCulloch, *J. Mater. Chem. C* **2017**, *5*, 4940.

[155] H. D. Pham, H. Hu, K. Feron, S. Manzhos, H. Wang, Y. M. Lam, P. Sonar, *Sol. RRL* **2017**, *1*, 1700105.

[156] Y. Li, Z. Xu, S. Zhao, B. Qiao, D. Huang, L. Zhao, J. Zhao, P. Wang, Y. Zhu, X. Li, X. Liu, X. Xu, *Small* **2016**, *12*, 4902.

[157] K. Yang, Q. Liao, J. Huang, Z. Zhang, M. Su, Z. Chen, Z. Wu, D. Wang, Z. Lai, H. Y. Woo, Y. Cao, P. Gao, X. Guo, *Angew. Chem. Int. Ed.* **2022**, *61*, 202113749.

[158] S. J. Park, S. Jeon, I. K. Lee, J. Zhang, H. Jeong, J.-Y. Park, J. Bang, T. K. Ahn, H.-W. Shin, B.-G. Kim, H. J. Park, *J. Mater. Chem. A* **2017**, *5*, 13220.

[159] L. Yang, F. Cai, Y. Yan, J. Li, D. Liu, A. J. Pearson, T. Wang, *Adv. Funct. Mater.* **2017**, *27*, 1702613.

[160] W. Li, H. Liu, C. Liu, W. Kong, H. Chen, W. Wang, H. Zhang, X. Zhang, C. Cheng, *J. Mater. Chem. A* **2020**, *8*, 16560.

[161] X. Lai, M. Du, F. Meng, G. Li, W. Li, A. K. K. Kyaw, Y. Wen, C. Liu, H. Ma, R. Zhang, D. Fan, X. Guo, Y. Wang, H. Ji, K. Wang, X. W. Sun, J. Wang, W. Huang, *Small* **2019**, *15*, 1904715.

[162] E. Zhu, J. Wang, J. Xu, L. Fu, R. Li, C. Yu, S. Ge, X. Lin, R. Chen, H. Wu, H. L. Wang, G. Che, *ACS Appl. Mater. Interfaces* **2021**, *13*, 13254.

[163] C. Wang, J. Hu, C. Li, S. Qiu, X. Liu, L. Zeng, C. Liu, Y. Mai, F. Guo, *Sol. RRL* **2019**, *4*, 1900389.

[164] N. Liu, X. Zong, Z. Wang, T. Cui, M. Liang, Y. Zhang, S. Xue, *Electrochim. Acta* **2019**, *296*, 283.

[165] Y. Wang, W. Chen, L. Wang, B. Tu, T. Chen, B. Liu, K. Yang, C. W. Koh, X. Zhang, H. Sun, G. Chen, X. Feng, H. Y. Woo, A. B. Djurisic, Z. He, X. Guo, *Adv. Mater.* **2019**, *31*, 1902781.

[166] I. Zimmermann, J. Urieta-Mora, P. Gratia, J. Aragó, G. Grancini, A. Molina-Ontoria, E. Ortí, N. Martín, M. K. Nazeeruddin, *Adv. Energy Mater.* **2016**, *7*, 1601674.

[167] S. S. Reddy, S. Shin, U. K. Aryal, R. Nishikubo, A. Saeki, M. Song, S.-H. Jin, *Nano Energy* **2017**, *41*, 10.

[168] Y. Wang, Q. Liao, J. Chen, W. Huang, X. Zhuang, Y. Tang, B. Li, X. Yao, X. Feng, X. Zhang, M. Su, Z. He, T. J. Marks, A. Facchetti, X. Guo, *J. Am. Chem. Soc.* **2020**, *142*, 16632.

[169] F. Gao, Y. Zhao, X. Zhang, J. You, *Adv. Energy Mater.* **2019**, *10*, 1902650.

[170] L. K. Ono, S. F. Liu, Y. Qi, *Angew. Chem. Int. Ed.* **2020**, *59*, 6676.

[171] R. Shang, Z. Zhou, H. Nishioka, H. Halim, S. Furukawa, I. Takei, N. Ninomiya, E. Nakamura, *J. Am. Chem. Soc.* **2018**, *140*, 5018.

[172] C.-H. Chen, Y.-T. Hsu, B.-C. Wang, C.-L. Chung, C.-P. Chen, *J. Phys. Chem. C* **2018**, *123*, 1602.

[173] Y. Chen, X. Xu, N. Cai, S. Qian, R. Luo, Y. Huo, S. W. Tsang, *Adv. Energy Mater.* **2019**, *9*, 1901268.

[174] N. Cai, F. Li, Y. Chen, R. Luo, T. Hu, F. Lin, S. M. Yiu, D. Liu, D. Lei, Z. Zhu, A. K. Jen, *Angew. Chem. Int. Ed.* **2021**, *60*, 20437.

[175] M. Mas-Montoya, P. Gomez, D. Curiel, I. da Silva, J. Wang, R. A. J. Janssen, *Chem. Eur. J.* **2020**, *26*, 10276.

[176] P. Gómez, J. Wang, M. Más-Montoya, D. Bautista, C. H. L. Weijtens, D. Curiel, R. A. J. Janssen, *Sol. RRL* **2021**, *5*, 2100454.

[177] C. U. Kim, E. D. Jung, Y. W. Noh, S. K. Seo, Y. Choi, H. Park, M. H. Song, K. J. Choi, *EcoMat* **2021**, *3*, 12084.

[178] F. Lang, M. A. Gluba, S. Albrecht, J. Rappich, L. Korte, B. Rech, N. H. Nickel, *J. Phys. Chem. Lett.* **2015**, *6*, 2745.

[179] T. Bauer, T. Schmaltz, T. Lenz, M. Halik, B. Meyer, T. Clark, *ACS Appl. Mater. Interfaces* **2013**, *5*, 6073.

[180] P. J. Hotchkiss, S. C. Jones, S. A. Paniagua, A. Sharma, B. Kippelen, N. R. Armstrong, S. R. Marder, *Accounts Chem. Res.* **2012**, *45*, 337.

[181] F. Ambrosio, N. Martsinovich, A. Troisi, *J. Phys. Chem. Lett.* **2012**, *3*, 1531.

[182] A. Magomedov, A. Al-Ashouri, E. Kasparavičius, S. Strazdaite, G. Niaura, M. Jošt, T. Malinauskas, S. Albrecht, V. Getautis, *Adv. Energy Mater.* **2018**, *8*, 1801892.

[183] A. Al-Ashouri, A. Magomedov, M. Roß, M. Jošt, M. Talaikis, G. Chistiakova, T. Bertram, J. A. Márquez, E. Köhnen, E. Kasparavičius, S. Levcenco, L. Gil-Escrig, C. J. Hages, R. Schlatmann, B. Rech, T. Malinauskas, T. Unold, C. A. Kaufmann, L. Korte, G. Niaura, V. Getautis, S. Albrecht, *Energy Environ. Sci.* **2019**, *12*, 3356.

[184] E. Yalcin, M. Can, C. Rodriguez-Seco, E. Aktas, R. Pudi, W. Cambarau, S. Demic, E. Palomares, *Energy Environ. Sci.* **2019**, *12*, 230.

[185] E. Aktas, N. Phung, H. Köbler, D. A. González, M. Méndez, I. Kafedjiska, S.-H. Turren-Cruz, R. Wenisch, I. Lauermann, A. Abate, E. Palomares, *Energy Environ. Sci.* **2021**, *14*, 3976.

[186] E. Li, E. Bi, Y. Wu, W. Zhang, L. Li, H. Chen, L. Han, H. Tian, W. H. Zhu, *Adv. Funct. Mater.* **2019**, *30*, 1909509.

[187] E. Li, C. Liu, H. Lin, X. Xu, S. Liu, S. Zhang, M. Yu, X. M. Cao, Y. Wu, W. H. Zhu, *Adv. Funct. Mater.* **2021**, *31*, 2103847.

[188] A. Ullah, K. H. Park, H. D. Nguyen, Y. Siddique, S. F. A. Shah, H. Tran, S. Park, S. I. Lee, K. K. Lee, C. H. Han, K. Kim, S. Ahn, I. Jeong, Y. S. Park, S. Hong, *Adv. Energy Mater.* **2021**, *12*, 2103175.

[189] N. Singh, A. Mohapatra, C.-W. Chu, Y.-T. Tao, *Org. Electron.* **2021**, *98*, 106297.

[190] E. Arkan, E. Yalcin, M. Unal, M. Z. Y. Arkan, M. Can, C. Tozlu, S. Demic, *Mater. Chem. Phys.* **2020**, *254*, 123435.

[191] E. Arkan, M. Unal, E. Yalcin, M. Z. Yigit Arkan, S. Yurtdas, M. Can, C. Tozlu, S. Demic, *Mater. Sci. Semicond. Process.* **2021**, *123*, 105514.

[192] E. Arkan, M. Z. Yigit Arkan, M. Unal, E. Yalcin, H. Aydin, C. Celebi, M. Can, C. Tozlu, S. Demic, *Opt. Mater.* **2020**, *105*, 109910.

[193] A. Al-Ashouri, E. Kohnen, B. Li, A. Magomedov, H. Hempel, P. Caprioglio, J. A. Marquez, A. B. Morales Vilches, E. Kasparavicius, J. A. Smith, N. Phung, D. Menzel, M. Grischek, L. Kegelmann, D. Skroblin, C. Gollwitzer, T. Malinauskas, M. Jost, G. Matic, B. Rech, R. Schlatmann, M. Topic, L. Korte, A. Abate, B. Stannowski, D. Neher, M. Stolterfoht, T. Unold, V. Getautis, S. Albrecht, *Science* **2020**, *370*, 1300.

[194] R. Azmi, E. Ugur, A. Seitkhan, F. Aljamaan, A. S. Subbiah, J. Liu, G. T. Harrison, M. I. Nugraha, M. K. Eswaran, M. Babics, Y. Chen, F. Xu, T. G. Allen, A. U. Rehman, C. L. Wang, T. D. Anthopoulos, U. Schwingenschlogl, M. De Bastiani, E. Aydin, S. De Wolf, *Science* **2022**, *367*, 73.

[195] B. Chen, S. W. Baek, Y. Hou, E. Aydin, M. De Bastiani, B. Scheffel, A. Proppe, Z. Huang, M. Wei, Y. K. Wang, E. H. Jung, T. G. Allen, E. Van Kerschaver, F. P. Garcia de Arquer, M. I. Saidaminov, S. Hoogland, S. De Wolf, E. H. Sargent, *Nat. Commun.* **2020**, *11*, 1257.

[196] D. Song, S. Narra, M.-Y. Li, J.-S. Lin, E. W.-G. Diau, *ACS Energy Lett.* **2021**, *6*, 4179.

[197] M. M. Tepliakova, A. V. Akkuratov, S. A. Tsarev, P. A. Troshin, *Tetrahedron Lett*. **2020**, *61*, 152317.

[198] C. Zuo, D. Vak, D. Angmo, L. Ding, M. Gao, *Nano Energy* **2018**, *46*, 185.

[199] C. Zuo, A. D. Scully, D. Vak, W. Tan, X. Jiao, C. R. McNeill, D. Angmo, L. Ding, M. Gao, *Adv. Energy Mater*. **2019**, *9*, 1803258.

[200] J.-E. Kim, S.-S. Kim, C. Zuo, M. Gao, D. Vak, D.-Y. Kim, *Adv. Funct. Mater.***2019**, *29*, 1809194.

[201] M. Othman, F. Zheng, A. Seeber, A. S. R. Chesman, A. D. Scully, K. P. Ghiggino, M. Gao, J. Etheridge, D. Angmo, *Adv. Funct. Mater.* **2021**, *32*, 2110700.

[202] T. M. Schmidt, T. T. Larsen-Olsen, J. E. Carlé, D. Angmo, F. C. Krebs, *Adv. Energy Mater.* **2015**, *5,* 1500569.

[203] Z. Yang, C.-C. Chueh, F. Zuo, J. H. Kim, P.-W. Liang, A. K. Y. Jen, *Adv. Energy Mater*. **2015**, *5*, 1500328.

[204] W. Q. Wu, Z. Yang, P. N. Rudd, Y. Shao, X. Dai, H. Wei, J. Zhao, Y. Fang, Q. Wang, Y. Liu, Y. Deng, X. Xiao, Y. Feng, J. Huang, *Sci. Adv*. **2019**, *5*, 8925.

[205] J. Küffner, T. Wahl, M. Schultes, J. Hanisch, J. Zillner, E. Ahlswede, M. Powalla, *ACS Appl. Mater. Interfaces* **2020**, *12*, 52678.

[206] Y. Deng, C. H. Van Brackle, X. Dai, J. Zhao, B. Chen, J. Huang, *Sci. Adv*. **2019**, *5*, 7537.

[207] Y. Deng, Z. Ni, A. F. Palmstrom, J. Zhao, S. Xu, C. H. Van Brackle, X. Xiao, K. Zhu, J. Huang, *Joule* **2020**, *4*, 1949.

[208] Y. Deng, X. Zheng, Y. Bai, Q. Wang, J. Zhao, J. Huang, *Nat. Energy* **2018**, *3*, 560.

[209] J. Küffner, J. Hanisch, T. Wahl, J. Zillner, E. Ahlswede, M. Powalla, *ACS Appl. Mater. Interfaces* **2021**, *4*, 11700.

[210] B. Chen, Z. J. Yu, S. Manzoor, S. Wang, W. Weigand, Z. Yu, G. Yang, Z. Ni, X. Dai, Z. C. Holman, J. Huang, *Joule* **2020**, *4*, 850.

[211] K. Xiao, Y. H. Lin, M. Zhang, R. D. J. Oliver, X. Wang, Z. Liu, X. Luo, J. Li, D. Lai, H. Luo, R. Lin, J. Xu, Y. Hou, H. J. Snaith, H. Tan, *Science* **2022**, *376*, 762.

[212] X. Yang, D. Luo, Y. Xiang, L. Zhao, M. Anaya, Y. Shen, J. Wu, W. Yang, Y.-H. Chiang, Y. Tu, R. Su, Q. Hu, H. Yu, G. Shao, W. Huang, T. P. Russell, Q. Gong, S. D. Stranks, W. Zhang, R. Zhu, *Adv. Mater.* **2021**, *33*, 2006435.

[213] B. Chen, J. Song, X. Dai, Y. Liu, P. N. Rudd, X. Hong, J. Huang, *Adv. Mater*. **2019,** *31*, 1902413.

[214] T. Sekimoto, T. Matsui, T. Nishihara, R. Uchida, T. Sekiguchi, T. Negami, *ACS Appl. Mater. Interfaces* **2019**, *2*, 5039.

[215] H. A. Chen, C. W. Pao, *ACS Omega.* **2019**, *4*, 10950.

[216] T. J. Jacobsson, A. Hultqvist, A. García-Fernández, A. Anand, A. Al-Ashouri, A. Hagfeldt, A. Crovetto, A. Abate, A. G. Ricciardulli, A. Vijayan, A. Kulkarni, A. Y. Anderson, B. P. Darwich, B. Yang, B. L. Coles, C. A. R. Perini, C. Rehermann, D. Ramirez, D. Fairen-Jimenez, D. Di Girolamo, D. Jia, E. Avila, E. J. Juarez-Perez, F. Baumann, F. Mathies, G. S. A. González, G. Boschloo, G. Nasti, G. Paramasivam, G. Martínez-Denegri, H. Näsström, H. Michaels, H. Köbler, H. Wu, I. Benesperi, M. I. Dar, I. Bayrak Pehlivan, I. E. Gould, J. N. Vagott, J. Dagar, J. Kettle, J. Yang, J. Li, J. A. Smith, J. Pascual, J. J. Jerónimo-Rendón, J. F. Montoya, J.-P. Correa-Baena, J. Qiu, J. Wang, K. Sveinbjörnsson, K. Hirselandt, K. Dey, K. Frohna, L. Mathies, L. A. Castriotta, M. H. Aldamasy, M. Vasquez-Montoya, M. A. Ruiz-Preciado, M. A. Flatken, M. V. Khenkin, M. Grischek, M. Kedia, M. Saliba, M. Anaya, M. Veldhoen, N. Arora, O. Shargaieva, O. Maus, O. S. Game, O. Yudilevich, P. Fassl, Q. Zhou, R. Betancur, R. Munir, R. Patidar, S. D. Stranks, S. Alam, S. Kar, T. Unold, T. Abzieher, T. Edvinsson, T. W. David, U. W. Paetzold, W. Zia, W. Fu, W. Zuo, V. R. F. Schröder, W. Tress, X. Zhang, Y.-H. Chiang, Z. Iqbal, Z. Xie, E. Unger, *Nat. Energy* **2022**, *7*, 107.

[217] B. Yılmaz, R. Yıldırım, *Nano Energy* **2021**, *80*, 105546.

[218] R. E. Kumar, A. Tiihonen, S. Sun, D. P. Fenning, Z. Liu, T. Buonassisi, *Matter* **2022**, *5*, 1353.

Author biographies and photographs:

Kai Wang received his BS (2009) and PhD degree (2014) under the supervision of Prof. Yue Wang in Jilin University (China). Then he worked at King Abdullah University of Science & Technology as a postdoctoral researcher with Prof. Stefaan De Wolf. In 2020, he obtained his current professor position in Northwestern Polytechnical University (China) to continue his research interest including novel organic optoelectronic functional materials and their application in photovoltaic devices.

Stefaan De Wolf received his Ph.D. degree in 2005 from the Katholieke Universiteit Leuven in

Belgium, during which time he was also affiliated with IMEC. From 2005 to 2008, he was with the National Institute of Advanced Industrial Science and Technology (AIST), Tsukuba, Japan. In 2008, he joined the Photovoltaics and Thin-Film Electronics Laboratory, Ecole Polytechnique Federale de Lausanne (EPFL), Neuchatel, Switzerland, as a team leader for its activities on high-efficiency solar cells. Since September 2016 he has been an associate professor at the King Abdullah University of Science and Technology (KAUST) in Saudi Arabia, focusing on high-efficiency silicon and perovskite solar cells and their combinations in perovskite/silicon tandem solar cells, as well as photovoltaics for sunny and hot climates.

Organic Hole Transport Layers for Efficient, Stable and Scalable Inverted Perovskite Solar Cells

Yiguo Yao, Caidong Cheng, Chenyang Zhang, Hanlin Hu, Kai Wang, Stefaan De Wolf**

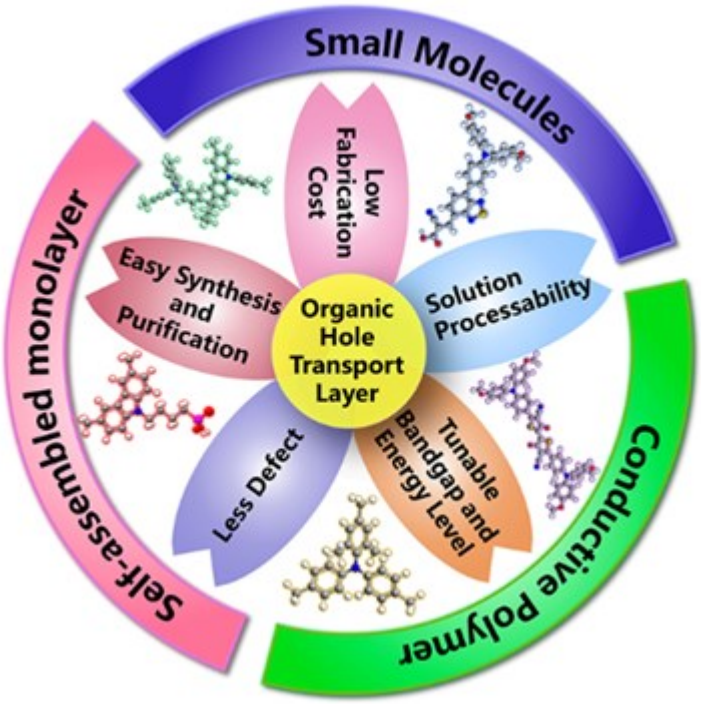

Inverted perovskite solar cells (PSCs) attract great attention due to the low temperature processing, negligible hysteresis and superior stability. Hole transport layers play a decisive role in carrier extraction, transport, and perovskite crystallizaiton. This review provides a comprehensive overview of the structural engineering of organic hole transport layers utilized in inverted PSCs is including conductive polymers, small molecules (SMs) and emerging self-assembled monolayers (SAMs).